

**Colloidal Nanoparticle Inks for Printing Functional Devices:
Emerging Trends and Future Prospects**

| | |
|-------------------------------|--|
| Journal: | <i>Journal of Materials Chemistry A</i> |
| Manuscript ID | TA-REV-07-2019-007552.R1 |
| Article Type: | Review Article |
| Date Submitted by the Author: | 16-Sep-2019 |
| Complete List of Authors: | Zeng, Minxiang; University of Notre Dame, Department of Aerospace and Mechanical Engineering Notre Dame Zhang, Yanliang; University of Notre dame, Department of Aerospace and Mechanical Engineering |
| | |

Colloidal Nanoparticle Inks for Printing Functional Devices: Emerging Trends and Future Prospects

Minxiang Zeng, Yanliang Zhang*

Department of Aerospace and Mechanical Engineering, University of Notre Dame, Notre Dame, IN, USA

**Corresponding Author: yzhang45@nd.edu*

ABSTRACT

Colloidal nanoparticles have been widely studied and proven to have unique and superior properties compared to their bulk form, which are attractive building blocks for diverse technologies, including energy conversion and storage, sensing, electronics, etc. However, transforming colloidal nanoparticles into functional devices while translating their unique properties from nanoscale to macroscale remains a major challenge. The development of advanced manufacturing methodologies that can convert functional nanomaterials into high-performance devices in a scalable, controllable and affordable manner presents great research opportunities and challenges for the next several decades. One promising approach to fabricate functional devices from nanoscale building blocks is additive manufacturing, such as 2D and 3D printing, owing to their capability of fast prototyping and versatile fabrication. Here, we review recent progresses and methodologies on additive printing of functional devices using colloidal nanoparticles inks with an emphasis on 2D nanomaterial-based inks. This review provides a comprehensive overview on four important and interconnected topics, including nanoparticle synthesis, ink formulation, printing methods, and device applications. New research opportunities as well as future directions are also discussed.

KEYWORDS: colloidal nanoparticles, ink printing, functional devices

Table of Content

| | |
|--|-----------|
| 1. Introduction | 3 |
| 2. Synthesis of 2D nanomaterials..... | 6 |
| 2.1. Bottom-up synthesis | 7 |
| 2.2. Top-down synthesis | 10 |
| 3. Ink formulation..... | 16 |
| 3.1. The colloidal stability of 2D nanomaterials..... | 17 |
| 3.2. Ink rheology of 2D nanomaterials | 25 |
| 3.3. Ink drying and particle assembly | 27 |
| 4. Printing strategies..... | 30 |
| 4.1. 2D printing..... | 31 |
| 4.2. 3D printing..... | 35 |
| 4.3. 4D printing..... | 39 |
| 5. Device applications of printed 2D nanomaterials..... | 43 |
| 5.1. Energy conversion and storage | 43 |
| 5.2. Sensing..... | 51 |
| 6. Conclusion and Future Perspectives..... | 60 |

1. Introduction

Colloidal nanoparticles are attractive building blocks for a wide range of emerging technologies, including electronics, optoelectronics, sensors, energy devices, etc. In the past several decades, various device fabrication technologies, such as photolithography, electroless plating, and physical/chemical vapor deposition, have been extensively investigated.^{1,2} However, these technologies rely on expensive equipment and/or multi-stage processes, which are not only difficult for fast prototyping and low-cost manufacturing, but also not compatible/sophisticated enough for building functional devices with colloidal nanoparticles. An alternative method to fabricate flexible/functional devices is additive manufacturing, such as three-dimensional (3D) printing.^{3,4} In the past several decades, significant development of printing technologies has been witnessed for converting printable nanoparticle inks into complex device architectures.⁵⁻⁷ A wide range of functional nanomaterials from zero-dimension (0D) quantum dots, to one-dimensional (1D) nanowires/nanofibers, and two-dimensional (2D) nanosheets, have been adopted as printable colloidal inks (**Figure 1**). All these progresses have created almost infinite possibilities for rapid prototyping and scalable and low-cost manufacturing of functional devices.⁸

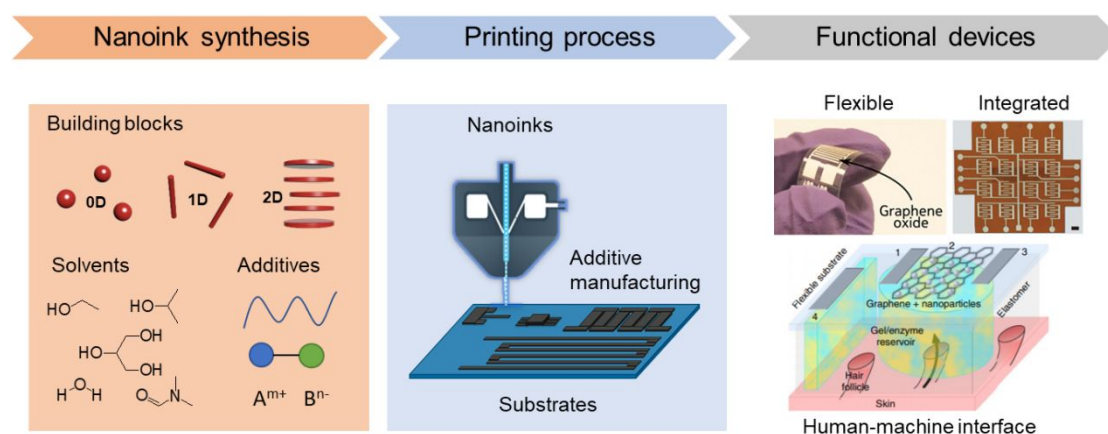


Figure 1. Additive manufacturing enables rapid transformation from nanoscale building blocks into macroscale functional devices. Adapted and reprinted by permission from Springer Nature.⁹
¹⁰ Copyright 2017&2018 Nature Publishing Group. Reproduced with permission from reference.¹¹ Copyright 2013 American Chemical Society.

Among various types of nanomaterials, 2D nanomaterials (2DM) are ultrathin nanostructures with unique optical, electrical, chemical, thermal and mechanical properties.^{12, 13} Since the rise of graphene family, a great variety of 2D nanomaterials have been synthesized and developed by bottom-up strategy from molecular precursors or top-down approach from their layered crystals.¹⁴ As shown in **Figure 2**, common 2D nanomaterials include graphene/graphene oxide/reduced graphene oxide (Gr/GO/rGO), transition metal dichalcogenides (TMDs), transition metal carbides/carbonitrides/nitrides (MXenes), black phosphorus (BP), hexagonal boron nitride (h-BN), graphitic carbon nitride (g-C₃N₄), layered double hydroxides (LDHs), transitional metals/metal oxides (TMOs/MOs), and other novel 2D nanostructures.¹² Graphene is a monolayer graphite with every carbon atom bonded to adjacent ones by σ bond, forming hexagonal 2D network with a thickness around 3.4 Å. TMDs also have a hexagonal surface structure similar to graphene, with the in-plane anion atoms in each layer split into two identical layers. MXenes are of general formula $M_{n+1}X_nT_x$ ($n = 1-3$), where M is transition metal (e.g., Ti or V), X is C and/or N, and T is surface anion (O, OH, F). For natural occurring 2DMs, clay minerals are 2D sandwich structures with octahedral metal hydroxide layers and tetrahedral silicate layers.¹⁵ LDHs, also known as anionic clays or hydrotalcite-like compounds, are often described by the general formula, $[M^{2+}_{1-x}M^{3+}_x(OH)_2]^{x+}A^{n-}_{x/n}\cdot yH_2O$, where M is metal ion and A represents an interlayer anion.^{16, 17}

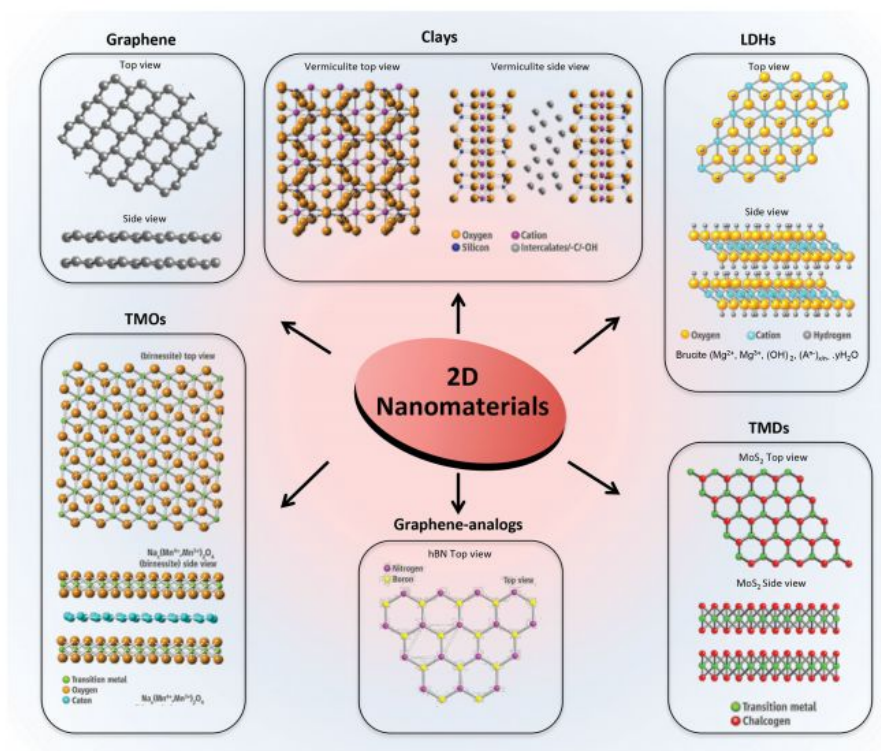


Figure 2. 2D nanomaterials and their structures. Reproduced with permission from reference.¹⁸ Copyright 2018 Wiley-VCH.

The extreme chemical diversity of 2D nanomaterials provides many opportunities, but also poses challenges for comprehensive assessments of specialized roles of 2DMs in device fabrication processes, such as printing-based manufacturing. In addition, high-performance 2D nanomaterials are not necessarily translated into high-quality inks for printing processes. The collective behaviour of 2D nanoparticles in colloidal inks can be influenced by many factors, such as particle size and surface chemistry, tendency of aggregation, ionic strength of the dispersion. Although several articles have made great effort on reviewing printing technologies of nanomaterials,^{3, 4, 7, 19-22} a comprehensive review that covers nanoscale building blocks (e.g., synthesis and surface engineering), mesoscopic colloidal interaction (e.g., aggregation and sedimentation), and macroscopic printing processes (e.g., 2D, 3D, and 4D printing) and device applications is missing. This review therefore proposes a framework for seeking a systematic understanding on fundamental correlations of materials chemistry and physics of 2DMs, ink

properties, printing processes, and corresponding device applications. With this in mind, the framework thus considers four key interactive aspects: 2D nanomaterial synthesis, ink formulation, printing processes, and device applications. Our vision is to undertake a meticulous examination of current research trends over the last decade with a focus on 2DMs compatible with printing processes. The review closes with a conclusion and outlook, suggesting future directions to inform researchers potentially disruptive printing technologies and applications of 2DMs.

2. Synthesis of 2D nanomaterials

Since the discovery of graphene, significant efforts have been invested on the synthesis of 2D materials, including liquid phase exfoliation, hydrothermal synthesis, etc. In this section, we mainly focus on solution-processable 2D nanomaterials such that some synthetic methods such as chemical vapor deposition will not be discussed. The synthetic strategies of 2D nanomaterials typically can be categorized into two kinds: bottom-up synthesis and top-down synthesis. Despite some exceptions, Table 1 aims to summarize the common preparation methods for 2D nanomaterials. Despite that not all of these synthetic methods have been explored for ink preparation, significant research opportunities still exist for synthesizing novel printable 2D nanostructures and establishing next-generation material library for printing technology as well as for developing new printing methodologies for a broad range of device applications.

Table 1: Overview of various 2D nanomaterials with their common preparation methods.

| | <i>Bottom-up</i> | | | <i>Top-down</i> | | |
|---------------------|-------------------------------|-----------------------------------|-------------------|----------------------------------|-----------------------|----------------------|
| | Hydrothermal/ Solvothermal | Ligand/ Template attachment | Self- assembly | Micro- mechanical cleavage | Liquid exfoliation | Selective etching |
| Gr/GO/rGO | +23, 24 | | | +25, 26 | +27, 28 | |
| TMDs | +29 | +30 | +31 | +32 | +33, 34 | |
| h-BN | +35, 36 | | | +37 | +38 | |
| Black phosphorus | | | | +39 | +40 | |

| | | | | | | |
|--------------|---|--|---|--|--|--|
| Metal oxides | +41 | +42, 43 | +44 | | +45 | |
| MXene | | +46 | | | | +47 |
| Clays | +48 | | | | +49 | |
| Comments | <i>Facile and applicable to large-scale production.</i> | <i>Provide good control on particle size and morphology.</i> | <i>Versatile but low structural robustness due to non-covalent bonding.</i> | <i>Good quality while often low yield.</i> | <i>High scalability and relatively low cost.</i> | <i>Strongly corrosive agents are often required.</i> |

2.1. Bottom-up synthesis

2.1.1 Hydrothermal/Solvothermal synthesis

As a representative wet-chemical synthesis approach, the hydrothermal/solvothermal synthesis involves water or other solvents in a sealed vessel, where reaction temperature can be higher than the boiling point of the solvent in order to generate high pressure to assist the reaction kinetics and increase the quality of crystal phase of as-prepared 2D nanomaterials.¹² Remarkably, the solvent and additives, such as ligands or surfactants, are crucial factors in determining the synthesis, morphology, and properties of 2D nanosheets. For example, ultrathin cobalt nanosheets with tunable oxide state can be prepared by using hydrothermal condition of butylamine and dimethylformamide (**Figure 3a**).⁵⁰ Single-layer noble metal nanosheets with lateral sizes of few hundred nanometers can be prepared using polyvinylpyrrolidone (PVP) as surfactants. Besides metal nanosheets, metal oxides and TMDs nanosheets have also been produced by hydrothermal/solvothermal techniques.

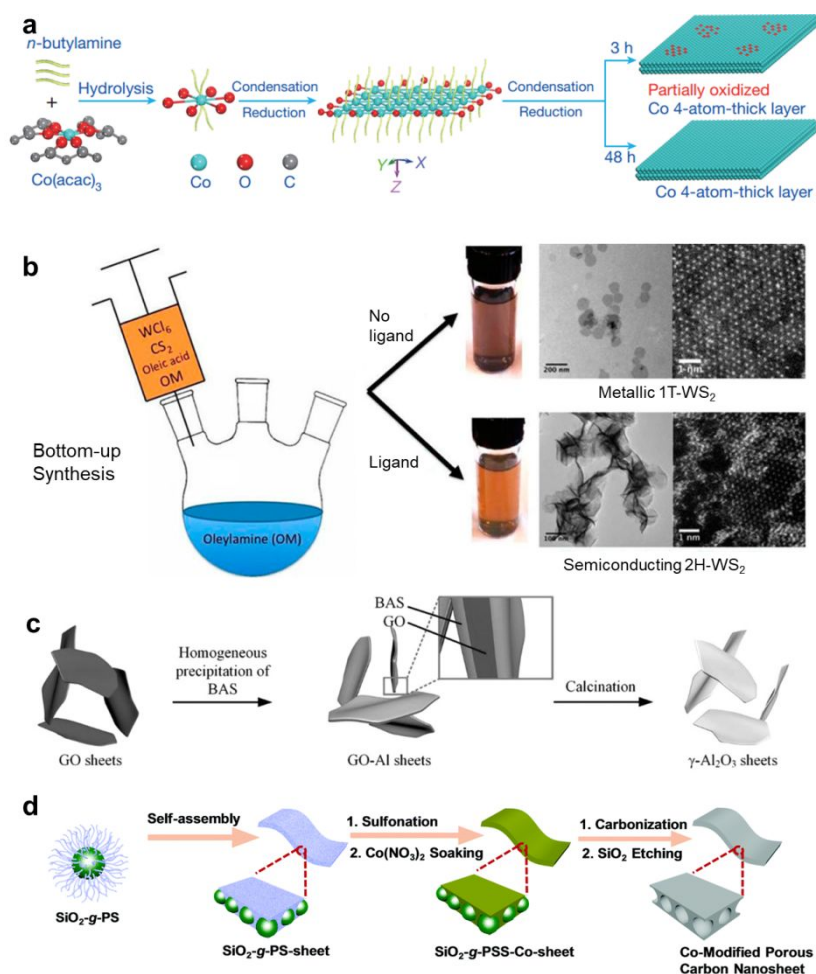


Figure 3. Examples of bottom-up synthesis of 2D nanomaterials. (a) Hydrothermal synthesis of cobalt nanosheets. Reprinted by permission from Springer Nature.⁵⁰ Copyright 2016 Nature Publishing Group. (b) Colloidal synthesis of WS₂ from small molecules. The formation of 1T-WS₂ and 2H-WS₂ can be actively controlled by adjusting reaction conditions. Reprinted by permission from reference.⁵¹ Copyright 2014 The Royal Society of Chemistry. (c) The bottom-up synthesis of Al₂O₃ nanosheets based on the 2D templates of GO reacting with basic aluminum sulfate (BAS). Reproduced with permission from reference.³⁰ Copyright 2016 Wiley-VCH. (d) Evaporation-induced bottom-up self-assembly approach for fabricating 2D porous carbon nanosheets. Reprinted by permission from reference.⁵² Copyright 2019 The Royal Society of Chemistry.

Although the hydrothermal/solvothermal synthesis is a facile and possibly scalable technique for producing 2DMs, it is difficult to fully understand the mechanisms in every single reaction as all the reaction kinetics occurs in a sealed system, which make it challenging to apply the same experimental condition to other 2DMs systems. Noteworthy, the hydrothermal synthesis is relatively sensitive to the experimental settings, which increase the challenge of precisely controlling the resulting 2D nanomaterials in different batches or different laboratories.

2.1.2 Ligand/template attachment method

Compared with traditional hydrothermal mechanism, the ligand attachment method demonstrates an unusual growth progression and realizes nanostructures with well-defined shapes.⁵³ During this process, neighboring nanocrystals or precursors are accumulated, attached, and fused with each other, forming single-crystalline 2D sheets to reduce high interfacial energy facets.¹² For example, taking advantage of the strong bonding of oleic acid on [100] facet, small PbS nanocrystals can grow into single-crystalline 2D PbS sheets. Studies also showed that other reagents, such as chlorine-containing reactants, can assist activating the oriented attachment progression. In general, the growth mechanism is typically based on oriented attachment of small crystals, after which epitaxial recrystallization into large 2D nanostructures occurs. Similar to hydrothermal mechanism, surfactants are critical for determining the size, shape, and nanostructures of 2DMs in ligand attachment method. As shown in **Figure 3b**, Mahler et al. demonstrated that the formation of either 2H-WS₂ or 1T-WS₂ highly depends on the ligand choice.⁵¹ Introducing small amount of hexamethyldisilazane (HMDS) into reaction system can lead to the formation of semiconducting 2H-WS₂ rather than the metallic 1T-WS₂.

Similar to the ligand attachment method, other templated strategies have been investigated for growing anisotropic nanostructures. As shown in **Figure 3c**, 2D GO nanosheets were used as 2D template to direct the growth of inorganic Al₂O₃ sheets.³⁰ During the synthesis, a thin layer of hydroxide of aluminum was first deposited on the GO sheets which was then removed using calcination treatment at 800 °C, leading to the transformation of aluminum

hydroxide to the Al_2O_3 nanosheets. As another 2D-templated example, the hexagonal close-packed (*hcp*) gold nanosheets can be prepared by using the GO as a starting template.⁵⁴ In addition, CuO nanoplates were also reported for templated synthesis of $\alpha\text{-Fe}_2\text{O}_3$ nanosheets, in which the CuO template was etched away during the nanosheet growth.⁵⁵ Numerous 2D semiconductor nanosheets, including CuInS_2 , $\text{CuIn}_x\text{Ga}_{1-x}\text{S}_2$, and $\text{Cu}_2\text{ZnSnS}_4$, have also been fabricated by 2D-templated synthesis processes.⁵⁶

2.1.3 Self-assembly of building blocks

Driven by the improvement of nanocrystal production, self-assembly of small building blocks has been developed to breed architectures with nanocrystal building blocks in an orientationally/positionally ordered manner, where pre-synthesized building blocks instinctively assemble with each other by physical/chemical interactions including electrostatic interactions, van der Waals interactions, hydrogen bonds, etc.⁵⁷ Both nanoparticles and nanowires were shown to self-assemble into 2D materials, such as polycrystalline 2D CdTe nanosheet or assembled Au nanosheets.^{31, 58} For example, the self-assembly of PbS nanowires has been demonstrated to produce anisotropic PbS nanosheet.⁵⁹ To better control the assembly process, interface-based self-assembly has been proposed to fabricate functional 2D nanomaterials.⁵² As shown in **Figure 3d**, spherical polystyrene-functionalized SiO_2 nanoparticles can self-assemble at the interface of the saturated NaCl solution and air. The 2D intermediate was then dispersed in sulfuric acid to preserve its nanosheet morphology followed by Co treatment to dope Co element in 2D sheets. After a simple carbonization and etching process, functional Co-modified carbon nanosheets were obtained.⁵²

In addition to nanocrystals, organic molecules can also be used as building blocks for self-assembly into 2D materials by electrostatic interactions, van der Waals interactions, and hydrogen bonds. Well-organized photonic nanosheets were demonstrated by self-assembly of nonionic surfactant hexadecylglyceryl maleate.⁶⁰ It is reasonable to expect that more novel 2D materials would be developed via self-assembly of building blocks strategy.

2.2. Top-down synthesis

2.2.1 Micromechanical cleavage

The ability to synthesize 2D materials with desired chemical composition, dimensions, crystalline phase, and surface properties is of particular significance. The micromechanical cleavage technique was used to prepare 2D nanosheets by exfoliating layered crystals. For example, using mechanical forces with Scotch tape, single/few layers of nanosheets can be achieved as the interlayered van der Waals forces have been overcome in bulk crystals. In 2004, Geim and co-workers first reported the micromechanical cleavage of graphite, where the bulk graphite can be attached to Scotch tapes followed by peeling into thin platelets with another adhesive surface.⁶¹⁻⁶⁴ By repeating such process several times, the desired thin flakes can be obtained. After attaching freshly cleaved thin films to a flat substrate and removing Scotch tapes, single- or few-layers of graphene can be acquired.

This micromechanical cleavage technique can be extended to exfoliate other layered materials, including MoS₂, NbSe₂, and *h*-BN.⁶³ Recently, the micromechanical cleavage technique has been employed to synthesize several ultrathin 2D nanomaterials ranging from TMDs,⁶⁵ to topological insulator,⁶⁶ and antimonene.⁶⁷ As a general method capable of fabricating all categories of nanosheets of which bulk crystals are layered structures, additional novel ultrathin 2D crystals are expected to be synthesized by this method. This methodology can be considered as a nondestructive process as no chemical reactions were required during the manufacturing process. Consequently, the exfoliated nanosheets retained the pristine crystal quality of their layered counterparts. The dimensions of the formed 2D structures can reach micrometer levels, which enable the mechanically cleaved nanosheet to become an ideal candidate to investigate the intrinsic mechanical, optical, and electronic properties of 2D nanomaterials.

Despite several advantages of the micromechanical cleavage method, disadvantages still remain: 1) the fabrication yield of this method is relatively low, and impurities such as thick flakes

always coexist with the single- or few-layer flakes; 2) The manufacturing speed is not competitive to other methods such as solution-based approaches. The low yield together with the slow manufacturing rate make it problematic to meet the requirements for many printing applications, especially for large-scale additive manufacturing; 3) the dimensions of the prepared 2D materials are hard to be regulated as the exfoliation route lacks the exactness, controllability, or repeatability; 4) Additional substrates are prerequisites to hold the formed 2D crystals during exfoliation, making it challenging for fabricating freestanding 2DM-based devices. Recent efforts have been made to improve micromechanical cleavage method, showing that using oxygen plasma treatment with additional heating during the exfoliation substantially improved the uniformity of interface contact and thus increased the production yield of 2D nanosheets.⁶⁸

2.2.2 Mechanical liquid exfoliation

Sonication has been commonly used as sources of mechanical forces for exfoliating layered bulk materials, which are generally dispersed in a particular solvent. As the liquid cavitation is induced by sonication, the waves of mechanical vibrations through the layered crystals produce an intensive tensile stress, resulting in the exfoliation of starting materials into thin sheets.⁶⁹ The 2D nanosheets can be separated from the suspension using centrifugation. To maximize the efficiency of liquid phase exfoliation, matching the interfacial energy between solvent and 2D materials can be an important factor. As it is relatively simple and effective without any complicated equipment, this sonication technique offers a low-cost approach for high-yield fabrication of 2D nanosheets. For example, a fairly high concentration of graphene nanosheets suspension was achieved by sonicating bulk graphite in isopropanol and chloroform.⁷⁰ ⁷¹ In addition to graphene, other 2D nanomaterials, including NbSe₂, Bi₂Te₃, and *h*-BN have also been prepared by this technique.⁷² The solvent systems play significant roles in the production of exfoliated nanosheets. It is noteworthy that although pure H₂O was constantly thought to be unsatisfactory for efficiently exfoliating layered bulk materials, a recent study showed that direct exfoliation and dispersion of 2D nanomaterials in pure H₂O can be achieved at elevated

temperatures.⁷³ The exfoliated nanosheets can be stabilized due to the presence of colloidal surface charges brought by edge functionalization or high polarity, leading to enhanced colloidal stability of 2D nanosheets. Such approach of exfoliating bulk materials in pure water makes this process promising for practical applications due to environmentally friendly and low-cost feature.

It is challenging to find an appropriate solvent for each layered bulk material, as the surface energy differs in different bulk crystals. Instead, the addition of polymers or surfactants provided another promising pathway for exfoliating 2D layered materials. The surface energy of the aqueous dispersion can be simply adjusted by introducing suitable surfactants, thus reducing the interfacial energy between layered bulk crystals and solvent and realizing effective exfoliation of layered constituents. For instance, pyrene derivatives are commonly used as dispersants for manufacturing graphene dispersions owing to their ability to form π - π stacking interaction with graphene sheets.^{74, 75} Through introducing repulsive electrostatic forces on graphene surface, pyrene derivatives can prevent sheet aggregation and consequently stabilize graphene in water.⁷⁶⁻⁷⁸ In addition to pyrene derivatives, other species have been employed for dispersing 2D nanosheets in inks: polystyrene (PS), polyvinyl chloride (PVC), ethyl cellulose (EC), polyvinylpyrrolidone, poly(isoprene-*b*-acrylic acid) (PI-*b*-PAA), poly[styrene-*b*-(2-vinylpyridine)] (PS-*b*-P2VP), P-123-polyoxyethylenes orbitanmonooleate, polyoxyethylene sorbitantriolate, polyoxyethylene dodecyl ether, polyoxyethylene octadecylether, polyoxyethyleneoctyl phenyl ether, bovine serum albumin (BSA), Pluronic P-123, *n*-dodecyl β -d-maltoside (DBDM), and Arabic gum from acacia tree.⁷⁹⁻⁸²

Although the sonication-assisted exfoliation method can be applicable for a wide range of 2D materials with higher fabrication rate than that of micromechanical cleavage processes, the fabrication rate remains relatively low to meet the requirement for industrial scale. In order to scale up the process, shear force-assisted method was proposed. Using a high-shear rotor-stator mixer, high shear rates in suspension can trigger the exfoliation process and produce exfoliated nanosheets in a much more efficient manner.⁸³ The shear-force device contains a mixing head

consisting of a rotor with a stator. Such technique was also used for exfoliating BP crystal into few-layer platelets. Additionally, the synthesis of exfoliated WS₂, MoS₂, and *h*-BN nanosheets were reported by using a kitchen blender.⁸⁴ Such results suggest that it is possible to use industrial stirring tank reactors for large-scale 2D materials production.

2.2.3 Intercalation-assisted liquid exfoliation

As a typical top-down approach, the ion intercalation strategy has been widely adopted to fabricate ultrathin 2D nanosheets. Small molecules and ionic species, including Li⁺, Na⁺, K⁺, can intercalate into the spaces between neighboring layers in layered bulk crystals, leading to the formation of intercalated compounds (**Figure 4**).^{33, 34} Consequently, the ion intercalation can considerably enlarge the interlayer distance of unexfoliated bulk crystals, facilitating the exfoliation process with shorter time. High yield of mono- to few-layer nanosheets can be achieved using a separation step to eliminate unexfoliated flakes by methods such as high-speed centrifugation. For example, the layered materials were treated with *n*-butyl lithium to yield a Li-intercalated structure in refluxed hexane solution for several days, and subsequently the nanosheet dispersion can be readily formed under sonication in water.

In spite of the accelerated exfoliation facilitated by ion intercalation, the intercalation process itself requires extended reaction time (for example, several days) and elevated temperature (for instance, 100 °C) for some compounds. The lateral dimensions, quantity of deficiencies, sheet concentration, and number of layers can be approximately adjusted by changing the tentative settings, including starting size of layered crystals, exfoliation time, exfoliation agents, and reaction temperature. During ion-intercalation, phase alteration sometimes occurs from semiconducting hexagonal (2H) and metallic octahedral (1T) phase for MoS₂ and WS₂, presenting a potent method for the phase engineering of TMDs.⁸⁵ Despite that some ions are able to intercalate into layered metal telluride or selenide, the use of ion intercalation strategy for exfoliating metal telluride or selenide remains challenging, as the intercalated metal telluride

or selenide are commonly unstable, leading to the decomposition of metal telluride/selenide during sonication.¹²

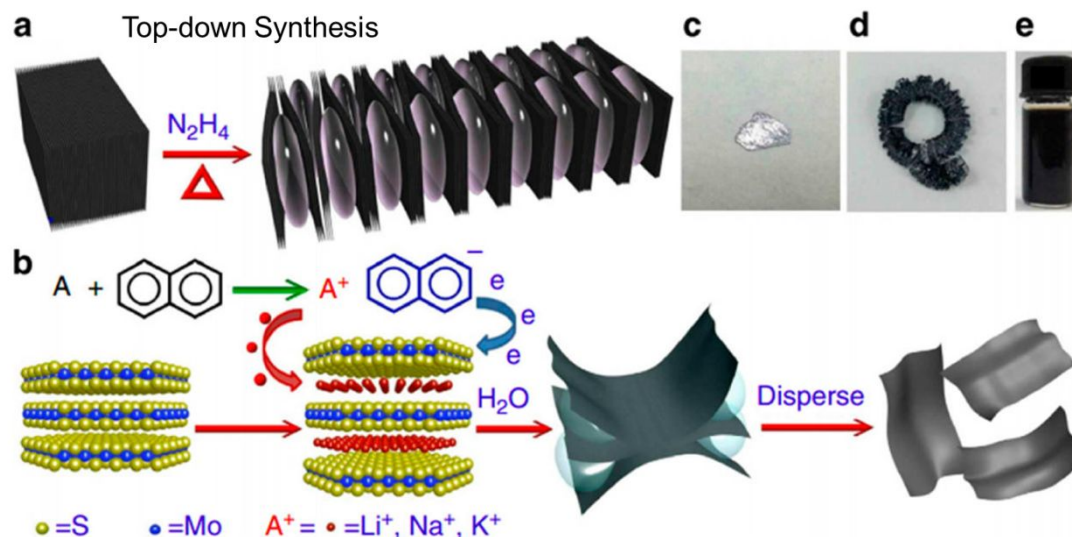


Figure 4. Examples of top-down synthesis of 2D nanomaterials. (a) The intercalation and (b) the exfoliation of MoS₂ using hydrazine and naphthalene. (c) Unexfoliated MoS₂ crystal. (d) Intercalated MoS₂ (e) Exfoliated MoS₂ in dispersion. Reprinted by permission from Springer Nature.³⁴ Copyright 2014 Nature Publishing Group.

The ion intercalation route, such as the use of butyl lithium, is difficult to regulate precisely, making it challenging to circumvent inadequate or over ion-intercalation. Recently, safer salt choices including NaCl and CuCl₂ were proposed as intercalates for the exfoliation of graphite powder into graphene. Upon heating at 100 °C to vaporize the water, the Cu²⁺ or Na⁺ can be intercalated into interlayer spacing of graphite.⁸⁶ After sonicating in DMF or NMP for a short time, up to 65% (1–5 layers) yield of graphene sheets can be produced with large lateral sizes up to tens of micrometers.

2.2.4 Oxidation-assisted Liquid Exfoliation

In oxidation-assisted exfoliation of graphite, commonly known as the Hummers' method, strong oxidizing agents, such as potassium permanganate or sodium persulfate, were applied to

oxidize graphite, and the oxidation of graphite produces hydrophilic functional groups on each graphene layer, resulting in enlarged d-spacing of bulk graphite.^{87, 88} With increased treatment time and temperature, the expanded graphite oxides bulk materials were exfoliated into 2D graphene oxide monolayers, or possibly transformed into small-sized 2D graphene quantum dots. This technique enables large-scale synthesis of single-layer GO nanosheets in aqueous solution. It is noteworthy that the oxygen-containing functional groups of GO can be partially eliminated using reduction strategy to form reduced GO nanosheets. Up to now, electrochemical reduction, thermal annealing, photochemical reduction, and chemical reduction were reported to remove GO's oxygen-containing groups.⁸⁹ Since the residual groups may still exist, the conductivity of reduced GO commonly cannot compete with graphene nanosheets produced from CVD method or mechanical exfoliation.

2.2.5 Selective etching

The selective etching method can prepare 2D nanosheets of MXenes, a type of metal carbides or carbonitrides.^{90, 91} MAX phases have a common formula of $M_{n+1}AX_n$ ($n = 1, 2, \text{ or } 3$), where M, A, and X represent early transition metal, element of group IIIA or IVA, and C and/or N, respectively.⁹²⁻⁹⁴ A clear difference between MAX phase materials and conventional van der Waals layered crystals lies in the metallic bonds between $M_{n+1}X_n$ layers which shows much more robust interaction than weak forces of TMDs, graphite, and BP. Consequently, an elective etching technique based on acidic HF solution is often required to remove the "A" layers without destroying the bonds in $M_{n+1}X_n$ layers. The resulting etched materials with loosely packed layers can be readily exfoliated into 2D nanosheets under sonication. Up to now, this technique has been magnificently useful for synthesizing many different types of MXenes including Al_3C_3 , Ta_4C_3 , Mo_2TiC_2 , Nb_2C , Ti_4N_3 , $Mo_2Ti_2C_3$, Ti_3CN , Mo_2CT_x , Cr_2TiC_2 , Ti_2C , V_2C , $(Ti_{0.5}, Nb_{0.5})_2C$, and $(V_{0.5}, Cr_{0.5})_3C_2$. However, several limitations still exist in this technique as it is difficult to apply this process to prepare other ultrathin 2D nanosheets, such as TMDs.

3. Ink formulation

While 2D materials show intriguing properties at the nanoscale, these particles cannot be directly used until being processed and formulated into printable inks for device fabrication. One important goal of ink formulation is to convert or integrate nanoscale building blocks into a stable colloidal dispersion. The use of 2DM-based inks for printing has received increasing research interests in recent years, likely due to: (i) significant advances in solution-processable 2DMs and 2DM derivatives on which the surface chemistry and nanostructure can be on-demand controlled, and (ii) fast development of printing technologies that provides a variety of processing options. Herein, major principles of colloidal ink systems and recent developments in 2DM-based inks are discussed.

3.1. The colloidal stability of 2D nanomaterials

For most nanoparticle-based inks, the colloidal stability of the ink particles is one of the most essential elements in preparation of high-quality inks. In a liquid medium, the colloidal behavior of 2D nanomaterials can be estimated through the Derjaguin-Landau-Verwey-Overbeek (DLVO) theory, which predicts the aggregation trend of nanoparticles quantitatively. As shown in **Figure 5a**, DLVO theory combines the potential energy of the van der Waals attraction (P_A , red) and the electrostatic repulsion (P_R , blue) because of the electric double layers. **Figure 5a** also presents a typical total energy profile (P_{total} , green) along with the separation distance of particles: the primary minimum and secondary minimum represent the aggregation state and colloidally stable state, respectively. For 2D particles, the DLVO theory can be represented in Equation (1)-(4):⁹⁵

$$P_A = -\frac{A}{12\pi} \left\{ \frac{1}{d^2} + \frac{1}{(d+2\delta)^2} - \frac{2}{(d+\delta)^2} \right\} \quad (1)$$

$$P_R = \frac{64k_B T I N_A}{\kappa} \left\{ \tanh \left(\frac{e\psi_0}{4k_B T} \right) \right\}^2 e^{-\kappa d} \quad (2)$$

$$\kappa^{-1} = \sqrt{\frac{k_B T \epsilon_0 \epsilon_r}{2N_A e^2 I}} \quad (3)$$

$$P_{total} = P_A + P_R = -\frac{A}{12\pi} \left\{ \frac{1}{d^2} + \frac{1}{(d+2\delta)^2} - \frac{2}{(d+\delta)^2} \right\} + \frac{64k_B T I N_A}{\kappa} \left\{ \tanh \left(\frac{e\psi_0}{4k_B T} \right) \right\}^2 e^{-\kappa d} \quad (4)$$

Where δ is the thickness of 2D materials, A is the Hamaker constant of materials, d is the average distance of 2D materials, κ^{-1} is the Debye screening length, N_A is $6.02 \times 10^{23} \text{ mol}^{-1}$ (Avogadro constant), ϵ_0 is the vacuum permittivity, ϵ_r is the relative permittivity of water, k_B is the Boltzmann constant, ψ_0 is the surface potential of 2D materials, I is the concentration of free ions.

Despite being a simplified model of colloidal particle interaction, DLVO theory provides some important insights to understand the aggregation of 2D nanoparticles. A small Debye length κ^{-1} (the thickness of the diffuse electric double layer) often leads to a reduced repulsive potential energy which is likely to form aggregation. For example, Chowdhury et al. observed that GO nanosheets tend to aggregate at high salt concentration due to electrical double layer compression.⁹⁶ It is also intuitive that the aggregation occurs when 2D particles are processed in a high volume concentration (a small average distance d), as shown in **Figure 5a**. However, there are studies showing that DLVO theory is not effective in describing colloidal nanosystems in dilute dispersions with low salt concentrations.^{97, 98}

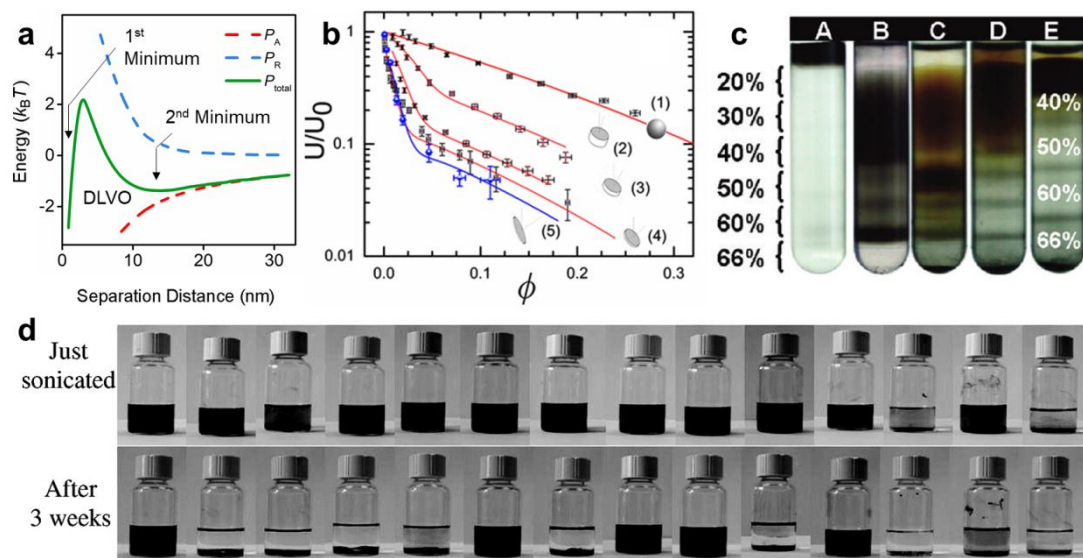


Figure 5. (a) DLVO theory of colloidal particles in dispersion. (b) Dimensionless sedimentation speed of 2D particles. Reproduced with permission from reference.⁹⁹ Copyright 2010 American Physical Society. (c) Ultracentrifuge separation of monodispersed graphene using density gradient. Reproduced with permission from reference.¹⁰⁰ Copyright 2010 American Chemical Society. (d) The colloidal stability of graphene oxide in different solvents. From left to right, the solvents are water, acetone, methanol, ethanol, 1-propanol, ethylene glycol, dimethyl sulfoxide, dimethylformamide, N-methyl-2-pyrrolidone, pyridine, tetrahydrofuran, dichloromethane, xylene, and hexane. Reproduced with permission from reference.¹⁰¹ Copyright 2008 American Chemical Society.

In addition to the tendency to aggregate, gravitational sedimentation can also play an important role in the colloidal stability of ink system. According to Stokes' law, the terminal sedimentation velocity of an individual spherical particle in a fluid is a function of the particle size, the force of gravity, the viscosity of the fluid and the density difference between the particle and the fluid, as shown in Equation (5):¹⁰²

$$U_0 = \frac{D^2 \cdot \Delta\rho \cdot g}{18\mu}$$

(5)

Where D is the diameter of the sphere, $\Delta\rho$ is the density difference between the particle and the solvent, g is the gravity constant, and μ is the solvent viscosity.

According to Stokes' Law, reducing particle size and increasing solution viscosity can promote particle dispersibility, in prevent of rapid sedimentation due to the gravity. Indeed, these sedimentation parameters have been used to develop methods for preparation and separation of monodispersed 2D materials (**Figure 5c**). For example, Sun et al. reported a density-gradient ultracentrifuge separation method to separate chemically modified graphene by sheet size and surface chemistry.¹⁰⁰ By optimizing the parameters, including the density gradient and centrifugation speed/time, graphene nanosheets with reduced polydispersity were obtained.

In addition to the particle size, the particle shape and volume fraction (ϕ) can also strongly affect the sedimentation speed. Compared with spherical nanoparticles, He et al.⁹⁹ found that anisotropic 2D nanosheets showed a higher resistance to the sedimentation owing to a stronger backflow of particles, as shown in **Figure 5b**. There is clear decreasing trend of dimensionless sedimentation rate upon increasing the particle volume fraction ϕ . For batch sedimentation, backflow moves opposite to the sedimentation direction to compensate the volume flux of settling colloidal particles. Such hydrodynamic force from the backflow can retard the sedimentation of colloidal particles. Thus, increasing ϕ can decrease the dimensionless sedimentation speed U/U_0 . These results indicated the unique advantages of 2D nanomaterials in preparing high-quality nanoinks.

Appropriate solvents are often critical to promote the colloidal stability of 2DMs. The desirable features of solvents include suitable viscosity, matched surface tension, and optimal Hansen/Hildebrand solubility parameters.^{103, 104} Having been used in industries such as paints and coatings, Hansen distance (R_a , often refer as Hansen solubility parameter) can be expressed as follows:

$$R_a = \sqrt{(\delta_{D,A} - \delta_{D,B})^2 + (\delta_{P,A} - \delta_{P,B})^2 + (\delta_{H,A} - \delta_{H,B})^2} \quad (6)$$

Where δ_D is the energy from dispersion forces of molecules A and B, δ_P is the energy from dipolar intermolecular force between molecules A and B, and δ_H is the energy from hydrogen bonds between molecules A and B.

The two molecules are likely to dissolve if R_a is a small value. Hernandez et al.¹⁰⁵ evaluated the dispersibility of graphene in 40 solvents and obtained Hansen solubility parameters of graphene sheets. It was found that some high boiling point organic solvents showed optimal Hansen solubility parameters for graphene, such as dimethylformamide and N-methyl-2-pyrrolidone. The dispersion stability of GO in various solvent systems have been shown in **Figure 5d**.¹⁰¹ Due to the hydrophilic nature of GO, several hydrophobic solvents, including dichloromethane and hexane, showed poor solubility for dispersing GO. The boiling point of

solvents is another important factor. For example, screen printing prefers solvents of relatively slow evaporation rates to circumvent possible clogging of the screen mesh related to rapid drying. On the other hand, more volatile solvents, such as isopropanol (IPA), are required for high-speed processes such as gravure and flexographic printing. In the aspect of environment, the development of good green solvents can be highly beneficial for large-scale application of printing processes.¹⁰⁶ It is worth mentioning that using mixtures of solvent can allow additional control on the boiling point, surface tension and solubility parameters.^{107, 108}

Alternatively, surfactants can be employed for electrostatic and/or steric stabilisation.^{77, 109, 110} As shown in **Figure 6a**, surfactants are amphiphilic species that have hydrophobic groups as well as hydrophilic groups. These molecules can strongly adsorb on the surface of 2D materials to further reduce the interfacial tension between particles and solvents, facilitating colloidal stability of inks. The addition of surfactants commonly allows higher concentrations of 2DMs for printing applications. It has been demonstrated that ionic surfactants, such as cetyltrimethylammonium bromide (CTAB) and sodium dodecyl sulfate (SDS), can be used to prepare monolayer MoS₂ nanosheets in water.¹¹¹ The dispersions are stabilized by electrostatic repulsive force between MoS₂ nanosheets, and interestingly the sign of surface charge on nanosheets, either positive or negative, can be controlled by the choice of surfactants (**Figure 6b**). A recent study also suggested that the surfactant sodium dodecyl benzene sulfonic acid sodium salt (SDBS) can not only enhance the colloidal stability of nanoparticles (e.g., carbon nanotube (CNT)), but also improved the film adhesion through an ink aging process.¹¹²

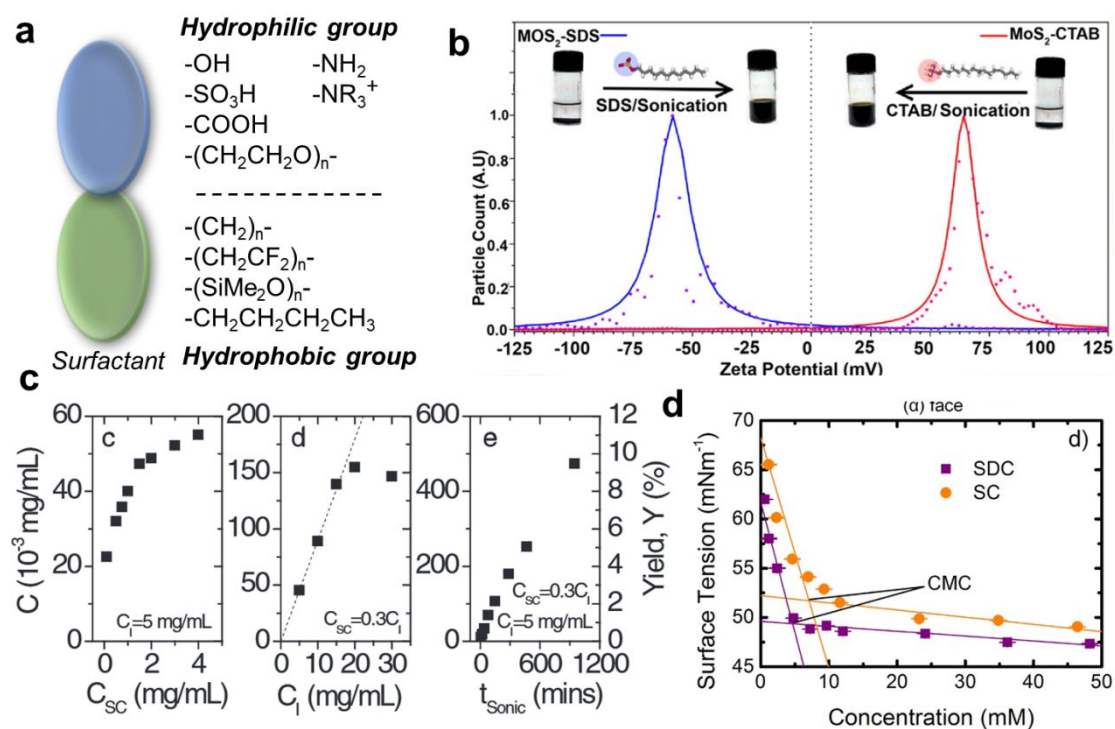


Figure 6. (a) Schematic illustration of examples of hydrophilic and hydrophobic groups of surfactants. (b) Electrostatic stabilization of MoS₂ in water by cationic (cetyltrimethylammonium bromide, CTAB) or anionic surfactants (sodium dodecyl sulfate, SDS). Reproduced with permission from reference.¹¹¹ Copyright 2015 American Chemical Society. (c) The dispersed particle concentration C increases monotonically with the concentration of surfactant sodium cholate (C_{sc}), initial concentration of unexfoliated bulk materials (C_I), and sonication time (t_{sonic}). Reproduced with permission from reference.¹¹³ Copyright 2011 Wiley-VCH. (d) The surface tension of sodium cholate (SC) and sodium deoxycholate (SDC) solutions decreases with surfactant concentration until reaching the critical micelle concentration (CMC). Reproduced with permission from reference.¹¹⁴ Copyright 2016 Wiley-VCH.

Among various types of surfactants, facial amphiphiles with a quasi-flat molecular structure (e.g. sodium cholate (SC) and sodium deoxycholate (SDC)) are particularly effective for dispersing 2D materials.¹¹⁵ When SC surfactants and 2D materials interact in water, the surfactant molecules are adsorbed onto the surface of the 2D flakes, leading to the formation of temporary charge. This can balance the aggregation forces (e.g., van der Waals force), and hence facilitate

the dispersing or exfoliating processes.¹¹⁵ The induced charge of exfoliated 2D sheets can enhance electrostatic repulsion which further prevents reaggregation.¹¹⁶ Smith et al. systematically investigated the SC in stabilizing aqueous dispersions of WS₂, MoTe₂, MoSe₂, NbSe₂, TaSe₂, and h-BN nanosheets.¹¹³ As shown in **Figure 6c**, it was found that the dispersed concentration increased monotonically with surfactant concentration (C_{sc}), initial concentration of unexfoliated bulk materials (C_I), and sonication time (C_{Sonic}). It is worth mentioning that if surfactant concentration is above critical micelle concentration (CMC), the excess addition of surfactant would not continuously improve the concentration of 2DMs as the surfactant molecules will spontaneously arrange into micelles. The CMC values of surfactants can be easily determined by measuring interfacial tension with surfactant concentration (**Figure 6d**).¹¹⁴ Below CMC, further addition of the surfactant causes a considerable decrease in the surface tension as the surfactant molecules assemble at the solution-particle or solution-air interface. It is also worth noting that the addition of co-surfactant, such as tetrahydrofuran and pentanol, may increase the CMC such that surfactant needs to reach higher concentration to form micelles.¹¹⁷ This co-solvent strategy could be valuable for preparing highly concentrated 2DM dispersion, though a systematic study on co-solvent effect and corresponding mechanism for printing processes has not been conducted so far.

In addition to surfactants, other additives (normally <5 wt%) may be used to modify or tailor specific properties of ink systems. Examples of 2D nanomaterials with corresponding ink formulations were shown in **Table 2**. A recent work also demonstrated that the use of ionic liquid electrolyte can reduce the overall fabrication cost of solar cells by avoiding one extra cell sealing step in the conventional solar cell sealing process.¹¹⁸ In addition, various types of polymers have been added during ink formulation, such as sodium carboxymethylcellulose (Na-CMC), polyvinylpyrrolidone, and ethyl cellulose.^{119, 120} The polymers can attach onto or encapsulate the 2D material flakes, and hence provide a physical separation between the flakes to allow enhanced exfoliation and stabilization.¹²¹ Liang *et al.* demonstrated the addition of ethyl cellulose in ethanol

for exfoliation and stabilization of graphene flakes using this strategy.¹²² The authors suggested that the ethyl cellulose worked as a colloidal stabilizer and prevented the graphene flakes from aggregation.¹²² Additives may also be selected to modify certain functionalities. For instance, defoaming agents (e.g. short-chain alcohols) may be used to suppress undesired bubble formation during the printing of aqueous inks. Alkalis can be added into inks to carefully adjust pH value to improve the solubility of polymer binders (e.g., ethyl cellulose). In fact, the binders can be either polymers (e.g., cellulose and its derivatives) or inorganic precursors (e.g., chalcogenidometallate).^{21, 123} Binders can form an integral part of formulated inks, connecting the nanomaterials to each other and/or to the substrate. Such binding process can occur by simply drying and solidifying during solvent evaporation, while sometimes curing processes (e.g. thermal annealing or exposure to UV light) are required in order to form cross-linked structures. The appropriate choice of binders can improve certain property and performance of the printed devices, such as mechanical strength or stability/durability against hazard conditions. For example, hydrophobic polymers can promote the resistance of printed composite to moisture.²¹

Table 2: Examples of 2D nanomaterials with corresponding ink formulations and printed device applications. *The ink formulation includes the main solvents and applicable additives in parentheses.

| | Synthesis | Ink formulation* | Printed device applications |
|---|--------------------|---------------------------------------|---|
| MoS ₂ | Liquid exfoliation | Terpineol/ethanol (Ethyl cellulose) | Inkjet inks for FETs ¹²⁴ |
| WS ₂ | Liquid exfoliation | Propylene glycol/water (Triton X-100) | Inkjet inks for photodetectors ¹²⁵ |
| SnS ₂ | Liquid exfoliation | Ethanol | Inkjet inks for gas sensors ¹²⁶ |
| Black phosphorus | Liquid exfoliation | Acetonitrile | Inkjet inks for humidity sensors ¹²⁷ |
| MXene | Selective etching | Water | Direct ink writing for supercapacitors ¹²⁸ |
| Bi ₂ Te _{2.8} Se _{0.2} | Solvothermal | Terpineol (Disperbyk-110) | Screen-printing inks for thermoelectrics ¹²⁹ |
| Bi ₂ Te _{2.7} Se _{0.3} | Solvothermal | Ethanol/glycol/glycerol | Aerosol jet inks for thermoelectrics ¹³⁰ |

| | | | |
|-----------------|------------------------------------|-------------------------------------|--|
| h-Boron nitride | Liquid exfoliation | Water (Na-CMC) | Inkjet inks for dielectrics ¹³¹ |
| Gr | Liquid exfoliation | IPA (PVP) | Inkjet inks for humidity sensors ¹³² |
| Gr | Commercial Gr ¹³³ | Water/IPA (Na-CMC) | Flexographic inks for solar cells ¹³³ |
| Gr | Liquid exfoliation | Terpineol/ethanol (Ethyl cellulose) | Gravure inks for conductive devices ¹³⁴ |
| Gr | Commercial Gr ¹³⁵ | Ethanol (PANI) | Screen printing inks for supercapacitors ¹³⁵ |
| GO | Hummers' method | Water | Direct ink writing for batteries ¹³⁶ |
| rGO | Hummers' method, NaBH ₄ | Water/Ethanol | Gravure printing inks for functional substrates ¹³⁷ |

3.2. Ink rheology of 2D nanomaterials

The rheological properties of the nanomaterial-based inks (*e.g.* viscosity and elasticity) can significantly affect the printing consistency and performance. The viscosity of inks describes the resistance to flow at a certain shear due to internal friction, and is defined as the ratio of the shear stress to shear rate.¹³⁸ Ink viscosity is a crucial factor for most printing techniques. For example, inkjet printing generally requires low viscosity of 2D material dispersion, whereas viscous yet fluent inks are preferred for screen printing. **Figure 7a** shows the common range of viscosities for 2D and 3D printing of 2DMs. A higher viscosity means that the fluid is more difficult to flow and is more resistant to stress. A typical fluid can be categorized into Newtonian fluids or non-Newtonian fluids. A Newtonian fluid is a fluid with a linear shear stress/shear rate relationship, *i.e.* a constant viscosity. However, the dispersion of 2D materials commonly shows reduced shear stress under increased shear rate, which is known as shear thinning. Yang et al.¹³⁹ investigated the shear-induced properties of aqueous dispersions of GO nanosheets. As shown in **Figure 7b**, the authors found strong shear-thinning behaviour of GO which showed a yield stress for all concentrations. Holmqvist et al. reported that 2D gibbsite suspensions showed the same shear-thinning behavior.¹⁴⁰ Such effect of 2D materials is caused by the alignment of ordered structures along the shear direction. These shear-thinning fluids were also termed as pseudoplastic fluids, enabling the ink to flow with less resistance force at higher shear rates. The pseudoplastic

behaviour is important for ink formulation, as in this case the ink particles are more readily dispersed under stress due to better shear-driven mixing. For example, the pseudoplastic nature allows the ink to smoothly flow during the printing process by transferring from component to component and from roll to roll (high shear rate), but is prevented from overspreading once being printed onto the substrates (low shear rate).¹⁴¹ For 3D printing of polymers, shear thinning limits the entanglement of polymer chains, allowing smooth extrusion of viscous inks, such as biological hydrogels, through the nozzle. Owing to these benefits, many researchers have tried to enhance the shear thinning properties of bioinks.¹⁴²

As opposed to pseudoplastic fluid, a dilatant fluid shows increased viscosity under shear. A dilatant fluid is usually highly concentrated suspensions in a colloidal form. On the other hand, Bingham fluids exhibit yield stress, such that the fluids need to overcome this finite stress to flow. A Bingham fluid may behave as Bingham plastic of which the viscosity is constant upon stress, or Bingham pseudoplastic of which the viscosity decreases under stress. The rheology behaviors of these non-Newtonian fluids were summarized in **Figure 7c**.

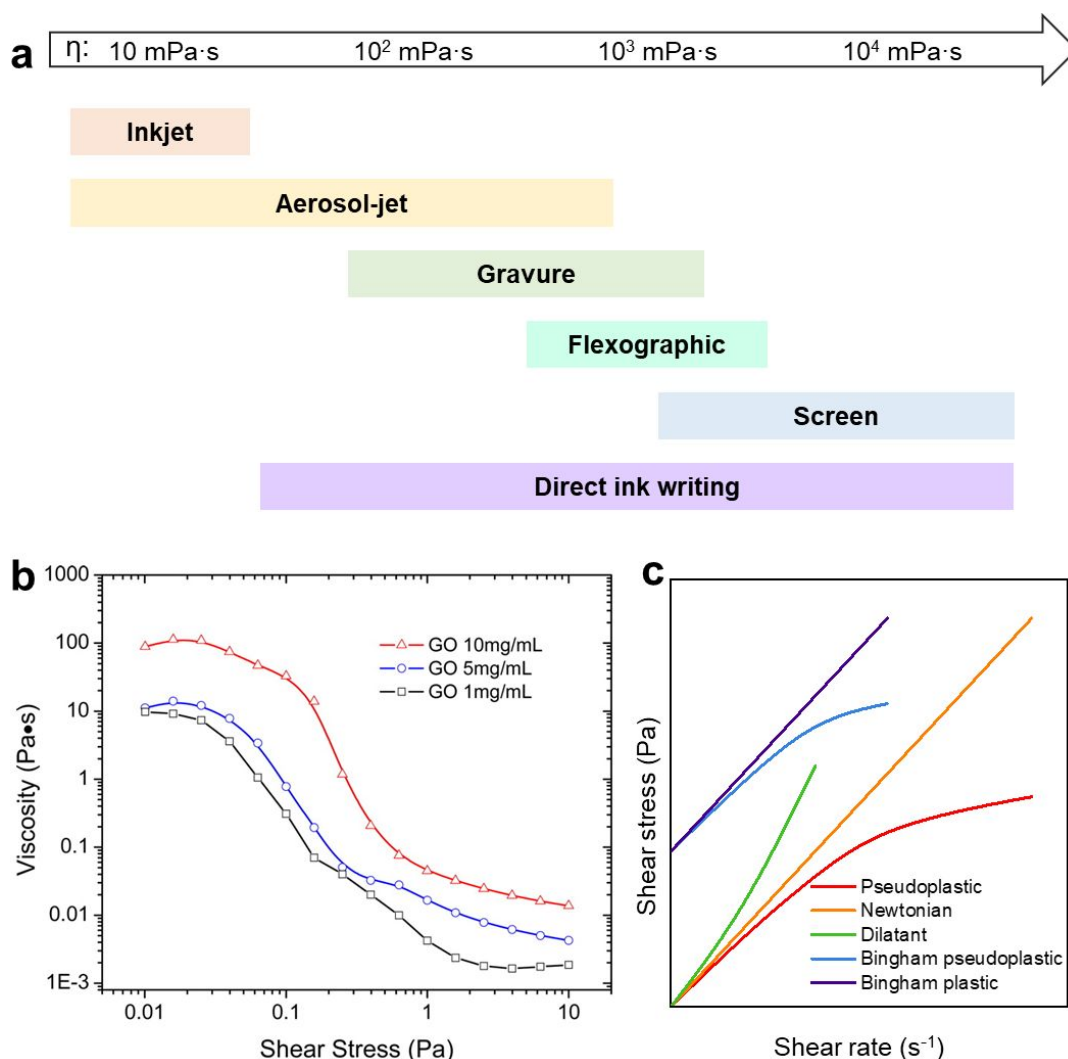


Figure 7. (a) Typical viscosity range of function inks for different printing technologies. (b) Shear thinning behaviour of GO nanosheets. Reproduced with permission from reference.¹³⁹ Copyright 2013 American Chemical Society. (c) Newtonian and non-Newtonian fluids with shear stress as a function of shear rate.

3.3. Ink drying and particle assembly

The interaction of ink droplets on the substrate after deposition is another essential step during printing. Depending on the droplet velocity and material properties, the droplet may splash or keep its shape after deposition. The spreading of ink over a solid surface is determined by the wettability of substrates toward inks.¹⁴³ In general, a good wetting of ink on substrate results in a small contact angle ($\ll 90^\circ$), while a large contact angle ($\gg 90^\circ$) indicates a poor wetting (**Figure**

8a). For instance, contact angle of 0° indicates superwetting and spreading, while 180° shows a perfect non-wetting case. A good wetting means that the ink is capable of spreading over and maintaining contact with the solid surface for a continuous feature, in which the interfacial tension between substrate and inks is much smaller than that of substrate and air or that of ink and air. Therefore, for aqueous inks, hydrophilic substrates (e.g. glass) with low interfacial energies for water are easy to wet, while hydrophobic polymers (e.g. polytetrafluoroethylene) are relatively difficult to wet.^{22, 144} In the case of poor wetting, the printed ink tends to retract and bead up due to the high interfacial tension, leading to a discontinuous material deposition. To change the wetting of substrates, several strategies including surface modification, polymer coating, and plasma etching have been developed.^{22, 28, 145-147} For example, to address the poor wetting of PDMS, Trantidou et al. proposed a two-step method of the deposition of polyvinyl alcohol after the plasma treatment.¹⁴⁸ The PDMS with a hydrophilic surface was achieved and remained stable in air for 9 days (**Figure 8b**).

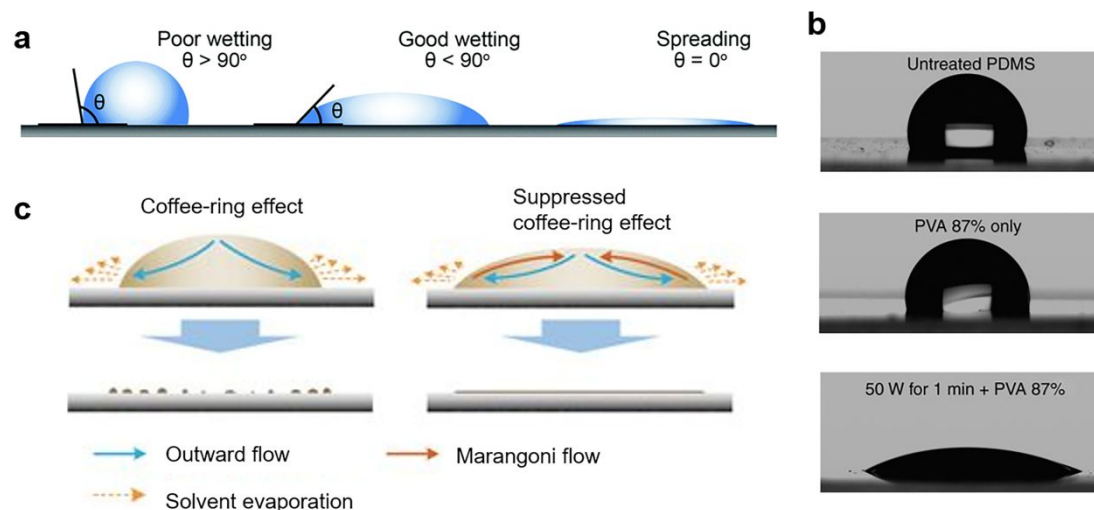


Figure 8. (a) The ink-substrate interaction showing poor wetting (left), good wetting (middle), and spreading behaviour (right). Reproduced with permission from reference.²¹ Copyright 2018 Royal Society of Chemistry. (b) An example of surface modification of PDMS. The plasma etching followed by PVA treatment allows for hydrophilic coating of PDMS for a long period of time. Reprinted by permission from Springer Nature.¹⁴⁸ Copyright 2017 Nature Publishing Group.

(c) Coffee ring effect (left) and suppressed coffee-ring effect (right) by Marangoni flow. Reprinted by permission from Springer Nature.¹⁴⁹ Copyright 2017 Nature Publishing Group.

Although the good wetting and spreading can improve the continuity of printed film, the over spreading of inks on substrates tends to increase drop size, which limits the printing resolution for most nozzle-based printing processes.^{150, 151} To overcome this challenge, several strategies based on surface modification of substrates have been developed. For example, Siringhaus et al. demonstrated that the surface patterning of substrates can greatly improve the printing resolution of inkjet-printed polymer transistors.¹⁵² Alteration of the surface charge can enhance the printing resolution.¹⁵³ The surface alteration can be used for printing dots or lines on 2D substrates. Also, correct amount of drop overlap is beneficial and interaction between the droplets can be important factors for precisely printing micro-lines of different sizes. For inkjet printing of biomaterials (such as tissue), the interfacial energy is vital for drop interactions, and printed bio-inks should be stable enough to keep their shape prior to solidification.¹⁵⁴ For nozzle-based 3D printing, surface modification methods may not be feasible as ink droplets are collected on top of each other, making interactions between drops even more significant than generating 2D structures with droplet overlap.^{151, 155}

During ink drying, the coffee ring effect is a common and unwanted phenomenon.¹⁵⁶ Such effect can be attributed to a non-uniform solvent evaporation across the droplet during the ink drying process. **Figure 8c** shows a droplet deposited onto a substrate, where the evaporation of the solvent occurs.¹⁴⁹ During drying processes, the solvent evaporation speed is typically highest at the edge of printed drops due to the highest surface area to volume ratio. Such uneven evaporation of the solvent results in an outward convection flow that moves from the droplet centre to the edges to replenish the evaporated solvents.¹⁵⁶ During the outward flow, the dispersed nanomaterials are carried and deposited at the droplet edges, leaving little to no material at the droplet centre. To mitigate the coffee-ring effect, significant efforts have been made. For example, Song's group reported a kinetics-controlled deposition mechanism to overcome coffee-ring

effect.¹⁵⁷ It was found that higher temperature enabled surface capture effect and thus uniform particle deposition. In addition to elevated temperature, introducing co-solvent with different boiling point can also help reduce coffee-ring effect. In preparation of BP-based inks, Hu et al. included 10 vol% 2-butanol (boiling point 100 °C) to induce a recirculating Marangoni flow that compensates the strong capillary outflow.¹⁴⁹ Therefore, reduced coffee-ring effect was observed and an improved printing resolution was achieved.

Overall, considering the rapid development of printing processes and vast chemical diversity of 2D materials, much more research will be needed to realize molecular-level understanding and control of colloidal behavior of 2DMs in inks that would benefit the design of printing processes.

4. Printing strategies

The use of printing originates from ancient China where replaceable/moveable wooden or ceramic letterpress was used for letter reproduction. Nowadays, the ability of printing for efficient conversion of materials into devices has been considered as one of the most promising solutions for rapid prototyping and advanced manufacturing. In the past decades, a large number of new printing strategies based on nanomaterials, including metals, semiconductors, and insulators, have emerged for a wide variety of applications.^{20, 158} Based on the dimensionality of printing processes, additive printing of nanomaterials can be mainly categorised into three types: 2D printing, 3D printing, and 4D printing. Several factors, such as printing mechanisms, dispensing pressure, printing speed, nozzle diameter, stage temperature, are crucial for successful printing of 2D materials. In this section, we will discuss the printing strategies of colloidal nanomaterials (particularly 2DMs) and critically evaluate their performances in these three kinds of printing processes. Some common examples of 2D printing, 3D printing, and 4D printing methods and their features and applications were shown in **Table 3**.

Table 3: Common examples of colloidal ink printing methods, their printing dimensionality, capabilities and features, and application examples. *The viscosity data are collected from references [20-22] and [158-171]. **The viscosity of ink filament for fused deposition modelling (FDM) is highly dependent on the fusing temperature and the nature of filament polymers.¹⁵⁹ ***The direct ink writing (DIW) method also includes the microextrusion-based bioprinting, with higher-viscosity inks for constructing structural materials and lower-viscosity inks to provide a suitable environment for maintaining cell viability and function.¹⁵⁸

| Printing methods | Dimensionality | Capabilities & Features | Ink viscosity* (mPa·s) | Application examples |
|------------------|----------------|---|-------------------------------------|--|
| Screen | 2D | Tolerate high viscosity, high particle load | 1000–10000 | Flexible electronics, ¹⁶⁰ Electrocatalysis ¹⁶¹ |
| Flexographic | 2D | Good uniformity and low production cost | 1000-2000 | Solar cells ¹³³ |
| Gravure | 2D | High throughput, thickness control | 100–1000 | Acetone sensor, ¹⁶² conductive pattern. ¹³⁴ |
| Aerosol jet | 2D/3D | High resolution, expanded material types | 1-1000 | Thermoelectrics, ¹⁶³ Stretchable interconnects ¹⁶⁴ |
| Inkjet | 2D/3D/4D | High accuracy and Uniformity; good spatial resolution | 1-50 | FETs, ¹⁶⁵ photodetector, ¹²⁵ strain probe, ¹⁶⁶ All-solid-state supercapacitor, ¹⁶⁷ Shape-changing soft actuators. ¹⁶⁸ |
| FDM | 3D/4D | Good for polymer-particle composite | 10 ⁵ -10 ⁷ ** | Flexible circuits, ¹⁶⁹ Shape memory composite ¹⁷⁰ |
| DIW | 3D/4D | Easy to print, low cost | 30-10 ⁷ *** | Lithium ion batteries; ¹³⁶ Soft robotics ¹⁷¹ |

4.1. 2D printing

Template-based and nozzle-based printing are probably two most studied methodologies for 2D printing of 2DMs. As examples of nozzle-based printing, inkjet printing and aerosol jet printing are non-contact, high-resolution, mask-less patterning technology, while common template-based printing including gravure printing, flexographic printing, and screen printing is particularly advantageous in low-cost and large-scale manufacturing.

Inkjet printing techniques are regarded as a versatile manufacturing tool *via* pushing the ink to form discrete droplets from a nozzle. As shown in **Figure 9a**, a thermal inkjet printer uses a thin-film heater to heat a thin layer of fluid, producing a vapor bubble in a few microseconds, which ejects a liquid drop.¹⁷² During printing, the initial actuation pressure of thermal inkjet printer is close to the saturated vapor pressure of the solvent at the superheat limit.¹⁷³ Piezoelectric inkjet printing process is another popular type of inkjet printing, which is based on the mechanical force of piezoelectric units to create pulses for droplet formation.¹⁷⁴ Nozzles of inkjet printing are typically in the size of 10–30 μm in diameter, while droplet volume is normally in the range of 1–20 pL.

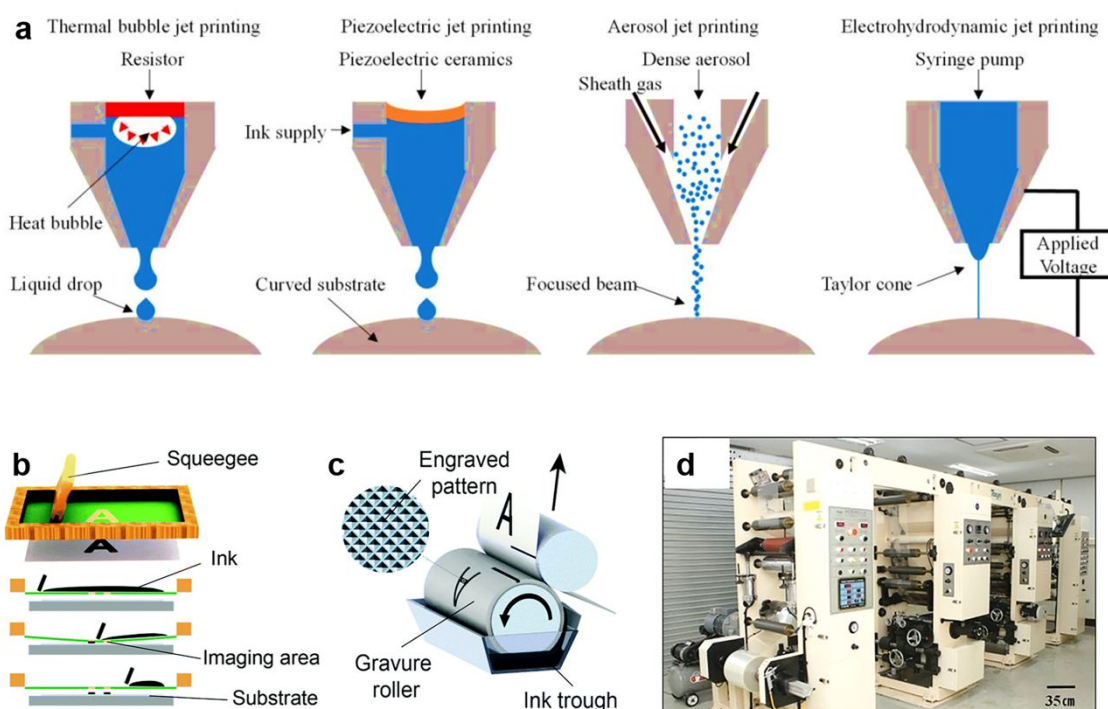


Figure 9. (a) Schematic illustration of various nozzle-based printing technologies. Reproduced with permission from reference.¹⁷² Copyright 2019 The Royal Society of Chemistry. (b) Schematic illustration of screen-printing of inks on substrates. (c) Schematic figure showing working principles of gravure printing. Reproduced with permission from reference.²¹ Copyright 2018 The Royal Society of Chemistry. (d) Photo of commercial gravure printer for printing electrodes on plastic foils. Reproduced with permission from IEEE.¹⁷⁵ Copyright 2010 IEEE.

To ensure smooth inkjet printing of colloidal nanoparticles, the size of 2DMs should be no more than 2% of the nozzle diameter to avoid nozzle clogging.¹⁷⁶ For example, small-sized WS₂ and h-BN particles can be directly used for inkjet printing in a low-cost and scalable manner.¹⁶⁵ In addition to particle size, inkjet printing requires relatively low ink viscosity (normally <50 mPa·s), which limits the types of polymer additives for ink formulation.^{177, 178} One common option is ethyl cellulose which can behave as colloidal stabilizer for 2D sheets.¹⁷⁷ The polymeric binders may be removed by thermal sintering or photonic sintering.^{177, 179} These post-printing treatments, although very effective, may lead to additional cost, and more importantly, can limit the choices of substrates due to the temperature intolerance.

The aerosol jet printing uses the aerodynamic focusing of aerosolized droplets to reliably transfer inks to surfaces.¹⁸⁰ This approach starts with aerosolizing inks using sonication force or shear pressure, forming aerosolized droplets with size of 2–5 microns (**Figure 9a**). Then, nitrogen was used as carrier gas to transport aerosol cloud to a printhead, where a co-flowing sheath gas focuses the droplets to a 10–100 μm-diameter jet with a velocity of ~80 m/s. One striking advantage of aerosol jet printing lies on its flexibility, as it can tolerate wide viscosity range from 1 mPa·s to around 1000 mPa·s, far beyond the range of conventional inkjet printing systems (5–50 mPa·s). Aerosol jet printing techniques have emerged as a powerful tool in electronics manufacturing.¹⁸¹ Up to date, a variety of materials, including nanoparticles, polymers, and biomaterials, are printable by aerosol jet printing onto various substrates such as glass, polyimide, silicon, and PDMS.¹⁸¹⁻¹⁸⁵ It is worth noting that the aerosol jet print head can work relatively far from the substrates such that aerosol jet printing is capable of printing on a curved surface. With appropriate design of printing model and precise modulation of printing parameters, the conformal printing of nanomaterials on 3D curved substrates can be readily achieved with reliable quality.

Screen printing is a template-based process whereby ink is transferred onto the substrate through a stencil screen made of a fine, porous mesh of fabric, silk, synthetic fibres or metal

threads. As shown in **Figure 9b**, the pores of the mesh are selectively blocked (typically using photo-polymerised resins) in the non-printing areas, whereas the remaining pores are kept exposed to allow ink to flow through.¹⁸⁶ Screen-printing ink formulations typically include polymeric binders due to the requirement of high ink viscosities. Several polymer binders show satisfactory performances for screen printing applications, including ethyl cellulose, polyaniline (PANI),¹⁸⁷ and PVP/polyvinyl alcohol (PVA).¹⁶⁰ Screen printing of 2D nanomaterials have attracted recent attention due to the ability to process high concentration of 2DMs. For example, Zhang *et al.* developed a rGO-based ink using ethyl cellulose as the polymer binder.¹⁸⁸ Owing to the good conductivity of 2D rGO, such 2DM-based ink was used to fabricate counter-electrodes of dye-sensitized solar cells.¹⁸⁸ However, high-temperature annealing was required to effectively remove organic binders from the rGO composite, which undermined the attachment of rGO on substrates. Although graphene has typically been the most studied 2D nanomaterial, other 2DMs, such as MoS₂¹⁶¹ and h-BN,¹⁸⁹ have also been reported recently.

As a large-scale commercial technology, high-speed roll-to-roll (R2R) printing (e.g., gravure and flexographic) has been extensively used to fabricate labels, smart packaging, and organic light-emitting diode.^{190, 191} For R2R gravure printing (**Figure 9c**), a predesigned pattern is first scratched on plastic/metal cylinders that are then used to print the pattern on substrates. Such procedure may be repeated several times to print multiple layers of functional inks which is important for high-throughput continuous operation (**Figure 9d**).¹⁷⁵ In 2014, Secor *et al.* reported a gravure printing of graphene for the fabrication of conductive pattern.¹³⁴ The graphene was prepared by liquid phase exfoliation (LPE) and then transferred into terpeneol/ethanol system during ink formulation, in which the ethyl cellulose was used to adjust ink properties for smooth gravure printing.¹³⁴ To ensure a high-resolution gravure printing, it was found that the small platelet size of the LPE graphene (~50 nm in diameter with average thickness of ~2 nm) was beneficial. It was demonstrated that a high-resolution (~30 μm) patterning of graphene on Kapton was obtained, leading to the formation of electrically conductive stripes.¹³⁴ Compared with

gravure printing, flexographic printing takes a slightly more complex ink transfer process. To form graphic patterns, soft and flexible relief printing plates are mounted onto a plate cylinder. Ink is first applied to the surface of a screened anilox roller, which is rolled through an ink trough to fill the cells with ink. Unlike gravure printing, the cells of anilox roller are not the graphic-forming part and are used primarily for metering the amount of ink to ensure continuous patterns. Baker *et al.* demonstrated the flexographic printing of graphene in 2014.¹³³ A graphene/sodium carboxymethylcellulose ink was first formulated in water/IPA solutions, and then printed on indium tin oxide (ITO) glasses to prepare counter-electrodes for photovoltaics. The graphene/polymer binder ratio was controlled to suit flexographic printing.¹³³

The various types of 2D printing techniques offer a straightforward, flexible, and cost-effective solution for the fast fabrication of functional devices with satisfactory resolution. Owing to the continuous operation and high printing efficiency, 2D flexographic printing and gravure printing have shown tremendous potential for large-scale manufacturing of electronic circuits and sensors. However, the printing of bulk 3D devices using conventional 2D printing techniques remains a challenge.

4.2. 3D printing

Since its conception from 1980s, three-dimensional printing has gained unprecedented levels of interests from academic community as well as industry, leading to inestimable possibilities for fast prototyping. The 3D printing begins with the formation of a virtual model, followed by the deposition/polymerization of starting materials, and post-treatment of the printed objects. 3D-printing technologies are commonly grouped into following major categories:⁴ (1) material jetting (e.g. inkjet printing), (2) extrusion/micro-extrusion (e.g. direct ink writing), (3) photopolymerization, (4) powder-bed fusion, and (5) lamination. Herein, we will only discuss mostly used methods for additive 3D printing of colloidal 2D materials, which are (1) and (2). Comprehensive review of 3D printing can be found in other recent literatures.^{7, 151}

Direct ink writing (DIW) and inkjet printing are arguably two most prevalent strategies for 3D printing of colloidal nanoparticles because of its straightforward procedure, cost effectiveness, flexible choice of materials, and ability to construct highly sophisticated 3D structures without additional masking requirements.⁵ After being extruded under an external pressure (**Figure 10a**) or ejected in form of droplets by nozzles (**Figure 10b**), the inks solidify to form 3D objects either through gelation, phase transition, or simply solvent evaporation.²⁰ The printing resolution of the direct ink writing is normally determined by the size of printing nozzles, and various predesigned substrates may be used during DIW, such as hemispherical antennas (**Figure 10c**), suggesting broad utility in electronics and optoelectronics.^{192, 193} One striking feature of DIW is the flexibility of printable ink options that include not only shear-thinning nanoparticle dispersions, but also exceedingly viscous hydrogels. Such advantage of DIW allows for an unrivalled freedom of material choices and preparation of suitable inks.^{158, 194, 195} The viscoelastic properties of certain inks have enabled self-supporting structures, such as 3D butterfly design (**Figure 10d**).¹⁹⁴ As early as 2015, García-Tuñón et al.¹⁹⁶ formulated GO inks that possessed good elastic shear modulus to construct self-supporting 3D structures via DIW (**Figure 10e**). After drying and thermal reduction, an ultra-light graphene device was obtained with elastomeric behavior and decent conductivity.

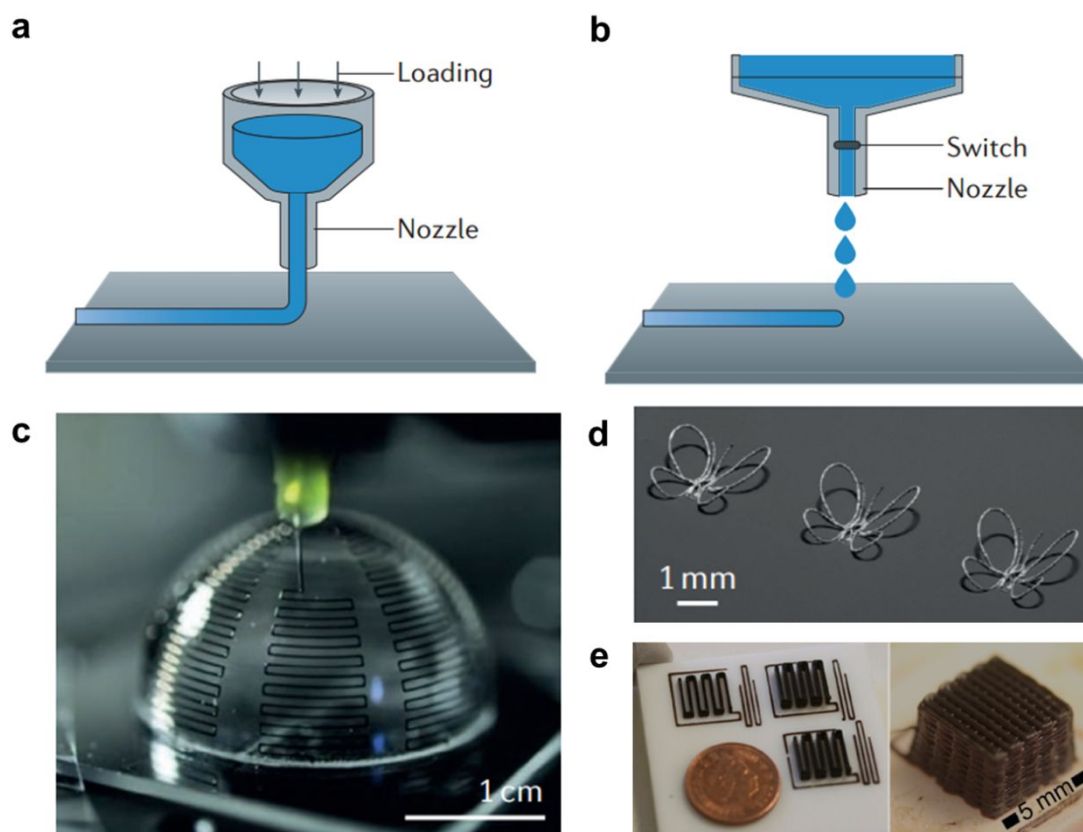


Figure 10. (a) Schematic illustration showing working principle of extrusion-based 3D printing. (b) Schematic of jetting-based 3D printing. Reprinted by permission from Springer Nature.¹⁹⁷ Copyright 2017 Nature Publishing Group. (c) Photo of printed antenna on a hemispherical surface. Reproduced with permission from reference.¹⁹³ Copyright 2011 Wiley-VCH. (d) Self-supported structures by 3D printing. Reprinted by permission from reference.¹⁹⁴ Copyright 2016 National Academy of Sciences. (e) Optical images of 3D printed graphene devices. Reproduced with permission from reference. Copyright 2015 Wiley-VCH.¹⁹⁶

Fused deposition modelling (FDM) is another popular 3D-printing technique that has been commercialized for years.¹⁹⁸ FDM is capable of layer-by-layer constructing complex three-dimensional structures by extruding liquefied plastic or metal filaments, while a nozzle moves along the x, y, and z axes. After extrusion from the nozzle and landing onto the substrate, solidification of inks occurs, which relies on the temperature-induced phase transition of polymers. Despite relatively low resolution and precision, the FDM method still has several advantages

including easy operation and low operating costs.¹⁹⁹ Among various types of polymer filaments, poly(lactic acid) (PLA) and acrylonitrile-butadiene-styrene (ABS) are the two popular choices for FDM. To date, FDM printing of nanocomposites including ABS/graphene,²⁰⁰ PLA/graphene,²⁰¹ and PLA/LFP/carbon²⁰² was reported. In preparation of filaments of PLA/graphene, rGO and polylactic acid were blended at elevated temperature to form composite powders.¹⁶⁹ After the FDM printing, the obtained 2D and 3D flexible circuits showed good mechanical performance. However, it is worth noting that high content of PLA (94 wt%) may lower the electrical conductivity (476 S/m), whereas increasing the concentration of rGO or post-treatment (such as thermal sintering) may mitigate this issue.

As discussed previously, inkjet and aerosol-jet printing are non-contact fabrication techniques that were originally developed for 2D printing. However, these two printing techniques can be redesigned for 3D printing purposes. Owing to their drop-on-demand characteristics, inkjet printing and aerosol jet printing are promising solutions toward rapid and economical deposition of inks on various substrates according to predesigned patterns.²⁰³ In 2017, Panat's group demonstrated highly intricate microscale 3D networks based on aerosol jet printing techniques.¹⁶⁴ Without using any supporting materials, sophisticated nanoarchitectures with nearly fully dense truss elements, including microscaffolds as well as microlattices, were realized. In the past decade, inkjet printing of 3D graphene aerogels or hydrogels has attracted enormous interest and achieved some progresses.²⁰⁴ For instance, Chi et al. reported an inkjet printable graphene/polyaniline (Gr-PANI) composite ink that was prepared by ball milling and ultrasonication.¹⁶⁷ Such 2DM-based ink was printed on freestanding graphene paper to form a three-dimensional hybrid electrode. With good mechanical flexibility, the printed Gr-PANI and gel electrolyte created an all-solid-state symmetric supercapacitor that showed a decent energy density as well as high cycling durability.

Although various types of 2D nanomaterials have been successfully printed in the past decade, the 3D printing of 2DMs has mainly focused on extrusion-based processes (e.g. direct ink

writing and fused deposition modelling). Innovative printing approaches are highly desirable to expand the scope of printable 3D devices and to make full use of 2DMs functionalities, which may lead to the development of intelligent structures that are multifunctional, adaptive, and programmable.

4.3. 4D printing

The ability of some 3D fabricated materials to evolve in a predefined shape, pattern, and structures over time has given rise to a new term called “4D printing”.²⁰⁵ However, not all 3D printing technologies that generate active components such as printed flexible hinges are regarded as 4D printing as they do not exhibit ‘smart’ behaviour such as self-folding, self-actuating and shape changing.²⁰⁶ It has been suggested that some of the distinguishing features of 4D printing involve fabricating a physical object using suitable additive manufacturing techniques, and laying down successive layers of stimuli-responsive materials with varying properties.²⁰⁷ After printing process, the object responds to stimuli from the natural environment or through human intervention, leading to a physical/chemical change of state over time. The 4D printing with shape-morphing features has been considered as a powerful paradigm for designing and fabricating multi-functional hierarchical structures.²⁰⁸

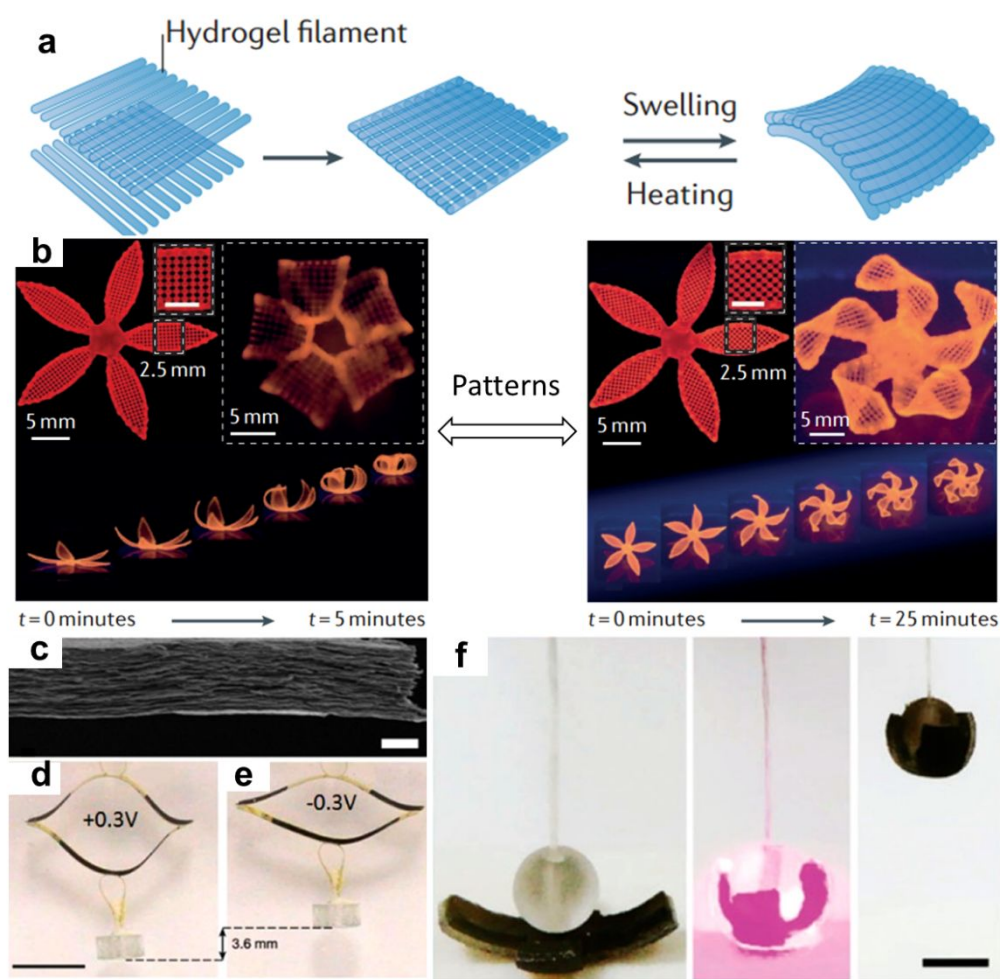


Figure 11. (a) Schematic showing working principle of 4D printing of hydrogel. Upon swelling, the shape of printed hydrogel tends to deform to enable additional control of the final structure. (b) Two hydrogel patterns with flower geometries and different petal patterns. Reprinted by permission from Springer Nature.^{197, 209} Copyright 2016&2017 Nature Publishing Group. (c-e) Dynamic expansion and contraction of MoS₂ electrode. Reprinted by permission from Springer Nature.²¹⁰ Scale bar is 1 cm. Copyright 2017 Nature Publishing Group. (f) Photos of MoS₂ composite hydrogels showing shape deformation and self-wrapping motions under remote control of light or heat. Scale bar is 1 cm. Reprinted by permission from reference.²¹¹ Copyright 2016 The Royal Society of Chemistry.

In the past few years, several research fields have emerged, including shape memory alloys (SMAs),²¹² self-evolving structures,²¹³ soft actuators/robotics,^{168,214} active origami, and controlled sequential folding.²¹⁵ For example, 4D printing of hydrogel was demonstrated based on the swelling ability of composite ink coupled with anisotropic design of printing patterns (**Figure 11a**).^{197, 209} Anisotropic swelling properties of different filament layers induced a controlled deformation and curvature of printed hydrogels. Reversible changes in 3D shapes are feasible with deswelling using external stimuli, such as heat. As shown in **Figure 11b**, several key factors including printed patterns, the swelling ratios, and elastic moduli can be used to tailor the final structural and properties of 4D-printed products. Theoretical mechanics models that expand the classical Timoshenko theory can be useful guidelines for predicting and developing new 4D-printed devices.²¹⁶ In addition, hydrogels are able to be laminated against passive materials for producing a self-evolving joint capable of twisting, curling, and folding upon swelling.^{205, 213}

Owing to the atomically thin structure and ultralow bending stiffness of 2D materials, many of these 2DMs have huge potential for fabricating stimuli-responsive materials, which are the key components for successful 4D printing.²¹⁷ Acerce *et al.* showed that the dynamic expansion and contraction of electrode films prepared by restacking exfoliated metallic MoS₂ nanosheets can produce considerable mechanical forces (**Figure 11c-e**).²¹⁰ MoS₂ electrode films can lift masses that are more than 150 times that of the electrode in the scale of ~cm. Such actuation of MoS₂ film can be attributed to the suitable elastic modulus and good conductivity of the metallic 1T phase. In addition to voltage response, Lei *et al.* reported a MoS₂ composite hydrogel that showed anisotropic actuation with thermo- and photo-responses. In this composite hydrogel, MoS₂ worked as a photothermal transduction component, allowing for remote control of hydrogel actuators (**Figure 11f**).²¹¹ The structural deformation and self-wrapping actions of the hydrogels were demonstrated using light or heat as external stimuli.

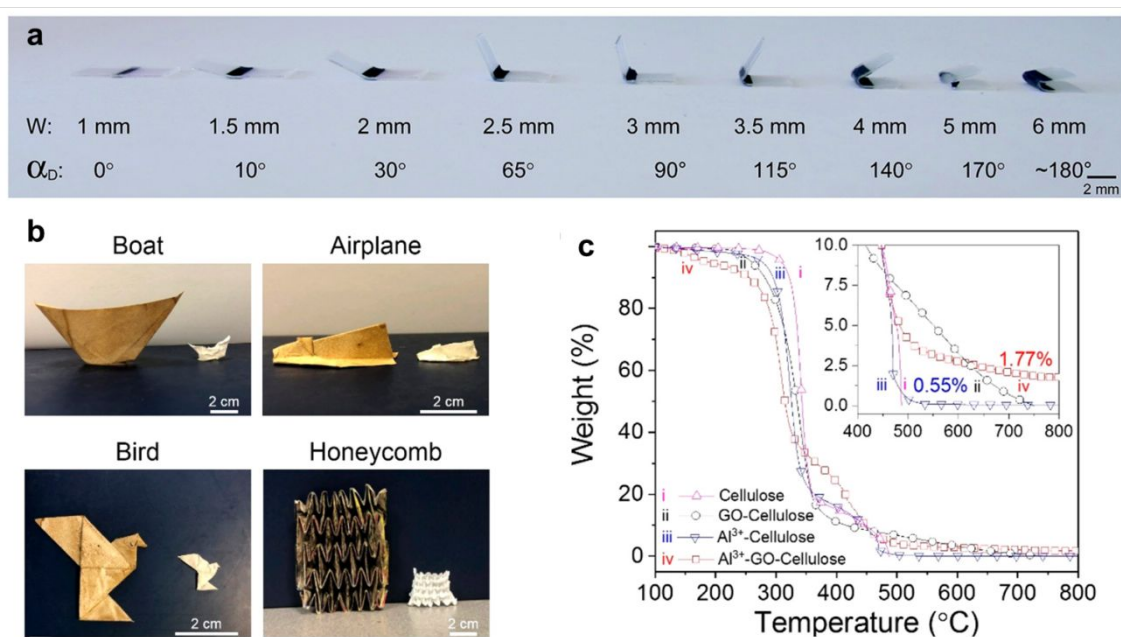


Figure 12. (a) 4D-printed self-folding graphene composite induced by microwave. Reproduced with permission from reference.²¹⁸ Copyright 2015 The Royal Society of Chemistry. (b) Photographic images of various reconfigurable origamis enabled by GO-template inks. (c) The removal of GO template using heat. Reproduced with permission from reference.²¹⁹ Copyright 2019 American Chemical Society.

Duncan et al.²¹⁸ established self-folding of pre-strained polymer films by microwaves (**Figure 12a**). Printed graphene composite films absorbed and converted microwaves energy into heat which causes the polymer to shrink and fold. The dihedral angle is directly proportional to the hinge width printed on the polymer sheet and it is possible to self-fold all the way to 180°. As shown in **Figure 12b**, Yang et al.²¹⁹ showed the transformation of robotic materials from GO/cellulose template to various soft metal oxide (MO) composites. The metalized GO glue enabled the fabrication of complex MO origamis and origami assemblies. After thermal treatment to remove the template (**Figure 12c**), the reproduced MO origamis were further stabilized with thin elastomers, forming composite origamis that can be used as functional backbones of soft robotics. The functionalities of MO backbones can be thoroughly controlled by introducing different metal precursors in the GO/cellulose template. Despite these advances, 4D printing of

2D nanomaterials remains an underexplored avenue for the fabrication of multifunctional, programmable, and smart structures/devices.

5. Device applications of printed 2D nanomaterials

Although significant development of 2DM-based devices has been seen in the past decade, device applications based on additive manufacturing of 2D nanomaterials are only beginning to emerge. This section provides a snapshot of some representative device applications based on 2DM printing, with an emphasis on energy and sensing devices.

5.1. Energy conversion and storage

The generation/storage of electric energy from sustainable sources, such as waste heat, wind and sun light, is one of the pressing challenges for modern society in 21st century.^{220, 221} A great number of energy technologies are emerging as possible solutions for bridging the gaps between global energy supply and demand. Here, thermoelectrics, supercapacitors, batteries, and solar cells are used as a few representative examples to illustrate potential energy applications of additive printing using 2DMs.

5.1.1. Thermoelectrics

When it comes to global energy consumption and supply, sustainable energy is one of the most crucial sources for securing long-term electricity supply. Thermoelectric (TE) materials have gained huge attentions due to the ability to convert waste heat to electric energy.²²²⁻²²⁶ Printing techniques that rapidly transform thermoelectric inks into TE devices with predesigned shapes have great potentials to accelerate practical applications of TE technology.^{227, 228} Up to now, a great variety of TE materials ranging from inorganic nanoparticles (such as Bi_2Te_3 , Sb_2Te_3 , $\text{Bi}_{0.5}\text{Sb}_{1.5}\text{Te}_3$, $\text{Bi}_2\text{Te}_{2.7}\text{Se}_{0.3}$, PbTe , $\text{Ca}_3\text{Co}_4\text{O}_9$, etc.) to organic polymers (such as poly(3,4-ethylenedioxythiophene) polystyrene sulfonate) have been successfully integrated in printing techniques.^{130, 229-232} As printable 2D nanomaterials, few-layer graphene has been reported in inkjet printing processes for fabricating flexible thermoelectric thin films (**Figure 13a-c**).²³³ The

printed graphene films exhibit electrical transport akin to that of few-layer graphene, and glassy thermal transport originated from disordered nanostructures. The thermoelectric power factor of the printed films is determined to be $18.7 \pm 3.3 \mu\text{W m}^{-1} \text{K}^{-2}$. Such inkjet-printed thermoelectric devices confirmed the feasibility of low-cost thermoelectric applications, allowing for the harvest of electric energy from body heat in wearable applications.

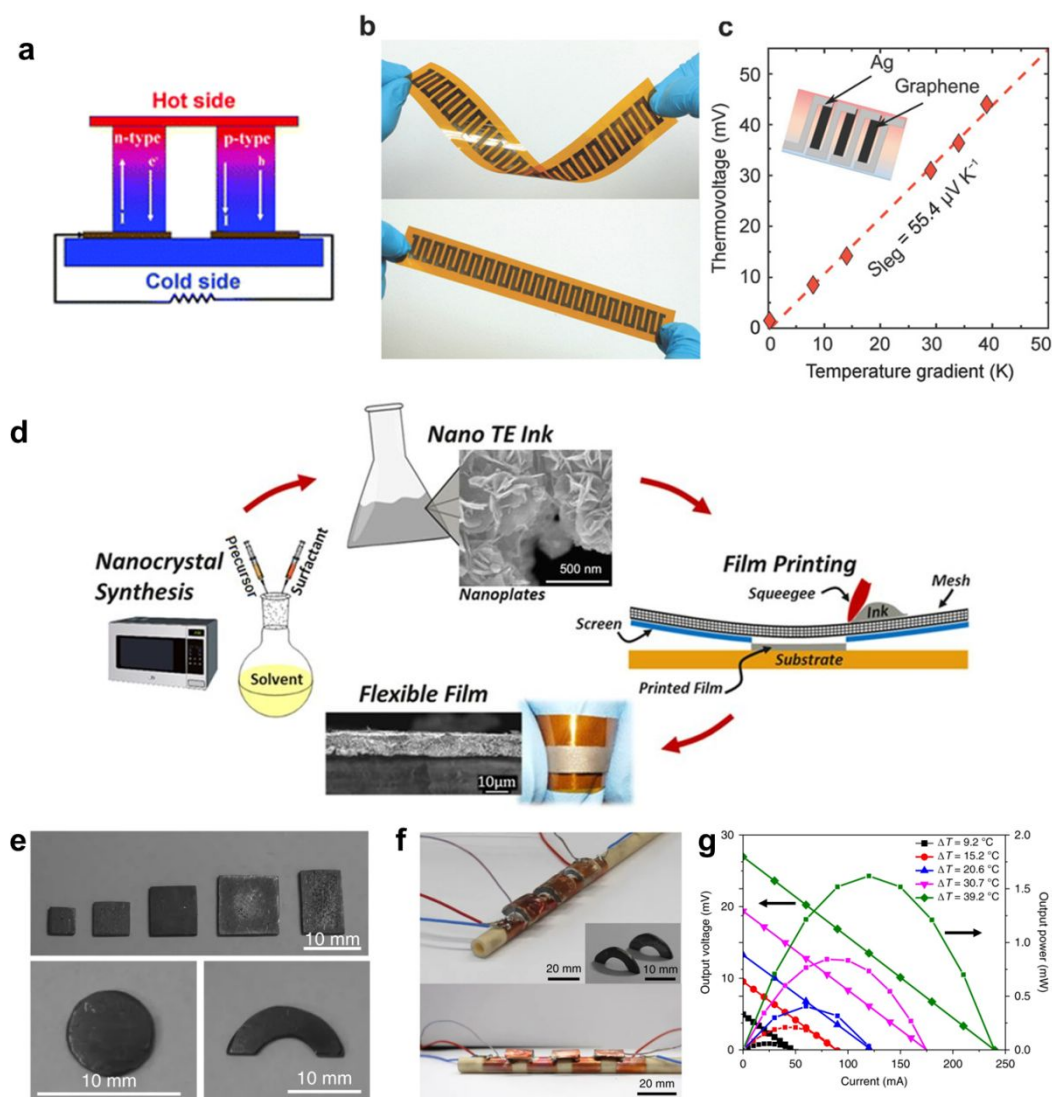


Figure 13. Printable 2D materials for thermoelectric (TE) applications. (a) Schematic demonstration of a thermoelectric device for power generation. Reproduced with permission from reference.²²⁶ Copyright 2009 The Royal Society of Chemistry. (b) Printed flexible TE devices. (c) Voltage output of Ag/graphene devices as a function of temperature gradient.

Reproduced with permission from reference.²³³ Copyright 2018 Wiley-VCH. (d) Screening printing process of flexible TE films using $\text{Bi}_2\text{Te}_{2.8}\text{Se}_{0.2}$ nanoplate ink. Reprinted by permission from Springer Nature.¹²⁹ Copyright 2016 Nature Publishing Group. (e) Photos of the printed TE materials with different shapes. (f) Images of the printed conformal TE devices. (g) Output voltage and power of the printed TE devices. Reprinted by permission from Springer Nature.¹²³ Copyright 2018 Nature Publishing Group.

In addition to graphene, additive printing of other 2D nanomaterials have been reported. For example, Zhang's group demonstrated high-performance flexible films and devices by screen printing bismuth telluride based nanoplate inks synthesized using a microwave-stimulated wet-chemical method (**Figure 13d**).¹²⁹ The films showed an unprecedented peak ZT of 0.43 at 175 °C and superior flexibility with negligible changes of electrical conductivity after 150 bending cycles. A flexible thermoelectric device fabricated using the printed films produces a high-power density of 4.1 mW/cm² under a temperature difference of 60 °C. A high-performance PbTe based flexible film was also demonstrated by Zhang's group by scalable and low-cost printing, with conservative estimate of ZT above 1 at 350 °C.²³⁴ These high-performance and flexible thermoelectric devices present an important step to make thermoelectrics a viable technology for a broad range of applications.

Although significant efforts have been made in printable TE materials, the large-scale applications of printed TE devices remain a challenge due to two main reasons: 1) The electrical conductivity of the printed TE materials is often lower than their single-crystalline bulk counterparts, leading to unsatisfactory output power and low figure-of-merit ZT values; 2) conformal printing of TE devices on different shapes that can fit the geometries of heat sources, such as hot pipelines, remains difficult. To address these issues, Kim et al. proposed a extrusion-based 3D-printing approach to fabricate thermoelectric materials with geometries suitable for heat sources.¹²³ Bi_2Te_3 -based TE materials were integrated with inorganic binders using Sb_2Te_3 chalcogenidometallate during ink formulation. After printing and sintering, various shapes of TE

devices were obtained and readily integrated onto pipeline systems (**Figure 13e-f**). Homogenous thermoelectric performance was observed in 3D-printed materials, of which the ZT values of 0.9 for p-type and 0.6 for n-type were comparable to their bulk counterparts. The TE devices showed a maximum output voltage of 27.0 mV and maximum power of 1.62 mW at a temperature difference of 39 °C (**Figure 13g**). In addition to extrusion-based 3D-printing methods, a 3D conformal aerosol jet printing was demonstrated to deposit solution-processed Bi₂Te_{2.7}Se_{0.3} nanoplate inks onto both 2D planar and 3D curved substrates.²³⁵ Within seconds of photonic sintering process, the electrical conductivity of the printed film was dramatically improved from non-conductive to 2.7×10^4 S/m. A power factor of $730 \mu\text{Wm}^{-1}\text{K}^{-2}$ was achieved for the printed flexible films with good stability after 500 bending cycles.

5.1.2. Supercapacitors

Based on the double-layer effect, supercapacitors enable rapid charging and discharging through the storage and release of electrical energy in a short period of time.^{236, 237} Owing to their large specific surface area, 2D materials have emerged as encouraging candidates for developing high-performance supercapacitors/ultracapacitors.^{14, 238, 239} For example, Pumera's group and Banks' group have applied graphene/PLA into functional electrodes for supercapacitors through fused deposition modelling printing.^{240, 241} In another example, the micro-extrusion 3D printing method was effectively used for the fabrication of rGO-based micro-supercapacitors.²⁴² The printed GO films were first treated with hydrogen iodide (HI), followed by the deposition of PVA-H₂SO₄ gel as the electrolyte. A capacitance of $41.8 \text{ F} \cdot \text{cm}^{-3}$ at $0.06 \text{ A} \cdot \text{cm}^{-3}$ was obtained for the printed micro-supercapacitor. To further improve the capacity of supercapacitors, Jiang et al. fabricated graphene aerogel microlattices with rich hierarchical pores and high electrical conductivity.²⁴³ During the printing process, a facile ion-induced gelation method was demonstrated to directly print aerogel microlattices from GO-based ink (**Figure 14a-c**). Using Ca²⁺ as ionic gelators, aqueous GO solution was transformed into printable gel ink, leading to the

formation of free-standing 3D structures with programmable microlattices at ambient conditions. The gravimetric capacitance (C_g) of supercapacitors is $213 \text{ F}\cdot\text{g}^{-1}$ at $0.5 \text{ A}\cdot\text{g}^{-1}$ and $183 \text{ F}\cdot\text{g}^{-1}$ at $100 \text{ A}\cdot\text{g}^{-1}$, and retains over 90% after 50000 cycles.

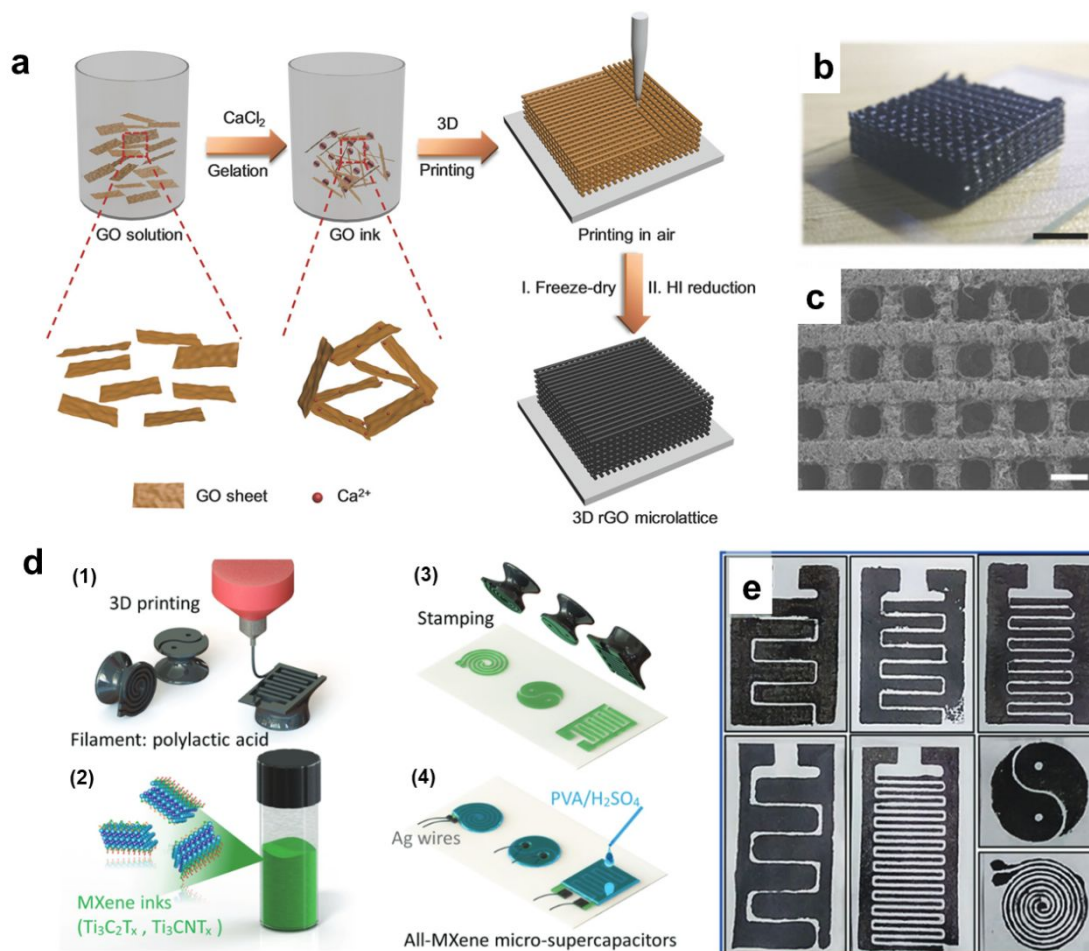


Figure 14. Printable 2D materials for supercapacitors. (a) 3D printing of graphene oxide into supercapacitors. (b) Photographic image of a printed supercapacitor with microscopic porous morphology (c) SEM image of a printed graphene supercapacitor. Scale bars of (b) and (c) are 5 mm and 500 μm , respectively. Reproduced with permission from reference.²⁴³ Copyright 2018 Wiley-VCH. (d) The fabrication of MXene-based supercapacitors by 3D printing and ink transferring using stamps. (e) Photos of several MXene-based supercapacitors. Reproduced with permission from reference.²⁴⁴ Copyright 2018 Wiley-VCH.

In addition to graphene, other conductive 2D materials have also been investigated for fabricating supercapacitors. Recently, Zhang et al. developed a stamping strategy to transform 2D titanium carbide or carbonitride inks into supercapacitors.²⁴⁴ As shown in **Figure 14d**, this process started with stamp fabrication by FDM method using PLA filaments. Next, the 3D-printed stamp was covered with MXene inks ($\text{Ti}_3\text{C}_2\text{T}_x$ or Ti_3CNT_x), and hard-pressed onto flexible substrates to generate all-MXene supercapacitors. Several MXene-based micro-supercapacitors were rapidly manufactured with a wide variety of designs (**Figure 14e**), which showed good cycle life (>10000 cycles) and excellent capability (capacitance retention of 82% at $800 \mu\text{A}\cdot\text{cm}^{-2}$).

5.1.3. Batteries

Supercapacitors are ideal when a rapid charging is desirable to fill a short-term power demand, while batteries are required to supply long-term electric energy. Thanks to the rapid development of printing technologies, direct print of 2D nanomaterials has been increasingly investigated for applications including Li–O₂ batteries,²⁴⁵ Li–S batteries,²⁴⁶ and Na-ion batteries.²⁴⁷ For example, graphene/PLA composites have been used in the rapid manufacturing of 3D printed freestanding anodes for lithium-ion batteries.^{240, 248} In 2016, Hu's group developed a fully 3D-printed lithium-ion battery by additive printing of GO-based inks as well as gel polymer electrolyte (**Figure 15**).¹³⁶ Lithium titanium oxide ($\text{Li}_4\text{Ti}_5\text{O}_{12}$, LTO) and lithium iron phosphate (LiFePO_4 , LFP) were added into anode and cathode materials, respectively. The 3D-printed LTO anode and LFP cathode showed stable cycling performance with specific capacities of $\approx 170 \text{ mA g}^{-1}$ and $\approx 160 \text{ mA}\cdot\text{h}\cdot\text{g}^{-1}$, respectively. A fully 3D-printed cell presented a high electrode mass loading of $18 \text{ mg}\cdot\text{cm}^{-2}$ when normalized to the overall area of the battery. The full cell delivered initial charge and discharge capacities of 117 and $91 \text{ mA}\cdot\text{h}\cdot\text{g}^{-1}$. In 2018, the same group described the use of holey graphene oxide (hGO) for 3D printing of lithium–oxygen battery without the use of additives or binders.²⁴⁵ The 3D printed hGO meshes exhibited hierarchical porosity: nanoscale (4–25 nm holes on hGO), microscale ($\sim 10 \mu\text{m}$ pores introduced by lyophilization), and macroscale ($< 500 \mu\text{m}$ square pores of the mesh). The 3D printed mesh's

multi-level porosities improved active-site utilization as well as mass/ionic transport, leading to enhanced performance of Li–O₂ battery performance in comparison with vacuum filtration method. In order to explore the role of hierarchical porosity, specifically nanoporosity, on electrochemical performance, GO nanosheets without nanoholes were prepared and compared with regards to their performance in battery. The mesh cathodes of hGO outperformed that of conventional GO under the full discharge condition, and showed better cycling depth and stability.

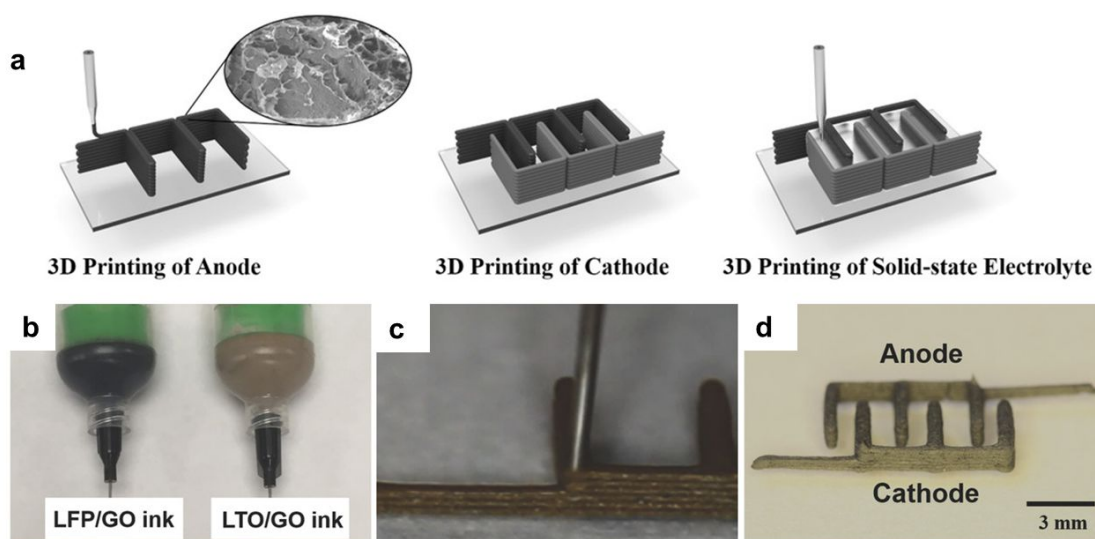


Figure 15. Printable 2D materials for batteries. (a) Schematic illustration of the 3D-printed battery electrodes as well as the electrolyte. (b) Photos of LFP/GO and LTO/GO inks. (c) Digital image displaying the printing process. (d) Optical images of 3D-printed interdigitated electrodes. Reproduced with permission from reference.¹³⁶ Copyright 2016 Wiley-VCH.

5.1.4. Solar cells

Owing to the extraordinary optical and electrical properties, several colloidal nanoparticles (e.g. graphene) have been widely used in various solar cell systems including heterojunction solar cells (HSCs),²⁴⁹ organic solar cells (OSC),²⁵⁰ dye/QDs sensitized solar cells (DSSCs),^{251, 252} and perovskite solar cells (PSCs).²⁵³⁻²⁵⁶ For example, Hashmi et al. developed inkjet infiltrated carbon-based printed perovskite solar cells with high stability and reproducibility.²⁵⁷ As shown in **Figure 16a-e**, the authors demonstrated that the perovskite

precursor ink is highly stable, printable, and controllable, and can directly be used to fabricate porous triple layered printed PSCs with a high overall conversion efficiency of 9.53% without the need of hole transporting materials. Owing to its high conductivity, 2D MXene nanosheets were used in silicon solar cells to form an Ohmic junction with n^+ -Si (**Figure 16f**).²⁵⁸ The metallic feature enabled MXene to effectively extract the photogenerated electrons from the active layer, leading to a decrease in device contact resistance and the suppression of charge carrier recombination. An improved open-circuit voltage and a high short-circuit current density were observed with a maximum power conversion efficiency of 11.5%. Despite that spin/drop coating was used for the majority of the photovoltaic works published in the literature to date, printing techniques have emerged as a promising approach for fast prototyping and scalable manufacturing of solar cells.^{259, 260} A wide range of materials including graphite,²⁵⁷ carbon nanotubes,²⁶¹ and dye molecules²⁶² have been incorporated in the printing of solar cells. In particular, the printing of 2D nanomaterials has been increasingly investigated in the past few years. For example, Hasan group demonstrated the use of graphene ink for fabricating dye-sensitized solar cells.²⁶³ In the fabrication of counter electrodes (CE), graphene ink showed good uniformity and consistency, as shown in **Figure 16g**. The authors also investigated the use of different dyes including natural dye extracts from *Pennisetum glaucum*, *Hibiscus sabdariffa* and *Caesalpinia pulcherrima* as well as the synthetic ruthenium-based dye N719, showing a maximum performance of ~3.0% conversion efficiency (**Figure 16h**). The inkjet-printed graphene electrode provided a cost-effective alternative, which has a material cost of only ~2.7% of the equivalent solution processed Pt-based electrodes. As another example of printed solar cells, MXene/CuSe nanosheets were screen-printed onto graphite sheet to form a counter electrode in quantum dot-sensitized solar cells.²⁶⁴ The authors combined the high electrical conductivity of MXene (Ti_3C_2) and rich active sites of CuSe for polysulfide electrolyte reduction.²⁶⁴ Therefore, such 2D composite CE enabled the photovoltaic device with an improved efficiency of 5.12%, which is higher than that of pristine CuSe CE (3.47%) or pristine Ti_3C_2 CE (2.04%).

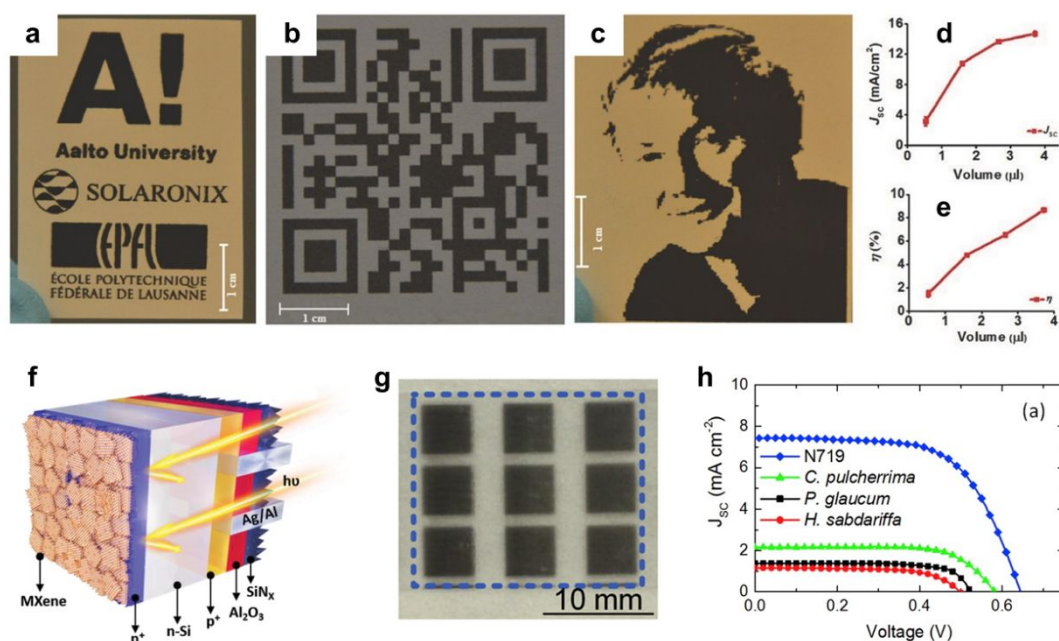


Figure 16. Printable colloidal nanomaterials for solar cells. (a-c) Demonstrations of inkjet-printed patterns using stable perovskite precursor ink, including (a) logos, (b) quick response (QR) code, (c) digital image. (d-e) The short circuit current density (J_{sc}) and efficiency (η) of PSCs by adjusting the volume of printing perovskite precursor ink, leading to the precise tuning of photovoltaic performance. Reproduced with permission from reference.²⁵⁷ Copyright 2011 Wiley-VCH. (f) Schematic illustration of MXene-based silicon solar cells. Reproduced with permission from reference.²⁵⁸ Copyright 2019 Wiley-VCH. (g) Image of printed graphene electrodes showing good printing consistency. (h) Current–Voltage characteristic curves of graphene-based solar cells sensitized with different dyes (Natural tropical dye: extracts from *Pennisetum glaucum*, *Hibiscus sabdariffa* and *Caesalpinia pulcherrima*. Synthetic dye: N719). Reproduced with permission from reference.²⁶³ Copyright 2016 Elsevier B.V.

The printing of 2DM-based inks provides a versatile platform for the design and development of a broad range of devices for energy conversion and storage. With suitable printing methods, these energy devices can be printed on a wide variety of substrates, such as flexible and

transparent films, adjusting the conventional stereotypes of energy conversion and storage using rigid structures. More importantly, the printing technologies enable the energy devices with low dimension, high resolution and short fabrication time, which would serve as power supplies for the development of next-generation wearable electronics and sensors.

5.2. Sensing

The ability of 2DMs to respond to the environment with ultra-high surface sensitivity has been demonstrated as key characteristics for sensing applications. Moreover, 2DMs' exceptional optical/electrical properties, combined with the structural robustness and flexibility, enable these materials to be desired candidates for manufacturing next-generation sensors. Combined with printing technologies, we will highlight recent advances in functional devices for sensing physical, chemical, and biological stimuli/inputs.

5.2.1. Optoelectronic sensor

The fast-expanding market of optoelectronic devices, including photodetectors and UV sensors, calls for innovative production of nanostructures from optoelectronic materials in a low-cost, high-throughput, and large-scale fashion.^{19, 265} Printing is a versatile technology for deposition of ink materials and an emerging tool toward fast prototyping and manufacturing of optoelectronic sensors. As many optoelectronic sensors involve charge transfer or energy transfer processes, the electronic structure of the 2DMs plays an essential role in developing functional optoelectronics based on desired donor–acceptor pair. In particular, the versatility in the band gaps of 2D materials provides enormous opportunities in the field of optoelectronics (**Figure 17a**).

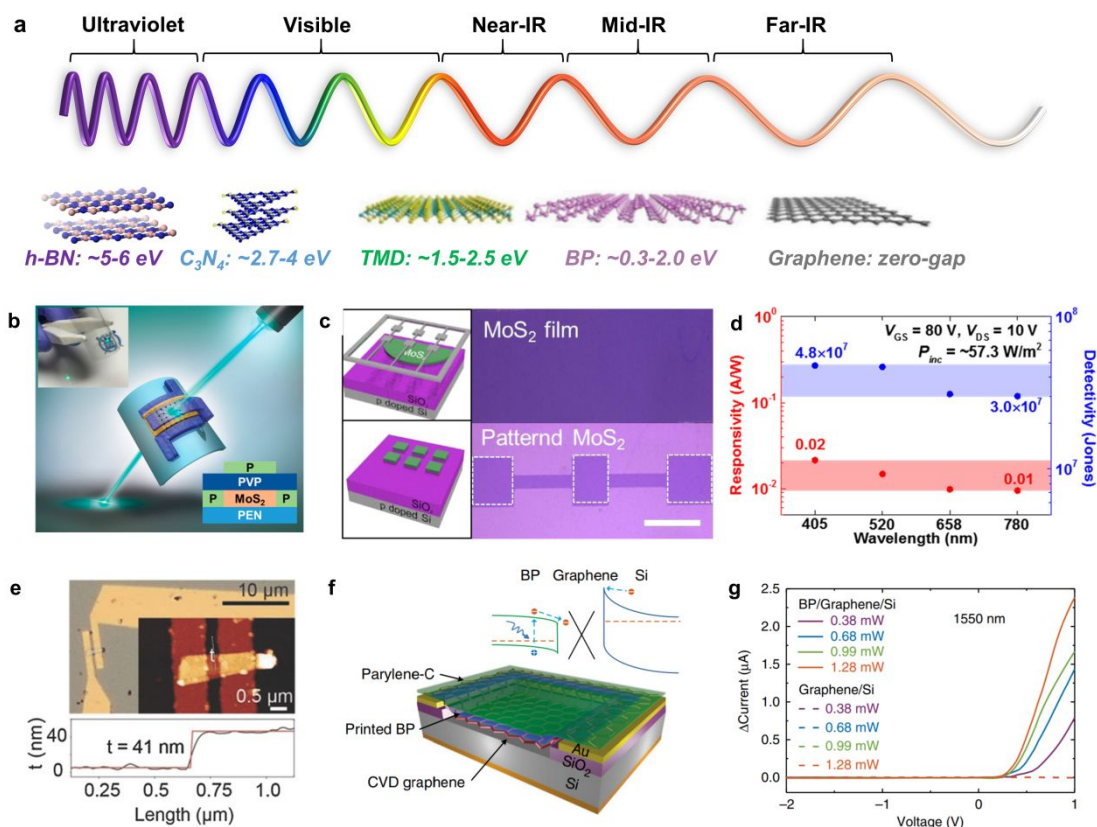


Figure 17. Optoelectronic sensors based on printable 2D nanomaterials. (a) The electromagnetic wave spectrum and the band gap ranges of different 2D nanomaterials. Reproduced with permission from reference.²⁶⁶ Copyright 2017 National Academy of Sciences. (b-d) MoS₂ based phototransistors. Reproduced with permission from reference.²⁶⁷ Copyright 2017 American Chemical Society. (e) In₂Se₃ thin-film photodetectors with thickness of 41 nm. Reproduced with permission from reference.⁴⁰ Copyright 2018 Wiley-VCH. (f) Schematic illustration of printed black phosphorus (BP) photodetector. (g) The BP/Graphene/Si heterostructure showing high photoresponsivity to 1550 nm light. Reprinted by permission from Springer Nature.¹⁴⁹ Copyright 2017 Nature Publishing Group.

Semiconducting TMDs and BP have attracted lots of attentions because of their tunable band gaps as well as atomically thin structures. For example, Kim et al. reported a highly transparent MoS₂ phototransistor arrays on flexible polymer substrates by a drop-on-demand inkjet-printing technique.²⁶⁷ To fabricate the phototransistor arrays, the MoS₂ monolayers were selectively patterned using reactive ion etching system with O₂ plasma (**Figure 17 b-c**), followed

by inkjet printing of electrodes and dielectric layers. As shown in **Figure 17d**, the printed phototransistors showed good responsivity and detectivity in the range of 400 to 800 nm wavelength. In addition to MoS₂, solution-processable indium selenide (InSe) flakes were used to fabricate photodetector with high photo responsivities ($\approx 5 \times 10^7 \text{ A W}^{-1}$) that surpass previously reported solution-processed monolithic semiconductor photodetectors by three orders of magnitude (**Figure 17 e**).⁴⁰ The pristine InSe flakes were prepared by liquid-phase exfoliation in surfactant-free, deoxygenated co-solvent mixtures and the fabricated field-effect transistors by vacuum filtration and electron-beam lithography. Such solution-based process possesses huge potential for the scalable synthesis of InSe and its thin films, which showed excellent responsivity for film-based photodetectors.

Recently, two-dimensional black phosphorus has drawn significant research attentions owing to its unique structural and electrical properties.²⁶⁶ An inkjet-printable BP ink was developed for fabricating hybrid photodetector.¹⁴⁹ As shown in **Figure 17f**, printed BP was combined with graphene/Si Schottky junction to fabricate optoelectronic devices. To avoid possible oxidation or degradation in air, a layer of parylene-C was used to encapsulate the hybrid structure. Under 450 nm light source, a photoresponsivity of up to 164 mA W⁻¹ was observed. Interestingly, owing to the layer-dependent bandgap of BP (0.3–2.0 eV), the device can also respond to 1550 nm light (1.8 mA W⁻¹ photoresponsivity), as showed in **Figure 17g**.

For graphene, MXene and other low band-gap 2DMs, they have also been extensively studied as an electrical contact or a photoactive layer in optoelectronics. In addition, the good solution processability of GO allows the fully inkjet printing for graphene-based photodetectors. Manga *et al.* formulated an ionic solution ink by combining GO nanosheets with titanium bis(ammonium lactate) dihydroxide (TBA), and printed the ink on coplanar graphene-based electrodes, producing a fully inkjet-printed photodetector.²⁶⁸ Heterostructure graphene/WS₂/graphene junction was also utilized for photodetection.¹²⁵ This heterostructure device exhibited a photoresponsivity $>1 \text{ mA W}^{-1}$ (at 514 nm).

5.2.2. Chemical sensor

Recently, graphene, rGO, TMDs, and other 2D nanomaterials are emerging as active constituents for electrochemical sensing due to their superior electrical conductivity, excellent electrochemical properties, and large surface to volume ratios compared to traditional metal oxides and conducting polymers.²⁶⁹⁻²⁷² Printed 2DM chemical sensor was first reported in 2010, where inkjet printing of rGO platelets was achieved using aqueous surfactant-supported dispersions of rGO powder.²⁷³ Despite relatively low electrical conductivity ($\sigma \approx 15 \text{ S cm}^{-1}$), the rGO-based chemical sensor was able to detect chemically aggressive vapours at the parts per billion level using an air sample at room temperature. An increase in electrical conductivity was observed when the rGO sensor was exposed to highly oxidizing vapours, while there was an increase in resistance when it was exposed to organic vapours and reducing species, including hexanes, CH_3OH , and NH_3 . In addition to 2D printed sensors, 3D printing of reduced graphene oxide nanowires was realized to detect the CO_2 concentrations between 0.25% and 5% (**Figure 18a-b**).²⁷⁴ By accurately tuning the printing parameters, the authors fabricated 3D printed rGO wires with complex features, demonstrating controlled deposition direction as well as deposition positions. The 3D printing of 2DM-based nanowires show enormous potential to fabricate components of electrochemical sensing devices such as flexible sensing transducers.²⁷⁴

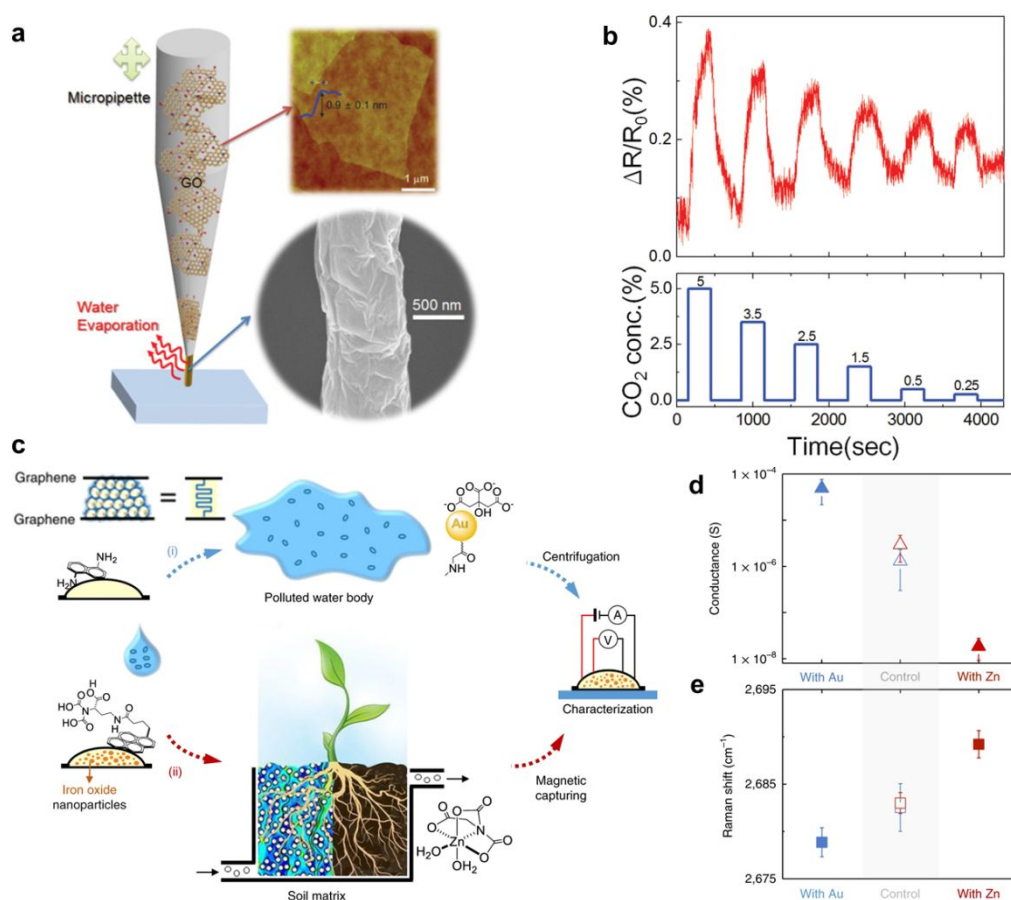


Figure 18. Printable 2D materials for chemical sensors. (a) 3D printing of reduced GO-based wires. (b) rGO nanowires for CO₂ sensing. Reproduced with permission from reference.²⁷⁴ Copyright 2015 Wiley-VCH. (c) Chemical sensors based on microprinted graphene–PS–graphene microparticles. (d) Surface conductance of graphene–PS–graphene microparticle on detecting gold nanoparticles and Zn²⁺. (e) Raman shift of graphene–PS–graphene microparticle on detecting gold nanoparticles and Zn²⁺. Reprinted by permission from Springer Nature.²⁷⁵ Copyright 2018 Nature Publishing Group.

Recently, Strano group integrated micro-printing technique with CVD-grown 2D materials to develop an “auto-perforation” technique that provides a means of spontaneous assembly for surfaces composed of two-dimensional molecular scaffolds.²⁷⁵ This innovative approach was based on controlled crack propagation in CVD-grown 2DM thin films, creating microparticles with a pair of enveloping 2D layers. In their work, the authors showcased a graphene–polystyrene–graphene (G-PS-G) microparticle which was used as a platform to detect

and monitor environmental stimuli. Such G-PS-G microparticles with amine groups can form interaction with gold nanoparticles (**Figure 18c**), and those with nitrilotriacetic acid (NTA) ligands can probe Zn^{2+} ions. Therefore, amine-modified devices revealed a significant increase in the surface conductivity for sensing gold nanoparticles, whereas a huge reduction was witnessed for the NTA-modified particles on Zn^{2+} exposure (**Figure 18d**). Raman shift of printed microsensor was also observed upon these chemical stimuli (**Figure 18e**).

In addition, there is an increasing emphasis on two areas in chemical sensing: 1) real-time monitoring; 2) ultrahigh-sensitivity detection.²⁷⁶ The real-time monitoring commonly relies on non-covalent interactions of 2D nanomaterials that enable a quick response and a fast recovery rate. Such non-covalent interactions, dependent on the type of analytes, include electrostatic force, hydrogen bonding, π - π interaction, and etc. To detect the trace amount of pollutants, strategies based on covalent linkages between analytes and 2D nanomaterials sometimes can be more suitable. As it allows analytes immobilize on the surface and to be stable during the assay, covalent linkages overcome the weakness of the supramolecular forces, particularly for biomolecule systems. The careful engineering of surface chemistry of 2D materials and novel designs enabled by printing techniques would be desirable to realize the next-generation high-performance chemical sensors.

5.2.3. Biosensor

2D materials appear to be a promising carrier platform for biological recognition elements owing to their high surface sensitivity and exceptional electronic property.²⁷⁷⁻²⁷⁹ To monitor glucose levels in the interstitial fluid, Lipani et al.⁹ developed a path-selective, non-invasive, transdermal glucose monitoring system by screen printing of graphene film, as shown in **Figure 19a**. It was suggested that glucose reacted with glucose oxidase to produce hydrogen peroxide, which was detected by the electrochemical sensor. With an increased density of graphene-decorating Pt nanoparticles, the limit of detection was improved to about $0.76 \mu\text{M}$. The authors also performed *in vivo* testing in which the glucose levels of healthy volunteers were monitored

by two of the array's pixel devices, during which lunch and a snack were ingested (**Figure 19b**). The results showed well-matched readout values that provided further confidence in the performance of the array.

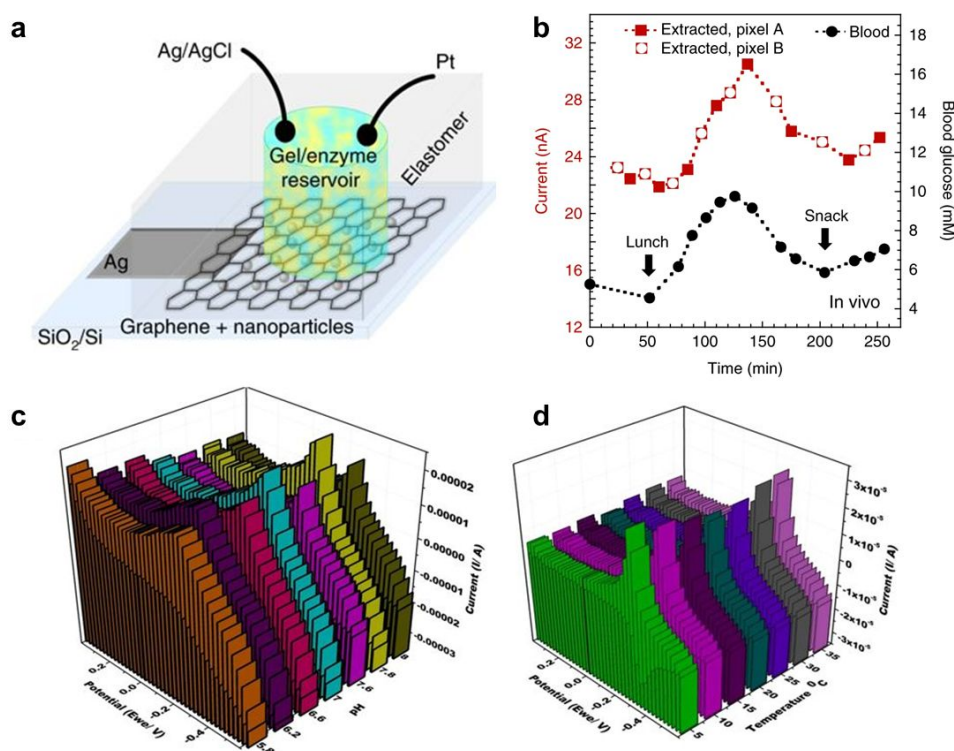


Figure 19. Printable 2D materials for biosensors. (a) Schematic demonstration of glucose sensing devices. A 3D electrochemical cell is formed by contacting the gel with Ag/AgCl (reference) and Pt (counter) electrodes. (b) The *in vivo* testing in which the glucose levels of healthy volunteers were monitored. Reprinted by permission from Springer Nature.⁹ Copyright 2018 Nature Publishing Group. (c-d) MoS₂-based biosensor on detecting the chikungunya virus DNA under the pH effect (c) and temperature effect (d). Reprinted by permission from Springer Nature.²⁸⁰

In addition to graphene, other 2D materials have been extensively investigated for printable biosensors, particularly MoS₂.²⁸¹⁻²⁸³ Recently, Singhal et al. developed a biosensor based on MoS₂ nanosheets for the selective detection of chikungunya virus.²⁸⁰ Owing to MoS₂'s exceptional biocompatibility, good electrochemical activity, and high specific surface, the biosensor exhibited a wide linear range of 0.1 nM to 100 μM towards the chikungunya virus DNA.

The biosensor also showed low limit of detection with 3.4 nM in a 3σ rule. As shown in **Figure 19c-d**, the pH response and temperature effect of the biosensor were studied, showing highest current response at 7.8 pH and 35 °C.

5.2.4. Other sensors

The rapid development of printing technology has enabled many other sensing and monitoring systems, such as temperature sensors, pressure gauges, and humidity detectors. Based on solution-processable colloidal nanoparticles, several printed temperature sensors have been demonstrated, showing strong potential in various research and industrial processes.²⁸⁴⁻²⁸⁶ Due to the excellent electrical, mechanical, and thermal properties, graphene and its derivatives have been widely used in developing sensors for temperature probing and monitoring.²⁸⁷⁻²⁸⁹ For example, a flexible resistive temperature sensor was inkjet-printed using graphene/PEDOT:PSS ink.²⁹⁰ The sensing device showed a negative temperature dependence of resistance with 0.06% per degree Celsius sensitivity. Very recently, Zhao et al. developed a printed tandem line-type temperature sensors based on reduced graphene oxide.²⁸⁹ The authors also used DIW printing method to fabricate MXenes/CNTs positive electrode and rGO/CNTs negative electrode, which were used as a supercapacitor to power the temperature sensors. The authors found that the temperature sensitivity of the printed integrated electronic device can reach 1.2% per degree Celsius in resistance.

Owing to 2D nanomaterials' exceptional mechanical properties and ultrathin thicknesses, they are emerging as attractive platform for strain sensors.²⁹¹⁻²⁹⁴ In a typical printed strain sensor, a conductive pattern can respond to geometric deformation that changes one or several key parameters of the sensor, such as resistance or capacitance.²⁹⁵⁻²⁹⁷ Casiraghi et al. reported inkjet printed strain gauges based on liquid-exfoliated graphene (**Figure 20 a-c**).¹⁶⁶ By adjusting several key printing parameters such as number of printing passes (**Figure 20 d-e**), gauge factor up to 125 was obtained, which led to high sensitivity (>20%) under small strains (0.3%). In another recent study, 2D MXene has been used to develop a flexible pressure sensor with interdigital

electrodes based on their change in d-spacing upon external pressure.¹⁰ An *in situ* transmission electron microscopy study directly illustrated a decrease in interlayer distances under pressure (Figure 20 f), providing a qualitative understanding of the working mechanism of MXene-based sensor. A great range of pressure can be detected using the MXene-based piezoresistive sensor with a decent gauge factor ($GF \sim 180$), good mechanical reversibility (over 4,000 times), and short response time (<30 ms). The authors also demonstrated a MXene-based sensor pixel array (4×4) for mapping the pressure distribution, as shown in Figure 20g-i. When an object (e.g. a watch) was positioned on the sensor arrays, the corresponding output at each pixel was recorded and measured, allowing for mapping local pressure distribution quantitatively.

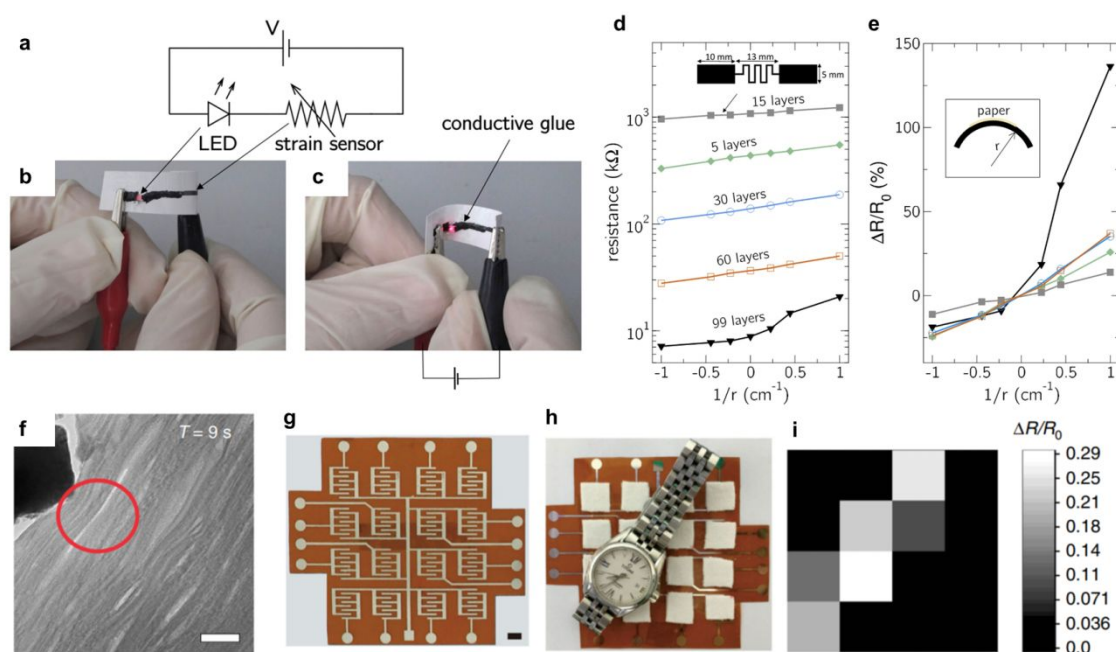


Figure 20. (a) Schematic of the simple circuit for graphene strain sensor. (b-c) Graphene sensing system under (b) tensile and (c) compressive strain. (d) Resistance as a function of the inverse of the bending radius and under different layer thicknesses. (e) Sensitivity as a function of $1/r$ under different layers. Reproduced with permission from reference.¹⁶⁶ Copyright 2018 Elsevier. (f) The *in situ* dynamic monitoring of MXene under an external pressure, showing the change of interlayer distance (scale bar is 40 nm). (g) 4×4 MXene-based sensor pixel arrays for sensing pressure distribution (scale bar is 5 mm). (h) A watch was positioned on the arrays. (i) The

corresponding resistance change was evaluated at each pixel. Reprinted by permission from Springer Nature.¹⁰ Copyright 2017 Nature Publishing Group.

Due to the ability to attract or interact with water molecules, numerous hydrophilic nanomaterials have recently attracted research interest in humidity sensing^{279, 298} and water-level monitoring.^{299, 300} Owing to the strong hydrophilic feature enabled by surface functional groups, 2DMs such as graphene oxides and MXene have been used in developing flexible/wearable humidity sensors.³⁰¹⁻³⁰⁴ For example, Yuan's group developed a flexible humidity sensor based on poly(3,4-ethylenedioxythiophene)/reduced graphene oxide/Au nanoparticles.²⁹⁸ Using inkjet printing techniques, the thin-film humidity sensor showed high conductivity and sensitivity with superior stability after 200 bending cycles. The sensor can respond to a wide range of humidity (11%–98% relative humidity), while producing a wide resistance change of 7%–52%. For some 2DMs (e.g., black phosphorus) of which the intrinsic conductivity is sensitive to ambient water, humidity sensors can also be developed through rational device design.³⁰⁵⁻³⁰⁷ For example, a thick-film black-phosphorus humidity sensor was fabricated with a high response to humidity change.³⁰⁵ Such humidity-response property showed decent stability after 3-month exposure to ambient condition with 25 % relative humidity. Compared with conventional thin-film sensor, the authors suggested that a thick film of BP nanosheets can be more robust for long-term humidity sensing in moderate humidity conditions.

6. Conclusion and Future Perspectives

In the past decade, colloidal nanoparticles have been extensively employed in a variety of printing processes because of their unique properties. In this review, we summarized and evaluated state-of-the-art progresses on colloidal nanoparticle synthesis, ink formulation and printing and device applications, and suggested high-priority areas for future research. As a perspective on possible future directions, we listed some emerging technologies and research

topics that could be potentially leveraged in the development of next-generation printed functional devices (**Table 4**).

Table 4: Examples of emerging trends of printing-related technologies and their applications in functional devices.

| | Emerging fields | Capabilities & Features | Example Applications | Reference |
|----------------------|-----------------------------|--|-----------------------------|------------------|
| Ink formulation | Orientation engineering | Ink particles can self-assemble or be direct-assembled into functional structures with high orientational ordering | Ordered/aligned devices | [320,321] |
| | Nanosurfactant | QD nanosurfactants stabilize graphene in water with high colloidal stability | Photonic materials | [28] |
| | Semiconductor binder/solder | Connecting semiconductor particles under mild conditions | Thermoelectrics, FETs | [123,308] |
| | Green solvent | Providing a low hazard, and highly scalable method | Transistor | [106] |
| Printing methodology | High throughput printing | A bar-coating technique (speed of 6 m min ⁻¹) enables large-area polymer circuits | Large-area electronics | [314] |
| | Volumetric printing | Printing entire complex objects on a time scale of seconds | Custom objects | [315,316] |
| | Embedded printing | Fabricating devices within extensible elastomeric matrices | Strain sensors | [319] |
| | Multi-material printing | Direct printing and mixing of multiple, high-quality materials by one printing process | Shape memory circuit | [317,318] |
| Substrate | Surface coating | Improve the printability of substrates | Microfluidics | [148] |
| | Prepatterned | Providing a customizable platform for generating 1D/2D patterns | Microcontact printing | [22,144] |
| | Smart substrate | Thermo-responsive polymers were used as reversible shape changing substrates | Soft actuators | [169] |
| Sintering /Annealing | Microwave annealing | Reduce GO into pristine graphene using 1- to 2-second pulses of microwaves | Hydrogen evolution | [325] |
| | Photonic sintering | Sintering of printed films on polymer substrates within seconds | Thermoelectrics | [130] |

The properties of 2D materials vary significantly, as expected from their diversity in chemical/electronic structures, from zero/small band gaps for some materials (*e.g.* graphene, MXene) to large band gaps for others (*e.g.* MoS₂, h-BN). The rich diversity of 2D materials in chemistry/physics offers numerous opportunities for formulating high-performance inks and printing functional devices, but also presents challenges for comprehensive understanding of specialized roles of 2DMs in printing process. The review considered four key aspects: 2D material synthesis, ink formulation, printing processes, and device applications.

In the section of 2D material synthesis, the rapid development of nanoparticle synthesis has accelerated progresses in preparing advanced 2D nanomaterials with controlled nanostructures. By using bottom-up or top-down approaches, ultrathin 2D nanomaterials have been synthesized with high yield and fast production speed. However, the commercial production (*e.g.* 1~100 kg level) of high-performance 2D nanomaterials remains a major challenge. For example, many LPE-based monolayer syntheses rely on ultrasonication for hours and even days, which makes it challenging for large-scale manufacturing of 2DMs. Methods that can consistently produce high-quality 2DMs with low cost and industrial scale are yet to be developed.

For processing inks, the ingredients (*e.g.* solvents, surfactants, and binders) play significant roles in determining the quality of inks, and thus innovations in ink additives can further improve the performance of printed devices. For example, the development of composition-matched molecular “solders” has demonstrated considerable improvement in device carrier mobility.³⁰⁸ In addition, surfactants can greatly reduce the interfacial tension and form steric and/or provide electrostatic stabilization for 2D nanomaterials in inks. However, the residue surfactant in printed devices often limits the overall functionalities of the 2D materials, which requires post-treatments to remove the surfactant. Therefore, one practical need to the large-scale applications of 2DM-based inks is the development of compatible ink additives such that they wouldn't compromise the performance of printed devices. A possible solution is to develop semiconducting/conducting nano-surfactants that do not undermine or even improve the device

functionalities of 2D materials. For instances, recent advances in colloidal nano-surfactants or so-called Pickering surfactants have shown that quantum dots,²⁸ graphene,³⁰⁹ MoS₂,³¹⁰ and 2D clays³¹¹⁻³¹³ can reduce surface tension and show “surfactancy” upon appropriate surface functionalization of nanoparticles. This could be a promising approach for preparing organic-free functional inks, and more works need to be done on this aspect.

In the past decade, the emergence of 2D/3D/4D printing has enabled rapid prototyping of macroscale functional devices from nanoscale building blocks.³¹⁴⁻³²⁰ Despite considerable progresses, there is still much to be done on comprehensive understanding and further optimization of ink rheological properties, drying process, and substrate-ink interactions. In addition, the fundamental understanding of the effect of 2D structure and chemical characteristics of 2DMs on above processes is critically important. As mentioned in Section 3.1, the colloidal stability of 2D particles in fluids is fundamentally different from spherical nanoparticle, such as the electrostatic repulsion energy and sedimentation rate. However, the impact of the unique dimensionality of 2DMs on printing technology remains poorly understood. Another possible direction to improve the overall performance of printed 2DMs is to design and develop novel printing processes. For example, multi-materials printing that integrates two or more 2D functional materials *in situ* during printing may enable fast prototyping and high-throughput discovery of novel heterostructures or nanocomposites. Successful examples of heterogeneous nanocompositing have been witnessed in the field of sensing. For instance, SnS₂, WS₂, MoS₂, and Ni₃S₂ have been adopted to enhance the performance of graphene/CNT based electrochemical sensors.²⁶⁹⁻²⁷²

On the other hand, although significant efforts have been made in printing functional devices, the electrical performance of printed 2D materials is often if not always lower than their single-crystalline counterparts. In order to further improve the charge/energy carrier transport of printed 2DM devices, methods that can align 2D materials with minimal defects are highly desirable. To achieve high alignment, the liquid-crystalline assembly of 2D nanoparticles into

ordered structures seems to be a promising approach. As 2D materials are intrinsically anisotropic, the dispersions of 2D particles have shown a fascinating diversity of liquid crystal phases, i.e. forming orientationally or positionally ordered structures.^{321, 322} This approach, combined with directed assembly tools, has been reported to significantly improve the device performance in terms of thermal conductivity and electrical capacity,^{323, 324} and could be applicable to additive printing processes. Innovative approaches of post-treatment (e.g. photonic sintering¹³⁰ or microwave treatment³²⁵) have also demonstrated great potential in improving the performance of solution-processed nanoparticle films.

For device design and development, a wider selection of 2D materials should be included. Newly-discovered 2D materials, including newly discovered tellurene and hematene,^{326, 327} have not been fully characterized and may enable translational applications. These and other undiscovered materials may have unprecedented properties that could hold the keys to new research breakthroughs. To push forward the development of a new generation of printable structures of 2D materials, it is of utmost importance to establish a fundamental structure-processing-property relationship by innovative theoretical efforts, such as machine learning method. For example, Rajan et al. developed machine-learning models to predict the band gap of MXene using kernel ridge (KRR), support vector (SVR), Gaussian process (GPR), and bootstrap aggregating regression algorithms.³²⁸ Theoretical/simulation works will be beneficial for better understanding the ink behavior of 2D nanomaterials that governs their utility in device applications.

Overall, unprecedented opportunities and challenges exist in printing colloidal nanoparticles for functional systems and transforming vast number of nanomaterials into next-generation technologies in a scalable and economic fashion.

AUTHOR INFORMATION**Corresponding Author**

* Email: yzhang45@nd.edu (Y. Z.).

ACKNOWLEDGEMENTS

We acknowledge funding support from the National Science Foundation under award CMMI-1747685, DARPA under DARPA HR00111820030, and U.S. Department of Energy under awards DE-NE0008712 and DE-NE0008701.

References

1. W. Zeng, L. Shu, Q. Li, S. Chen, F. Wang and X.-M. Tao, *Adv Mater*, 2014, **26**, 5310-5336.
2. X. Wang, X. Lu, B. Liu, D. Chen, Y. Tong and G. Shen, *Adv Mater*, 2014, **26**, 4763-4782.
3. K. Chen, W. Gao, S. Emaminejad, D. Kiriya, H. Ota, H. Y. Y. Nyein, K. Takei and A. Javey, *Adv Mater*, 2016, **28**, 4397-4414.
4. A. Ambrosi and M. Pumera, *Chem Soc Rev*, 2016, **45**, 2740-2755.
5. K. Fu, Y. Yao, J. Dai and L. Hu, *Adv Mater*, 2017, **29**.
6. Z. Zhan, J. An, Y. Wei, V. T. Tran and H. Du, *Nanoscale*, 2017, **9**, 965-993.
7. A. Kamyshny and S. Magdassi, *Chem Soc Rev*, 2019, **48**, 1712-1740.
8. Z. Cui, *Printed electronics: materials, technologies and applications*, John Wiley & Sons, 2016.
9. L. Lipani, B. G. R. Dupont, F. Doungmene, F. Marken, R. M. Tyrrell, R. H. Guy and A. Ilie, *Nat Nanotechnol*, 2018, **13**, 504-511.
10. Y. Ma, N. Liu, L. Li, X. Hu, Z. Zou, J. Wang, S. Luo and Y. Gao, *Nature communications*, 2017, **8**, 1207.
11. S. Borini, R. White, D. Wei, M. Astley, S. Haque, E. Spigone, N. Harris, J. Kivioja and T. Ryhänen, *ACS Nano*, 2013, **7**, 11166-11173.
12. C. Tan, X. Cao, X.-J. Wu, Q. He, J. Yang, X. Zhang, J. Chen, W. Zhao, S. Han, G.-H. Nam, M. Sindoro and H. Zhang, *Chem Rev*, 2017, **117**, 6225-6331.
13. Y. Liu, N. O. Weiss, X. Duan, H.-C. Cheng, Y. Huang and X. Duan, *Nature Reviews Materials*, 2016, **1**, 16042.
14. V. Nicolosi, M. Chhowalla, M. G. Kanatzidis, M. S. Strano and J. N. Coleman, *Science*, 2013, **340**, 1226419.
15. L. Fu, H. Yang, A. Tang and Y. Hu, *Nano Research*, 2017, **10**, 2782-2799.
16. A. I. Khan and D. O'Hare, *J Mater Chem*, 2002, **12**, 3191-3198.
17. H. T. Li, R. H. Liu, W. Q. Kong, J. Liu, Y. Liu, L. Zhou, X. Zhang, S. T. Lee and Z. H. Kang, *Nanoscale*, 2014, **6**, 867-873.
18. D. Chimene, D. L. Alge and A. K. Gaharwar, *Adv Mater*, 2015, **27**, 7261-7284.
19. M. Singh, H. M. Haverinen, P. Dhagat and G. E. Jabbour, *Adv Mater*, 2010, **22**, 673-685.
20. P. Chang, H. Mei, S. Zhou, K. G. Dassios and L. Cheng, *Journal of Materials Chemistry A*, 2019, **7**, 4230-4258.
21. G. Hu, J. Kang, L. W. T. Ng, X. Zhu, R. C. T. Howe, C. G. Jones, M. C. Hersam and T. Hasan, *Chem Soc Rev*, 2018, **47**, 3265-3300.
22. D. Tian, Y. Song and L. Jiang, *Chem Soc Rev*, 2013, **42**, 5184-5209.
23. Y. Q. Dong, J. W. Shao, C. Q. Chen, H. Li, R. X. Wang, Y. W. Chi, X. M. Lin and G. N. Chen, *Carbon*, 2012, **50**, 4738-4743.
24. K. Hu, X. Xie, T. Szkopek and M. Cerruti, *Chemistry of Materials*, 2016, **28**, 1756-1768.
25. K. S. Novoselov, A. K. Geim, S. V. Morozov, D. Jiang, Y. Zhang, S. V. Dubonos, I. V. Grigorieva and A. A. Firsov, *Science*, 2004, **306**, 666-669.
26. A. Geim and K. Novoselov, *Nat Mater*, 2007, **6**, 183-191.
27. D. C. Marcano, D. V. Kosynkin, J. M. Berlin, A. Sinitskii, Z. Z. Sun, A. Slesarev, L. B. Alemany, W. Lu and J. M. Tour, *ACS Nano*, 2010, **4**, 4806-4814.
28. M. Zeng, S. A. Shah, D. Huang, D. Parviz, Y.-H. Yu, X. Wang, M. J. Green and Z. Cheng, *ACS applied materials & interfaces*, 2017, **9**, 30797-30804.
29. Y. Peng, Z. Meng, C. Zhong, J. Lu, W. Yu, Z. Yang and Y. Qian, *Journal of Solid State Chemistry*, 2001, **159**, 170-173.
30. Z. Huang, A. Zhou, J. Wu, Y. Chen, X. Lan, H. Bai and L. Li, *Adv Mater*, 2016, **28**, 1703-1708.
31. Z. Tang, Z. Zhang, Y. Wang, S. C. Glotzer and N. A. Kotov, *Science*, 2006, **314**, 274-278.

32. D. J. Late, B. Liu, H. S. S. R. Matte, C. N. R. Rao and V. P. Dravid, *Advanced Functional Materials*, 2012, **22**, 1894-1905.
33. Z. Lin, Y. Liu, U. Halim, M. Ding, Y. Liu, Y. Wang, C. Jia, P. Chen, X. Duan, C. Wang, F. Song, M. Li, C. Wan, Y. Huang and X. Duan, *Nature*, 2018, **562**, 254-258.
34. J. Zheng, H. Zhang, S. Dong, Y. Liu, C. Tai Nai, H. Suk Shin, H. Young Jeong, B. Liu and K. Ping Loh, *Nature communications*, 2014, **5**, 2995.
35. B. Huo, B. Liu, T. Chen, L. Cui, G. Xu, M. Liu and J. Liu, *Langmuir*, 2017, **33**, 10673-10678.
36. Y. Kubota, K. Watanabe, O. Tsuda and T. Taniguchi, *Science*, 2007, **317**, 932-934.
37. C. Lee, Q. Li, W. Kalb, X.-Z. Liu, H. Berger, R. W. Carpick and J. Hone, *Science*, 2010, **328**, 76-80.
38. Y. Lin, T. V. Williams, T.-B. Xu, W. Cao, H. E. Elsayed-Ali and J. W. Connell, *The Journal of Physical Chemistry C*, 2011, **115**, 2679-2685.
39. J. D. Wood, S. A. Wells, D. Jariwala, K.-S. Chen, E. Cho, V. K. Sangwan, X. Liu, L. J. Lauhon, T. J. Marks and M. C. Hersam, *Nano letters*, 2014, **14**, 6964-6970.
40. J. Kang, S. A. Wells, V. K. Sangwan, D. Lam, X. Liu, J. Luxa, Z. Sofer and M. C. Hersam, *Adv Mater*, 2018, **30**, 1802990.
41. X. Zhang, P. Yu, H. Zhang, D. Zhang, X. Sun and Y. Ma, *Electrochimica Acta*, 2013, **89**, 523-529.
42. M. Liu, P.-Y. Chen and R. H. Hurt, *Adv Mater*, 2018, **30**, 1705080.
43. A. A. AbdelHamid, J. H. Soh, Y. Yu and J. Y. Ying, *Nano Energy*, 2018, **44**, 399-410.
44. R. Cai, D. Yang, K.-T. Lin, Y. Lyu, B. Zhu, Z. He, L. Zhang, Y. Kitamura, L. Qiu, X. Chen, Y. Zhao, Z. Chen and W. Tan, *J Am Chem Soc*, 2019, **141**, 1725-1734.
45. X. Rui, Z. Lu, H. Yu, D. Yang, H. H. Hng, T. M. Lim and Q. Yan, *Nanoscale*, 2013, **5**, 556-560.
46. X. Xiao, H. Yu, H. Jin, M. Wu, Y. Fang, J. Sun, Z. Hu, T. Li, J. Wu, L. Huang, Y. Gogotsi and J. Zhou, *ACS Nano*, 2017, **11**, 2180-2186.
47. M. Naguib, O. Mashtalir, J. Carle, V. Presser, J. Lu, L. Hultman, Y. Gogotsi and M. W. Barsoum, *ACS Nano*, 2012, **6**, 1322-1331.
48. Z. P. Xu and G. Q. Lu, *Chemistry of Materials*, 2005, **17**, 1055-1062.
49. Y. Kuroda, K. Ito, K. Itabashi and K. Kuroda, *Langmuir*, 2011, **27**, 2028-2035.
50. S. Gao, Y. Lin, X. Jiao, Y. Sun, Q. Luo, W. Zhang, D. Li, J. Yang and Y. Xie, *Nature*, 2016, **529**, 68.
51. B. Mahler, V. Hoepfner, K. Liao and G. A. Ozin, *J Am Chem Soc*, 2014, **136**, 14121-14127.
52. W. Mai, Y. Zuo, X. Zhang, K. Leng, R. Liu, L. Chen, X. Lin, Y. Lin, R. Fu and D. Wu, *Chem Commun*, 2019, **55**, 10241-10244.
53. T. Yu, B. Lim and Y. N. Xia, *Angew. Chem., Int. Ed.*, 2010, **49**, 4484.
54. X. Huang, S. Li, Y. Huang, S. Wu, X. Zhou, S. Li, C. L. Gan, F. Boey, C. A. Mirkin and H. Zhang, *Nature Communications*, 2011, **2**, 292.
55. W. Cheng, J. He, T. Yao, Z. Sun, Y. Jiang, Q. Liu, S. Jiang, F. Hu, Z. Xie, B. He, W. Yan and S. Wei, *J Am Chem Soc*, 2014, **136**, 10393-10398.
56. X.-J. Wu, X. Huang, X. Qi, H. Li, B. Li and H. Zhang, *Angewandte Chemie International Edition*, 2014, **53**, 8929-8933.
57. P. Simon, L. Bahrig, I. A. Baburin, P. Formanek, F. Roder, J. Sickmann, S. G. Hickey, A. Eychmuller, H. Lichte, R. Knipf and E. Rosseeva, *Adv. Mater.*, 2014, **26**, 3042.
58. Z. Wu, J. Liu, Y. Li, Z. Cheng, T. Li, H. Zhang, Z. Lu and B. Yang, *ACS Nano*, 2015, **9**, 6315-6323.
59. S. Acharya, B. Das, U. Thupakula, K. Ariga, D. D. Sarma, J. Israelachvili and Y. Golan, *Nano letters*, 2013, **13**, 409-415.
60. J. Niu, D. Wang, H. Qin, X. Xiong, P. Tan, Y. Li, R. Liu, X. Lu, J. Wu and T. Zhang, *Nature Communications*, 2014, **5**, 3313.

61. K. S. Novoselov, A. K. Geim, S. V. Morozov, D. Jiang, Y. Zhang, S. V. Dubonos, I. V. Grigorieva and A. A. Firsov, *Science*, 2004, **306**, 666.
62. K. S. Novoselov, A. K. Geim, S. V. Morozov, D. Jiang, M. I. Katsnelson, I. V. Grigorieva, S. V. Dubonos and A. A. Firsov, *Nature*, 2005, **438**, 197.
63. K. S. Novoselov, D. Jiang, F. Schedin, T. J. Booth, V. V. Khotkevich, S. V. Morozov and A. K. Geim, *Proc. Natl. Acad. Sci. U. S. A.*, 2005, **102**, 10451.
64. A. K. Geim and K. S. Novoselov, *Nat. Mater.*, 2007, **6**, 183.
65. H. Li, J. Wu, Z. Yin and H. Zhang, *Accounts Chem Res*, 2014, **47**, 1067-1075.
66. V. Goyal, D. Teweldebrhan and A. A. Balandin, *Appl Phys Lett*, 2010, **97**, 133117.
67. P. Ares, F. Aguilar-Galindo, D. Rodríguez-San-Miguel, D. A. Aldave, S. Díaz-Tendero, M. Alcamí, F. Martín, J. Gómez-Herrero and F. Zamora, *Adv Mater*, 2016, **28**, 6332-6336.
68. Y. Huang, E. Sutter, N. N. Shi, J. Zheng, T. Yang, D. Englund, H. J. Gao and P. Sutter, *ACS Nano*, 2015, **9**, 10612.
69. Y. Hernandez, V. Nicolosi, M. Lotya, F. M. Blighe, Z. Sun, S. De, I. T. McGovern, B. Holland, M. Byrne and Y. K. Gun'ko, *Nat. Nanotechnol.*, 2008, **3**, 563.
70. L. X. Xu, J. W. McGraw, F. Gao, M. Grundy, Z. B. Ye, Z. Y. Gu and J. L. Shepherd, *J. Phys. Chem. C*, 2013, **117**, 10730.
71. A. O'Neill, U. Khan, P. N. Nirmalraj, J. Boland and J. N. Coleman, *J. Phys. Chem. C*, 2011, **115**, 5422.
72. J. N. Coleman, M. Lotya, A. O'Neill, S. D. Bergin, P. J. King, U. Khan, K. Young, A. Gaucher, S. De and R. J. Smith, *Science*, 2011, **331**, 568.
73. J. Kim, S. Kwon, D.-H. Cho, B. Kang, H. Kwon, Y. Kim, S. O. Park, G. Y. Jung, E. Shin, W.-G. Kim, H. Lee, G. H. Ryu, M. Choi, T. H. Kim, J. Oh, S. Park, S. K. Kwak, S. W. Yoon, D. Byun, Z. Lee and C. Lee, *Nature communications*, 2015, **6**, 8294.
74. X. Dong, Y. Shi, Y. Zhao, D. Chen, J. Ye, Y. Yao, F. Gao, Z. Ni, T. Yu, Z. Shen, Y. Huang, P. Chen and L.-J. Li, *Physical Review Letters*, 2009, **102**, 135501.
75. M. Zhang, R. R. Parajuli, D. Mastrogiovanni, B. Dai, P. Lo, W. Cheung, R. Brukh, P. L. Chiu, T. Zhou and Z. Liu, *Small*, 2010, **6**, 1100-1107.
76. D. Parviz, S. Das, H. S. T. Ahmed, F. Irin, S. Bhattacharia and M. J. Green, *ACS Nano*, 2012, **6**, 8857-8867.
77. A. Ciesielski and P. Samori, *Chem Soc Rev*, 2014, **43**, 381-398.
78. S. Eigler and A. Hirsch, *Angewandte Chemie International Edition*, 2014, **53**, 7720-7738.
79. Y. T. Liang and M. C. Hersam, *J. Am. Chem. Soc.*, 2010, **132**, 17661.
80. R. J. Smith, P. J. King, M. Lotya, C. Wirtz, U. Khan, S. De, A. O'Neill, G. S. Duesberg, J. C. Grunlan and G. Moriarty, *Adv. Mater.*, 2011, **23**, 3944.
81. G. Guan, S. Zhang, S. Liu, Y. Cai, M. Low, C. P. Teng, I. Y. Phang, Y. Cheng, K. L. Duei and B. M. Srinivasan, *J. Am. Chem. Soc.*, 2015, **137**, 6152.
82. P. May, U. Khan, J. M. Hughes and J. N. Coleman, *J. Phys. Chem. C*, 2012, **116**, 11393.
83. K. R. Paton, E. Varrla, C. Backes, R. J. Smith, U. Khan, A. O'Neill, C. Boland, M. Lotya, O. M. Istrate and P. King, *Nat. Mater.*, 2014, **13**, 624.
84. E. Varrla, C. Backes, K. R. Paton, A. Harvey, Z. Gholamvand, J. McCauley and J. N. Coleman, *Chemistry of Materials*, 2015, **27**, 1129-1139.
85. D. Voiry, A. Mohite and M. Chhowalla, *Chem Soc Rev*, 2015, **44**, 2702-2712.
86. L. Niu, M. Li, X. Tao, Z. Xie, X. Zhou, A. P. A. Raju, R. J. Young and Z. Zheng, *Nanoscale*, 2013, **5**, 7202-7208.
87. X. Fan, W. Peng, Y. Li, X. Li, S. Wang, G. Zhang and F. Zhang, *Adv. Mater.*, 2008, **20**, 4490.
88. K. Erickson, R. Erni, Z. Lee, N. Alem, W. Gannett and A. Zettl, *Adv. Mater.*, 2010, **22**, 4467.
89. X. Huang, X. Qi, F. Boey and H. Zhang, *Chem Soc Rev*, 2012, **41**, 666-686.
90. M. Naguib, V. N. Mochalin, M. W. Barsoum and Y. Gogotsi, *Adv. Mater.*, 2014, **26**, 992.

91. X. Wang, S. Kajiyama, H. Iinuma, E. Hosono, S. Oro, I. Moriguchi, M. Okubo and A. Yamada, *Nat. Commun.*, 2015, **6**, 6544.
92. J. Halim, S. Kota, M. R. Lukatskaya, M. Naguib, M. Q. Zhao, E. J. Moon, J. Pitcock, J. Nanda, S. J. May, Y. Gogotsi and M. W. Barsou, *Adv. Funct. Mater.*, 2016, **26**, 3118.
93. P. Urbankowski, B. Anasori, T. Makaryan, D. Er, S. Kota, P. L. Walsh, M. Zhao, V. B. Shenoy, M. W. Barsouma and Y. Gogotsi, *Nanoscale*, 2016, **8**, 11385.
94. B. Anasori, Y. Xie, M. Beidaghi, J. Lu, B. Hosler, L. Hultman, P. Kent, Y. Gogotsi and M. W. Barsoum, *ACS Nano*, 2015, **9**, 9507.
95. K. Sano, Y. S. Kim, Y. Ishida, Y. Ebina, T. Sasaki, T. Hikima and T. Aida, *Nature Communications*, 2016, **7**, 12559.
96. I. Chowdhury, M. C. Duch, N. D. Mansukhani, M. C. Hersam and D. Bouchard, *Environmental Science & Technology*, 2013, **47**, 6288-6296.
97. G. R. Wiese and T. W. Healy, *Transactions of the Faraday Society*, 1970, **66**, 490-499.
98. T. Missana and A. Adell, *J Colloid Interf Sci*, 2000, **230**, 150-156.
99. P. He, A. F. Mejia, Z. D. Cheng, D. Z. Sun, H. J. Sue, D. S. Dinair and M. Marquez, *Phys Rev E*, 2010, **81**.
100. X. Sun, D. Luo, J. Liu and D. G. Evans, *ACS Nano*, 2010, **4**, 3381-3389.
101. J. I. Paredes, S. Villar-Rodil, A. Martínez-Alonso and J. M. D. Tascón, *Langmuir*, 2008, **24**, 10560-10564.
102. M. Bystrzejewski, A. Huczko and H. Lange, *Materials Chemistry and Physics*, 2008, **107**, 322-327.
103. J. N. Coleman, M. Lotya, A. O'Neill, S. D. Bergin, P. J. King, U. Khan, K. Young, A. Gaucher, S. De, R. J. Smith, I. V. Shvets, S. K. Arora, G. Stanton, H.-Y. Kim, K. Lee, G. T. Kim, G. S. Duesberg, T. Hallam, J. J. Boland, J. J. Wang, J. F. Donegan, J. C. Grunlan, G. Moriarty, A. Shmeliov, R. J. Nicholls, J. M. Perkins, E. M. Grievson, K. Theuwissen, D. W. McComb, P. D. Nellist and V. Nicolosi, *Science*, 2011, **331**, 568-571.
104. G. Cunningham, M. Lotya, C. S. Cucinotta, S. Sanvito, S. D. Bergin, R. Menzel, M. S. P. Shaffer and J. N. Coleman, *ACS Nano*, 2012, **6**, 3468-3480.
105. Y. Hernandez, M. Lotya, D. Rickard, S. D. Bergin and J. N. Coleman, *Langmuir*, 2010, **26**, 3208-3213.
106. B. Schmatz, A. W. Lang and J. R. Reynolds, *Advanced Functional Materials*, 2019, DOI: 10.1002/adfm.201905266.
107. K.-G. Zhou, N.-N. Mao, H.-X. Wang, Y. Peng and H.-L. Zhang, *Angewandte Chemie International Edition*, 2011, **50**, 10839-10842.
108. M. Yi, Z. Shen, S. Ma and X. Zhang, *Journal of Nanoparticle Research*, 2012, **14**, 1003.
109. X. Li, Y. Qin, C. Liu, S. Jiang, L. Xiong and Q. Sun, *Food Chem*, 2016, **199**, 356-363.
110. J. K. Lim, S. A. Majetich and R. D. Tilton, *Langmuir*, 2009, **25**, 13384-13393.
111. A. Gupta, V. Arunachalam and S. Vasudevan, *The Journal of Physical Chemistry Letters*, 2015, **6**, 739-744.
112. S. G. Hashmi, T. Moehl, J. Halme, Y. Ma, T. Saukkonen, A. Yella, F. Giordano, J. D. Decoppet, S. M. Zakeeruddin, P. Lund and M. Grätzel, *Journal of Materials Chemistry A*, 2014, **2**, 19609-19615.
113. R. J. Smith, P. J. King, M. Lotya, C. Wirtz, U. Khan, S. De, A. O'Neill, G. S. Duesberg, J. C. Grunlan, G. Moriarty, J. Chen, J. Wang, A. I. Minett, V. Nicolosi and J. N. Coleman, *Adv Mater*, 2011, **23**, 3944-3948.
114. R. C. T. Howe, R. I. Woodward, G. Hu, Z. Yang, E. J. R. Kelleher and T. Hasan, *Phys. Status Solidi B*, 2016, **253**, 911-917.
115. J. N. Coleman, *Adv Funct Mater*, 2009, **19**, 3680-3695.
116. T. Hasan, F. Torrisi, Z. Sun, D. Popa, V. Nicolosi, G. Privitera, F. Bonaccorso and A. C. Ferrari, *physica status solidi (b)*, 2010, **247**, 2953-2957.
117. P. K. Misra, B. K. Mishra and G. B. Behera, *Colloids and Surfaces*, 1991, **57**, 1-10.
118. S. G. Hashmi, M. Ozkan, J. Halme, K. D. Misic, S. M. Zakeeruddin, J. Paltakari, M. Grätzel and P. D. Lund, *Nano Energy*, 2015, **17**, 206-215.

119. T. Hasan, Z. Sun, F. Wang, F. Bonaccorso, P. H. Tan, A. G. Rozhin and A. C. Ferrari, *Adv Mater*, 2009, **21**, 3874-3899.
120. L. Guardia, M. J. Fernández-Merino, J. I. Paredes, P. Solís-Fernández, S. Villar-Rodil, A. Martínez-Alonso and J. M. D. Tascón, *Carbon*, 2011, **49**, 1653-1662.
121. A. Ciesielski, S. Haar, M. El Gemayel, H. Yang, J. Clough, G. Melinte, M. Gobbi, E. Orgiu, M. V. Nardi, G. Ligorio, V. Palermo, N. Koch, O. Ersen, C. Casiraghi and P. Samorì, *Angewandte Chemie International Edition*, 2014, **53**, 10355-10361.
122. Y. T. Liang and M. C. Hersam, *J Am Chem Soc*, 2010, **132**, 17661-17663.
123. F. Kim, B. Kwon, Y. Eom, J. E. Lee, S. Park, S. Jo, S. H. Park, B.-S. Kim, H. J. Im, M. H. Lee, T. S. Min, K. T. Kim, H. G. Chae, W. P. King and J. S. Son, *Nature Energy*, 2018, **3**, 301-309.
124. J. Li, M. M. Naiini, S. Vaziri, M. C. Lemme and M. Östling, *Advanced Functional Materials*, 2014, **24**, 6524-6531.
125. D. McManus, S. Vranic, F. Withers, V. Sanchez-Romaguera, M. Macucci, H. Yang, R. Sorrentino, K. Parvez, S.-K. Son, G. Iannaccone, K. Kostarelos, G. Fiori and C. Casiraghi, *Nat Nanotechnol*, 2017, **12**, 343.
126. X. Ma, Z. Xie, Z. Yang, G. Zeng, M. Xue and X. Zhang, *Materials Research Express*, 2018, **6**, 015025.
127. P. He, J. R. Brent, H. Ding, J. Yang, D. J. Lewis, P. O'Brien and B. Derby, *Nanoscale*, 2018, **10**, 5599-5606.
128. W. Yang, J. Yang, J. J. Byun, F. P. Moissinac, J. Xu, S. J. Haigh, M. Domingos, M. A. Bissett, R. A. W. Dryfe and S. Barg, *Adv Mater*, 2019, **0**, 1902725.
129. T. Varghese, C. Hollar, J. Richardson, N. Kempf, C. Han, P. Gamarachchi, D. Estrada, R. J. Mehta and Y. Zhang, *Scientific Reports*, 2016, **6**, 33135.
130. M. Saeidi-Javash, W. Kuang, C. Dun and Y. Zhang, *Advanced Functional Materials*, 2019, **29**, 1901930.
131. T. Carey, S. Cacovich, G. Divitini, J. Ren, A. Mansouri, J. M. Kim, C. Wang, C. Ducati, R. Sordan and F. Torrioni, *Nature Communications*, 2017, **8**, 1202.
132. S. Santra, G. Hu, R. C. T. Howe, A. De Luca, S. Z. Ali, F. Udrea, J. W. Gardner, S. K. Ray, P. K. Guha and T. Hasan, *Scientific Reports*, 2015, **5**, 17374.
133. J. Baker, D. Deganello, D. T. Gethin and T. M. Watson, *Materials Research Innovations*, 2014, **18**, 86-90.
134. E. B. Secor, S. Lim, H. Zhang, C. D. Frisbie, L. F. Francis and M. C. Hersam, *Adv Mater*, 2014, **26**, 4533-4538.
135. Y. Xu, M. G. Schwab, A. J. Strudwick, I. Hennig, X. Feng, Z. Wu and K. Müllen, *Advanced Energy Materials*, 2013, **3**, 1035-1040.
136. K. Fu, Y. Wang, C. Yan, Y. Yao, Y. Chen, J. Dai, S. Lacey, Y. Wang, J. Wan, T. Li, Z. Wang, Y. Xu and L. Hu, *Adv Mater*, 2016, **28**, 2587-2594.
137. G. Xiao, Y. Li, W. Shi, L. Shen, Q. Chen and L. Huang, *Applied Surface Science*, 2017, **404**, 334-341.
138. G. Pangalos, J. M. Dealy and M. B. Lyne, *Journal of Rheology*, 1985, **29**, 471-491.
139. X. Yang, C. Guo, L. Ji, Y. Li and Y. Tu, *Langmuir*, 2013, **29**, 8103-8107.
140. D. Kleshchanok, M. Heinen, G. Nägele and P. Holmqvist, *Soft Matter*, 2012, **8**, 1584-1592.
141. A. Goldschmidt and H.-J. Streitberger, *BASF handbook on basics of coating technology*, William Andrew, 2003.
142. C. B. Highley, C. B. Rodell and J. A. Burdick, *Adv Mater*, 2015, **27**, 5075-5079.
143. W. A. Zisman, in *Contact Angle, Wettability, and Adhesion*, American Chemical Society, 1964, vol. 43, ch. 1, pp. 1-51.
144. G. Pariani, R. Castagna, L. Oggioni, L. Colella, A. Nardi, S. Anzani, C. Bertarelli and A. Bianco, *Advanced Materials Technologies*, 2018, **3**, 1700325.
145. B. Xin and J. Hao, *Chem Soc Rev*, 2010, **39**, 769-782.

146. W.-K. Lee, W.-B. Jung, D. Rhee, J. Hu, Y.-A. L. Lee, C. Jacobson, H.-T. Jung and T. W. Odom, *Adv Mater*, 2018, **30**, 1706657.
147. M. Zeng, P. Wang, J. Luo, B. Peng, B. Ding, L. Zhang, L. Wang, D. Huang, I. Echols, E. Abo Deeb, E. Bordovsky, C.-H. Choi, C. Ybanez, P. Meras, E. Situ, M. S. Mannan and Z. Cheng, *ACS applied materials & interfaces*, 2018, **10**, 22793-22800.
148. T. Trantidou, Y. Elani, E. Parsons and O. Ces, *Microsystems & Nanoengineering*, 2017, **3**, 16091.
149. G. Hu, T. Albrow-Owen, X. Jin, A. Ali, Y. Hu, R. C. T. Howe, K. Shehzad, Z. Yang, X. Zhu, R. I. Woodward, T.-C. Wu, H. Jussila, J.-B. Wu, P. Peng, P.-H. Tan, Z. Sun, E. J. R. Kelleher, M. Zhang, Y. Xu and T. Hasan, *Nature communications*, 2017, **8**, 278.
150. P. G. Campbell, E. D. Miller, G. W. Fisher, L. M. Walker and L. E. Weiss, *Biomaterials*, 2005, **26**, 6762-6770.
151. T. Jungst, W. Smolan, K. Schacht, T. Scheibel and J. Groll, *Chem Rev*, 2016, **116**, 1496-1539.
152. H. Siringhaus, T. Kawase, R. H. Friend, T. Shimoda, M. Inbasekaran, W. Wu and E. P. Woo, *Science*, 2000, **290**, 2123-2126.
153. R. Cobas, S. Muñoz-Pérez, S. Cadogan, M. C. Ridgway and X. Obradors, *Advanced Functional Materials*, 2015, **25**, 768-775.
154. R. E. Saunders and B. Derby, *International Materials Reviews*, 2014, **59**, 430-448.
155. D. Soltman and V. Subramanian, *Langmuir*, 2008, **24**, 2224-2231.
156. R. D. Deegan, O. Bakajin, T. F. Dupont, G. Huber, S. R. Nagel and T. A. Witten, *Nature*, 1997, **389**, 827-829.
157. Y. Li, Q. Yang, M. Li and Y. Song, *Scientific Reports*, 2016, **6**, 24628.
158. S. V. Murphy and A. Atala, *Nature Biotechnology*, 2014, **32**, 773.
159. T. J. Coogan and D. O. Kazmer, *Journal of Rheology*, 2019, **63**, 141-155.
160. K. Arapov, E. Rubingh, R. Abbel, J. Laven, G. de With and H. Friedrich, *Adv Funct Mater*, 2016, **26**, 586-593.
161. S. J. Rowley-Neale, G. C. Smith and C. E. Banks, *ACS applied materials & interfaces*, 2017, **9**, 22539-22548.
162. L. Chen, L. Huang, Y. Lin, L. Sai, Q. Chang, W. Shi and Q. Chen, *Sensors and Actuators B: Chemical*, 2018, **255**, 1482-1490.
163. C. Dun, W. Kuang, N. Kempf, M. Saeidi-Javash, D. J. Singh and Y. Zhang, *Advanced Science*, 2019, **0**.
164. M. S. Saleh, C. Hu and R. Panat, *Science Advances*, 2017, **3**, e1601986.
165. F. Withers, H. Yang, L. Britnell, A. P. Rooney, E. Lewis, A. Felten, C. R. Woods, V. Sanchez Romaguera, T. Georgiou, A. Eckmann, Y. J. Kim, S. G. Yeates, S. J. Haigh, A. K. Geim, K. S. Novoselov and C. Casiraghi, *Nano letters*, 2014, **14**, 3987-3992.
166. C. Casiraghi, M. Macucci, K. Parvez, R. Worsley, Y. Shin, F. Bronte, C. Borri, M. Paggi and G. Fiori, *Carbon*, 2018, **129**, 462-467.
167. K. Chi, Z. Zhang, J. Xi, Y. Huang, F. Xiao, S. Wang and Y. Liu, *ACS applied materials & interfaces*, 2014, **6**, 16312-16319.
168. C. Yuan, D. J. Roach, C. K. Dunn, Q. Mu, X. Kuang, C. M. Yakacki, T. J. Wang, K. Yu and H. J. Qi, *Soft Matter*, 2017, **13**, 5558-5568.
169. D. Zhang, B. Chi, B. Li, Z. Gao, Y. Du, J. Guo and J. Wei, *Synthetic Metals*, 2016, **217**, 79-86.
170. Y. Liu, W. Zhang, F. Zhang, J. Leng, S. Pei, L. Wang, X. Jia, C. Cotton, B. Sun and T.-W. Chou, *Composites Science and Technology*, 2019, **181**, 107692.
171. Y. Kim, H. Yuk, R. Zhao, S. A. Chester and X. Zhao, *Nature*, 2018, **558**, 274-279.
172. Y. Huang, H. Wu, L. Xiao, Y. Duan, H. Zhu, J. Bian, D. Ye and Z. Yin, *Materials Horizons*, 2019, **6**, 642-683.
173. Z. Yin, Y. Huang, N. Bu, X. Wang and Y. Xiong, *Chinese Science Bulletin*, 2010, **55**, 3383-3407.

174. B.-J. de Gans and U. S. Schubert, *Macromolecular Rapid Communications*, 2003, **24**, 659-666.
175. J. Noh, D. Yeom, C. Lim, H. Cha, J. Han, J. Kim, Y. Park, V. Subramanian and G. Cho, *IEEE Transactions on Electronics Packaging Manufacturing*, 2010, **33**, 275-283.
176. F. Torrisi, T. Hasan, W. Wu, Z. Sun, A. Lombardo, T. S. Kulmala, G.-W. Hsieh, S. Jung, F. Bonaccorso, P. J. Paul, D. Chu and A. C. Ferrari, *ACS Nano*, 2012, **6**, 2992-3006.
177. E. B. Secor, P. L. Prabhmirashi, K. Puntambekar, M. L. Geier and M. C. Hersam, *The Journal of Physical Chemistry Letters*, 2013, **4**, 1347-1351.
178. J. Li, F. Ye, S. Vaziri, M. Muhammed, M. C. Lemme and M. Östling, *Adv Mater*, 2013, **25**, 3985-3992.
179. R. Danaei, T. Varghese, M. Ahmadzadeh, J. McCloy, C. Hollar, M. Sadeq Saleh, J. Park, Y. Zhang and R. Panat, *Advanced Engineering Materials*, 2019, **21**, 1800800.
180. J. A. Paulsen, M. Renn, K. Christenson and R. Plourde, 2012.
181. D. Zhao, T. Liu, J. G. Park, M. Zhang, J.-M. Chen and B. Wang, *Microelectronic Engineering*, 2012, **96**, 71-75.
182. C. Cao, J. B. Andrews and A. D. Franklin, *Advanced Electronic Materials*, 2017, **3**, 1700057.
183. K. Wang, Y.-H. Chang, C. Zhang and B. Wang, *Carbon*, 2016, **98**, 397-403.
184. W. Xie, X. Zhang, C. Leighton and C. D. Frisbie, *Advanced Electronic Materials*, 2017, **3**, 1600369.
185. Y. Xiao, Georgia Institute of Technology, 2019.
186. R. Leach, *The printing ink manual*, Springer Science & Business Media, 2012.
187. C. Xu, B. Xu, Y. Gu, Z. Xiong, J. Sun and X. S. Zhao, *Energ Environ Sci*, 2013, **6**, 1388-1414.
188. D. W. Zhang, X. D. Li, H. B. Li, S. Chen, Z. Sun, X. J. Yin and S. M. Huang, *Carbon*, 2011, **49**, 5382-5388.
189. A. M. Joseph, B. Nagendra, E. Bhoje Gowd and K. P. Surendran, *ACS Omega*, 2016, **1**, 1220-1228.
190. M. Jung, J. Kim, H. Koo, W. Lee, V. Subramanian and G. Cho, *Journal of nanoscience and nanotechnology*, 2014, **14**, 1303-1317.
191. J. Hast, M. Tuomikoski, R. Suhonen, K.-L. Väisänen, M. Välimäki, T. Maaninen, P. Apilo, A. Alastalo and A. Maanineny, *SID Symposium Digest of Technical Papers*, 2013, **44**, 192-195.
192. B. Y. Ahn, E. B. Duoss, M. J. Motala, X. Guo, S.-I. Park, Y. Xiong, J. Yoon, R. G. Nuzzo, J. A. Rogers and J. A. Lewis, *Science*, 2009, **323**, 1590-1593.
193. J. J. Adams, E. B. Duoss, T. F. Malkowski, M. J. Motala, B. Y. Ahn, R. G. Nuzzo, J. T. Bernhard and J. A. Lewis, *Adv Mater*, 2011, **23**, 1335-1340.
194. M. A. Skylar-Scott, S. Gunasekaran and J. A. Lewis, *Proceedings of the National Academy of Sciences*, 2016, **113**, 6137-6142.
195. J. A. Lewis, J. E. Smay, J. Stuecker and J. Cesarano, *Journal of the American Ceramic Society*, 2006, **89**, 3599-3609.
196. E. García-Tuñón, S. Barg, J. Franco, R. Bell, S. Eslava, E. D'Elia, R. C. Maher, F. Guitian and E. Saiz, *Adv Mater*, 2015, **27**, 1688-1693.
197. Y. Zhang, F. Zhang, Z. Yan, Q. Ma, X. Li, Y. Huang and J. A. Rogers, *Nature Reviews Materials*, 2017, **2**, 17019.
198. P. C. Sherrell and C. Mattevi, *Materials Today*, 2016, **19**, 428-436.
199. Y. Lin, Y. Gao, F. Fang and Z. Fan, *Nano Research*, 2018, **11**, 3065-3087.
200. X. Wei, D. Li, W. Jiang, Z. Gu, X. Wang, Z. Zhang and Z. Sun, *Scientific Reports*, 2015, **5**, 11181.
201. S. S. K. Mallineni, Y. Dong, H. Behlow, A. M. Rao and R. Podila, *Advanced Energy Materials*, 2018, **8**, 1702736.
202. H. Ragonés, S. Menkin, Y. Kamir, A. Gladkikh, T. Mukra, G. Kosa and D. Golodnitsky, *Sustainable Energy & Fuels*, 2018, **2**, 1542-1549.

203. N. Singh, C. Galande, A. Miranda, A. Mathkar, W. Gao, A. L. M. Reddy, A. Vlad and P. M. Ajayan, *Scientific Reports*, 2012, **2**, 481.
204. Q. Zhang, F. Zhang, S. P. Medarametla, H. Li, C. Zhou and D. Lin, *Small*, 2016, **12**, 1702-1708.
205. S. Tibbits, *Architectural Design*, 2014, **84**, 116-121.
206. R. Bogue, *Assembly Automation*, 2014, **34**, 16-22.
207. E. Pei, *Assembly Automation*, 2014, **34**, 310-314.
208. G. Liu, Y. Zhao, G. Wu and J. Lu, *Science Advances*, 2018, **4**, eaat0641.
209. A. Sydney Gladman, E. A. Matsumoto, R. G. Nuzzo, L. Mahadevan and J. A. Lewis, *Nat Mater*, 2016, **15**, 413.
210. M. Acerce, E. K. Akdoğan and M. Chhowalla, *Nature*, 2017, **549**, 370.
211. Z. Lei, W. Zhu, S. Sun and P. Wu, *Nanoscale*, 2016, **8**, 18800-18807.
212. S. Dadbakhsh, M. Speirs, J.-P. Kruth, J. Schrooten, J. Luyten and J. Van Humbeeck, *Advanced Engineering Materials*, 2014, **16**, 1140-1146.
213. D. Raviv, W. Zhao, C. McKnelly, A. Papadopoulou, A. Kadambi, B. Shi, S. Hirsch, D. Dikovskiy, M. Zyracki, C. Olguin, R. Raskar and S. Tibbits, *Sci Rep-Uk*, 2014, **4**, 7422.
214. A. Kotikian, R. L. Truby, J. W. Boley, T. J. White and J. A. Lewis, *Adv Mater*, 2018, **30**, 1706164.
215. Q. Ge, H. J. Qi and M. L. Dunn, *Appl Phys Lett*, 2013, **103**, 131901.
216. X.-Y. Tsai and L.-W. Chen, *Composite Structures*, 2002, **56**, 235-241.
217. W. Xu and D. H. Gracias, *ACS Nano*, 2019, **13**, 4883-4892.
218. D. Davis, R. Mailen, J. Genzer and M. D. Dickey, *RSC Adv*, 2015, **5**, 89254-89261.
219. H. Yang, B. S. Yeow, T.-H. Chang, K. Li, F. Fu, H. Ren and P.-Y. Chen, *ACS Nano*, 2019, **13**, 5410-5420.
220. K. J. Stevenson, V. Ozoliņš and B. Dunn, *Accounts Chem Res*, 2013, **46**, 1051-1052.
221. Z. Yang, J. Zhang, M. C. W. Kintner-Meyer, X. Lu, D. Choi, J. P. Lemmon and J. Liu, *Chem Rev*, 2011, **111**, 3577-3613.
222. L. E. Bell, *Science*, 2008, **321**, 1457-1461.
223. G. J. Snyder and E. S. Toberer, *Nat Mater*, 2008, **7**, 105.
224. C. Dun, C. A. Hewitt, Q. Li, Y. Guo, Q. Jiang, J. Xu, G. Marcus, D. C. Schall and D. L. Carroll, *Adv Mater*, 2017, **29**, 1702968.
225. C. Dun, C. A. Hewitt, Q. Li, J. Xu, D. C. Schall, H. Lee, Q. Jiang and D. L. Carroll, *Adv Mater*, 2017, **29**, 1700070.
226. A. J. Minnich, M. S. Dresselhaus, Z. F. Ren and G. Chen, *Energ Environ Sci*, 2009, **2**, 466-479.
227. J. H. We, S. J. Kim and B. J. Cho, *Energy*, 2014, **73**, 506-512.
228. S. J. Kim, H. Choi, Y. Kim, J. H. We, J. S. Shin, H. E. Lee, M.-W. Oh, K. J. Lee and B. J. Cho, *Nano Energy*, 2017, **31**, 258-263.
229. Z. Lu, M. Layani, X. Zhao, L. P. Tan, T. Sun, S. Fan, Q. Yan, S. Magdassi and H. H. Hng, *Small*, 2014, **10**, 3551-3554.
230. L. Yang, Z.-G. Chen, M. S. Dargusch and J. Zou, *Advanced Energy Materials*, 2018, **8**, 1701797.
231. M. Orrill and S. LeBlanc, *Journal of Applied Polymer Science*, 2017, **134**.
232. B. Zhang, J. Sun, H. E. Katz, F. Fang and R. L. Opila, *ACS applied materials & interfaces*, 2010, **2**, 3170-3178.
233. T. Juntunen, H. Jussila, M. Ruoho, S. Liu, G. Hu, T. Albrow-Owen, L. W. T. Ng, R. C. T. Howe, T. Hasan, Z. Sun and I. Tittonen, *Advanced Functional Materials*, 2018, **28**, 1800480.
234. C. Han, G. Tan, T. Varghese, M. G. Kanatzidis and Y. Zhang, *ACS Energy Letters*, 2018, **3**, 818-822.
235. M. Saeidijavash, W. Kuang, C. Dun and Y. Zhang, *Adv Funct Mater*, 2019, **0**.
236. Y. Shao, M. F. El-Kady, L. J. Wang, Q. Zhang, Y. Li, H. Wang, M. F. Mousavi and R. B. Kaner, *Chem Soc Rev*, 2015, **44**, 3639-3665.

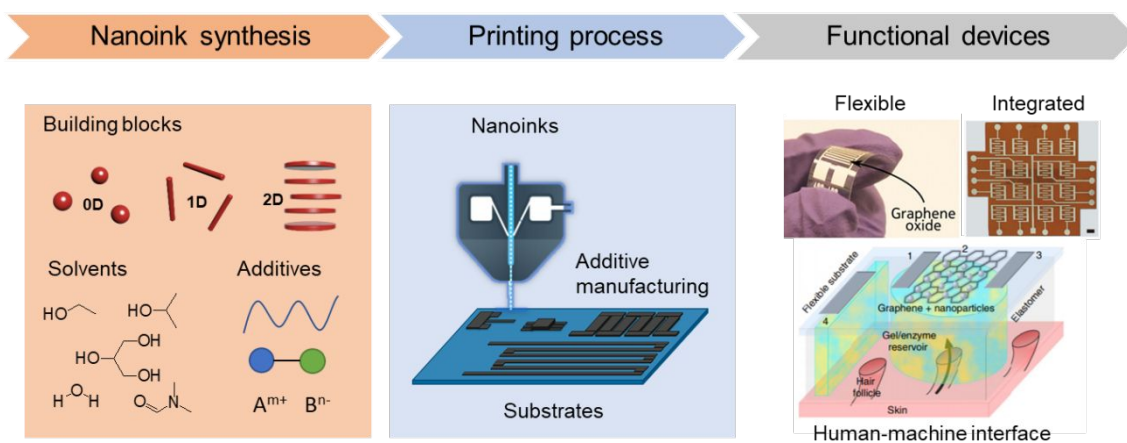
237. P. Simon and Y. Gogotsi, *Nat Mater*, 2008, **7**, 845.
238. R. Raccichini, A. Varzi, S. Passerini and B. Scrosati, *Nat Mater*, 2014, **14**, 271.
239. M. Xu, T. Liang, M. Shi and H. Chen, *Chem Rev*, 2013, **113**, 3766-3798.
240. C. W. Foster, M. P. Down, Y. Zhang, X. Ji, S. J. Rowley-Neale, G. C. Smith, P. J. Kelly and C. E. Banks, *Scientific Reports*, 2017, **7**, 42233.
241. R. Gusmão, M. P. Browne, Z. Sofer and M. Pumera, *Electrochemistry Communications*, 2019, **102**, 83-88.
242. G. Sun, J. An, C. K. Chua, H. Pang, J. Zhang and P. Chen, *Electrochemistry Communications*, 2015, **51**, 33-36.
243. Y. Jiang, Z. Xu, T. Huang, Y. Liu, F. Guo, J. Xi, W. Gao and C. Gao, *Adv Funct Mater*, 2018, **28**, 1707024.
244. C. Zhang, M. P. Kremer, A. Seral - Ascaso, S. H. Park, N. McEvoy, B. Anasori, Y. Gogotsi and V. Nicolosi, *Advanced Functional Materials*, 2018, **28**.
245. S. D. Lacey, D. J. Kirsch, Y. Li, J. T. Morgenstern, B. C. Zarket, Y. Yao, J. Dai, L. Q. Garcia, B. Liu, T. Gao, S. Xu, S. R. Raghavan, J. W. Connell, Y. Lin and L. Hu, *Adv Mater*, 2018, **30**, 1705651.
246. K. Shen, H. Mei, B. Li, J. Ding and S. Yang, *Advanced Energy Materials*, 2018, **8**, 1701527.
247. J. Ding, K. Shen, Z. Du, B. Li and S. Yang, *ACS Appl Mater Inter*, 2017, **9**, 41871-41877.
248. C. W. Foster, G.-Q. Zou, Y. Jiang, M. P. Down, C. M. Liaw, A. Garcia-Miranda Ferrari, X. Ji, G. C. Smith, P. J. Kelly and C. E. Banks, *Batteries & Supercaps*, 2019, **2**, 448-453.
249. M. Shanmugam, C. A. Durcan, R. Jacobs-Gedrim and B. Yu, *Nano Energy*, 2013, **2**, 419-424.
250. J.-M. Yun, Y.-J. Noh, C.-H. Lee, S.-I. Na, S. Lee, S. M. Jo, H.-I. Joh and D.-Y. Kim, *Small*, 2014, **10**, 2319-2324.
251. J.-Y. Lin, C.-Y. Chan and S.-W. Chou, *Chem Commun*, 2013, **49**, 1440-1442.
252. D. Barpuzary, A. Banik, G. Gogoi and M. Qureshi, *Journal of Materials Chemistry A*, 2015, **3**, 14378-14388.
253. A. Agresti, S. Pescetelli, A. L. Palma, A. E. Del Rio Castillo, D. Konios, G. Kakavelakis, S. Razza, L. Cinà, E. Kymakis, F. Bonaccorso and A. Di Carlo, *ACS Energy Letters*, 2017, **2**, 279-287.
254. X. Meng, X. Cui, M. Rager, S. Zhang, Z. Wang, J. Yu, Y. W. Harn, Z. Kang, B. K. Wagner, Y. Liu, C. Yu, J. Qiu and Z. Lin, *Nano Energy*, 2018, **52**, 123-133.
255. J. Yoon, H. Sung, G. Lee, W. Cho, N. Ahn, H. S. Jung and M. Choi, *Energ Environ Sci*, 2017, **10**, 337-345.
256. C.-C. Chung, S. Narra, E. Jokar, H.-P. Wu and E. Wei-Guang Diao, *Journal of Materials Chemistry A*, 2017, **5**, 13957-13965.
257. S. G. Hashmi, D. Martineau, X. Li, M. Ozkan, A. Tiihonen, M. I. Dar, T. Sarikka, S. M. Zakeeruddin, J. Paltakari, P. D. Lund and M. Grätzel, *Advanced Materials Technologies*, 2017, **2**, 1600183.
258. H.-C. Fu, V. Ramalingam, H. Kim, C.-H. Lin, X. Fang, H. N. Alshareef and J.-H. He, *Advanced Energy Materials*, 2019, **9**, 1900180.
259. X. Cao, C. Tan, X. Zhang, W. Zhao and H. Zhang, *Adv Mater*, 2016, **28**, 6167-6196.
260. F. Brunetti, A. Operamolla, S. Castro-Hermosa, G. Lucarelli, V. Manca, G. M. Farinola and T. M. Brown, *Adv Funct Mater*, 2019, **29**, 1806798.
261. S. G. Hashmi, J. Halme, Y. Ma, T. Saukkonen and P. Lund, *Advanced Materials Interfaces*, 2014, **1**, 1300055.
262. S. G. Hashmi, M. Özkan, J. Halme, S. M. Zakeeruddin, J. Paltakari, M. Grätzel and P. D. Lund, *Energ Environ Sci*, 2016, **9**, 2453-2462.
263. D. Dodoo-Arhin, R. C. T. Howe, G. Hu, Y. Zhang, P. Hiralal, A. Bello, G. Amaratunga and T. Hasan, *Carbon*, 2016, **105**, 33-41.
264. Y. Chen, D. Wang, Y. Lin, X. Zou and T. Xie, *Electrochimica Acta*, 2019, **316**, 248-256.

265. D. S. Hecht, L. Hu and G. Irvin, *Adv Mater*, 2011, **23**, 1482-1513.
266. X. Ling, H. Wang, S. Huang, F. Xia and M. S. Dresselhaus, *Proceedings of the National Academy of Sciences*, 2015, **112**, 4523-4530.
267. T.-Y. Kim, J. Ha, K. Cho, J. Pak, J. Seo, J. Park, J.-K. Kim, S. Chung, Y. Hong and T. Lee, *ACS Nano*, 2017, **11**, 10273-10280.
268. K. K. Manga, S. Wang, M. Jaiswal, Q. Bao and K. P. Loh, *Adv Mater*, 2010, **22**, 5265-5270.
269. S. Wu, Z. Zeng, Q. He, Z. Wang, S. J. Wang, Y. Du, Z. Yin, X. Sun, W. Chen and H. Zhang, *Small*, 2012, **8**, 2264-2270.
270. K.-J. Huang, L. Wang, Y.-J. Liu, T. Gan, Y.-M. Liu, L.-L. Wang and Y. Fan, *Electrochimica Acta*, 2013, **107**, 379-387.
271. J. Li, Z. Yang, Y. Tang, Y. Zhang and X. Hu, *Biosensors and Bioelectronics*, 2013, **41**, 698-703.
272. T.-W. Lin, C.-J. Liu and C.-S. Dai, *Applied Catalysis B: Environmental*, 2014, **154-155**, 213-220.
273. V. Dua, S. P. Surwade, S. Ammu, S. R. Agnihotra, S. Jain, K. E. Roberts, S. Park, R. S. Ruoff and S. K. Manohar, *Angewandte Chemie International Edition*, 2010, **49**, 2154-2157.
274. J. H. Kim, W. S. Chang, D. Kim, J. R. Yang, J. T. Han, G.-W. Lee, J. T. Kim and S. K. Seol, *Adv Mater*, 2015, **27**, 157-161.
275. P. Liu, A. T. Liu, D. Kozawa, J. Dong, J. F. Yang, V. B. Koman, M. Saccone, S. Wang, Y. Son, M. H. Wong and M. S. Strano, *Nat Mater*, 2018, **17**, 1005-1012.
276. C. Anichini, W. Czepa, D. Pakulski, A. Aliprandi, A. Ciesielski and P. Samorì, *Chem Soc Rev*, 2018, **47**, 4860-4908.
277. Y. Yuan, R. Li and Z. Liu, *Analytical Chemistry*, 2014, **86**, 3610-3615.
278. C.-H. Lu, H.-H. Yang, C.-L. Zhu, X. Chen and G.-N. Chen, *Angewandte Chemie International Edition*, 2009, **48**, 4785-4787.
279. S. Mao, J. Chang, H. Pu, G. Lu, Q. He, H. Zhang and J. Chen, *Chem Soc Rev*, 2017, **46**, 6872-6904.
280. C. Singhal, M. Khanuja, N. Chaudhary, C. S. Pundir and J. Narang, *Sci Rep-Uk*, 2018, **8**, 7734.
281. X. Gan, H. Zhao and X. Quan, *Biosensors and Bioelectronics*, 2017, **89**, 56-71.
282. B. Ryu, H. Nam, B.-R. Oh, Y. Song, P. Chen, Y. Park, W. Wan, K. Kurabayashi and X. Liang, *ACS Sensors*, 2017, **2**, 274-281.
283. M. Kukkar, A. Sharma, P. Kumar, K.-H. Kim and A. Deep, *Analytica Chimica Acta*, 2016, **939**, 101-107.
284. D. Katerinopoulou, P. Zalar, J. Sweelssen, G. Kiriakidis, C. Rentrop, P. Groen, G. H. Gelinck, J. van den Brand and E. C. P. Smits, *Advanced Electronic Materials*, 2019, **5**, 1800605.
285. C. Bali, A. Brandlmaier, A. Ganster, O. Raab, J. Zapf and A. Hübler, *Materials Today: Proceedings*, 2016, **3**, 739-745.
286. J. Zikulnig, C. Hirschl, L. Rauter, M. Krivec, H. Lammer, F. Riemelmoser and A. Roshanghias, *Flexible and Printed Electronics*, 2019, **4**, 015008.
287. D. Kong, L. T. Le, Y. Li, J. L. Zunino and W. Lee, *Langmuir*, 2012, **28**, 13467-13472.
288. S. Afroj, N. Karim, Z. Wang, S. Tan, P. He, M. Holwill, D. Ghazaryan, A. Fernando and K. S. Novoselov, *ACS Nano*, 2019, **13**, 3847-3857.
289. J. Zhao, Y. Zhang, Y. Huang, X. Zhao, Y. Shi, J. Qu, C. Yang, J. Xie, J. Wang, L. Li, Q. Yan, S. Hou, C. Lu, X. Xu and Y. Yao, *Journal of Materials Chemistry A*, 2019, **7**, 972-978.
290. T. Vuorinen, J. Niittynen, T. Kankkunen, T. M. Kraft and M. Mäntysalo, *Sci Rep-Uk*, 2016, **6**, 35289.
291. T.-H. Chang, K. Li, H. Yang and P.-Y. Chen, *Adv Mater*, 2018, **30**, 1802418.

292. X. Shi, S. Liu, Y. Sun, J. Liang and Y. Chen, *Advanced Functional Materials*, 2018, **28**, 1800850.
293. H. Song, I. Karakurt, M. Wei, N. Liu, Y. Chu, J. Zhong and L. Lin, *Nano Energy*, 2018, **49**, 7-13.
294. Z. Chen, Y. Hu, H. Zhuo, L. Liu, S. Jing, L. Zhong, X. Peng and R.-c. Sun, *Chemistry of Materials*, 2019, **31**, 3301-3312.
295. G. Hassan, J. Bae, A. Hassan, S. Ali, C. H. Lee and Y. Choi, *Composites Part A: Applied Science and Manufacturing*, 2018, **107**, 519-528.
296. J. Z. Gul, M. Sajid and K. H. Choi, *J Mater Chem C*, 2019, **7**, 4692-4701.
297. X. Fan, N. Wang, F. Yan, J. Wang, W. Song and Z. Ge, *Advanced Materials Technologies*, 2018, **3**, 1800030.
298. R. Zhang, B. Peng and Y. Yuan, *Composites Science and Technology*, 2018, **168**, 118-125.
299. P. Kruse, *Journal of Physics D: Applied Physics*, 2018, **51**, 203002.
300. Q. Yang, A. J. Yu, J. Simonton, G. Yang, Y. Dohrmann, Z. Kang, Y. Li, J. Mo and F.-Y. Zhang, *Journal of Materials Chemistry A*, 2017, **5**, 17841-17847.
301. H. An, T. Habib, S. Shah, H. Gao, A. Patel, I. Echols, X. Zhao, M. Radovic, M. J. Green and J. L. Lutkenhaus, *ACS Applied Nano Materials*, 2019, **2**, 948-955.
302. S.-J. Choi, H. Yu, J.-S. Jang, M.-H. Kim, S.-J. Kim, H. S. Jeong and I.-D. Kim, *Small*, 2018, **14**, 1703934.
303. Z. Zhen, Z. Li, X. Zhao, Y. Zhong, L. Zhang, Q. Chen, T. Yang and H. Zhu, *Small*, 2018, **14**, 1703848.
304. Z. Yang, A. Liu, C. Wang, F. Liu, J. He, S. Li, J. Wang, R. You, X. Yan, P. Sun, Y. Duan and G. Lu, *ACS Sensors*, 2019, **4**, 1261-1269.
305. P. Yasaei, A. Behranginia, T. Foroozan, M. Asadi, K. Kim, F. Khalili-Araghi and A. Salehi-Khojin, *ACS Nano*, 2015, **9**, 9898-9905.
306. D. J. Late, *Microporous and Mesoporous Materials*, 2016, **225**, 494-503.
307. M. B. Erande, M. S. Pawar and D. J. Late, *ACS applied materials & interfaces*, 2016, **8**, 11548-11556.
308. D. S. Dolzhenkov, H. Zhang, J. Jang, J. S. Son, M. G. Panthani, T. Shibata, S. Chattopadhyay and D. V. Talapin, *Science*, 2015, **347**, 425-428.
309. D. Luo, F. Wang, J. Zhu, F. Cao, Y. Liu, X. Li, R. C. Willson, Z. Yang, C.-W. Chu and Z. Ren, *Proceedings of the National Academy of Sciences*, 2016, 201608135.
310. I. Raj, M. Qu, L. Xiao, J. Hou, Y. Li, T. Liang, T. Yang and M. Zhao, *Fuel*, 2019, **251**, 514-522.
311. J. Luo, M. Zeng, B. Peng, Y. Tang, L. Zhang, P. Wang, L. He, D. Huang, L. Wang, X. Wang, M. Chen, S. Lei, P. Lin, Y. Chen and Z. Cheng, *Angewandte Chemie International Edition*, 2018, **57**, 11752-11757.
312. L. Zhang, Q. Lei, J. Luo, M. Zeng, L. Wang, D. Huang, X. Wang, S. Mannan, B. Peng and Z. Cheng, *Scientific Reports*, 2019, **9**, 163.
313. X. Wang, M. Zeng, Y.-H. Yu, H. Wang, M. S. Mannan and Z. Cheng, *ACS applied materials & interfaces*, 2017, **9**, 7852-7858.
314. S. G. Bucella, A. Luzio, E. Gann, L. Thomsen, C. R. McNeill, G. Pace, A. Perinot, Z. Chen, A. Facchetti and M. Caironi, *Nature Communications*, 2015, **6**, 8394.
315. M. Shusteff, A. E. M. Browar, B. E. Kelly, J. Henriksson, T. H. Weisgraber, R. M. Panas, N. X. Fang and C. M. Spadaccini, *Science Advances*, 2017, **3**, eaao5496.
316. B. E. Kelly, I. Bhattacharya, H. Heidari, M. Shusteff, C. M. Spadaccini and H. K. Taylor, *Science*, 2019, **363**, 1075-1079.
317. A. Reiser, M. Lindén, P. Rohner, A. Marchand, H. Galinski, A. S. Sologubenko, J. M. Wheeler, R. Zenobi, D. Poulikakos and R. Spolenak, *Nature Communications*, 2019, **10**, 1853.
318. X. Chen, X. Liu, M. Ouyang, J. Chen, O. Taiwo, Y. Xia, P. R. N. Childs, N. P. Brandon and B. Wu, *Sci Rep-Uk*, 2019, **9**, 3973.

319. J. T. Muth, D. M. Vogt, R. L. Truby, Y. Mengüç, D. B. Kolesky, R. J. Wood and J. A. Lewis, *Adv Mater*, 2014, **26**, 6307-6312.
320. H. Cui, R. Hensleigh, D. Yao, D. Maurya, P. Kumar, M. G. Kang, S. Priya and X. Zheng, *Nat Mater*, 2019, **18**, 234-241.
321. M. Zeng, D. King, D. Huang, C. Do, L. Wang, M. Chen, S. Lei, P. Lin, Y. Chen and Z. Cheng, *Proceedings of the National Academy of Sciences*, 2019, DOI: 10.1073/pnas.1906511116, 201906511.
322. M. Chen, A. Shinde, L. Wang, C. Ye, M. Zeng, Q. Yan, P. Lin, Y. Chen and Z. Cheng, *2D Materials*, 2019, **6**, 025031.
323. G. Xin, W. Zhu, Y. Deng, J. Cheng, L. T. Zhang, A. J. Chung, S. De and J. Lian, *Nature nanotechnology*, 2019, **14**, 168-175.
324. Y. Xia, T. S. Mathis, M.-Q. Zhao, B. Anasori, A. Dang, Z. Zhou, H. Cho, Y. Gogotsi and S. Yang, *Nature*, 2018, **557**, 409.
325. D. Voiry, J. Yang, J. Kupferberg, R. Fullon, C. Lee, H. Y. Jeong, H. S. Shin and M. Chhowalla, *Science*, 2016, **353**, 1413-1416.
326. Y. Wang, G. Qiu, R. Wang, S. Huang, Q. Wang, Y. Liu, Y. Du, W. A. Goddard, M. J. Kim, X. Xu, P. D. Ye and W. Wu, *Nature Electronics*, 2018, **1**, 228-236.
327. A. Puthirath Balan, S. Radhakrishnan, C. F. Woellner, S. K. Sinha, L. Deng, C. d. I. Reyes, B. M. Rao, M. Paulose, R. Neupane, A. Apte, V. Kochat, R. Vajtai, A. R. Harutyunyan, C.-W. Chu, G. Costin, D. S. Galvao, A. A. Martí, P. A. van Aken, O. K. Varghese, C. S. Tiwary, A. Malie Madom Ramaswamy Iyer and P. M. Ajayan, *Nature nanotechnology*, 2018, **13**, 602-609.
328. A. C. Rajan, A. Mishra, S. Satsangi, R. Vaish, H. Mizuseki, K.-R. Lee and A. K. Singh, *Chemistry of Materials*, 2018, **30**, 4031-4038.

TOC



Emerging trends and future perspective on nanoparticle synthesis and colloidal ink formulation, additive printing processes, and functional devices are highlighted.